Assessment of Climate Change Impact on the Net basin Supply of Lake Tana Water Balance

Zeryehun Haile Gebremariame

March, 2009

Assessment of Climate Change Impact on the Net Basin Supply of Lake Tana Water Balance

by

Zeryehun Haile Gebremariame

Thesis submitted to the International Institute for Geo-information Science and Earth Observation in partial fulfilment of the requirements for the degree of Master of Science in Geo-information Science and Earth Observation, Specialisation: Integrated watershed modelling and management

Thesis Assessment Board

Chairman	Dr. Ir. M.W. Lubczynski	WRS dep, ITC, Enschede
External Examiner	Dr. Ir. M.J. Booij	WREM dep, University of Twente,Enschede
First Supervisor	Dr. Ir. Christiaan van der Tol	WRS dep, ITC, Enschede
Second Supervisor	Dr. Ir. T.H.M. Rientjes	WRS dep, ITC, Enshede

INTERNATIONAL INSTITUTE FOR GEO-INFORMATION SCIENCE AND EARTH OBSERVATION
ENSCHEDE, THE NETHERLANDS

Disclaimer

This document describes work undertaken as part of a programme of study at the International Institute for Geo-information Science and Earth Observation. All views and opinions expressed therein remain the sole responsibility of the author, and do not necessarily represent those of the institute.

Abstract

Lake Tana is the largest fresh water lake in Ethiopia and the main source of the Blue Nile. Climate change has a significant impact on lake hydrology more than human impact such as deforestation and diversion of lake water for irrigation. Therefore studying the impact of climate change on the net basin supply of Lake Tana is important for sustainable utilization of the water resource in Ethiopia.

In this study the net basin supply of Lake Tana is predicted for different scenarios of climate change for three time windows: 2010-2039, 2040-2069 and 2070-2099. Net basin supply is the sum of all inflow to the lake and lake precipitation minus lake evaporation. Among the different GCMs the HadCM3 model is selected for this study since the model is widely used for climate change impact assessment. But the model output has coarse spatial resolution for this reason the statistical downscaling model (SDSM) is applied to downscale the climate variables to a finer resolution to match with hydrological modelling. For the SDSM the 30 years historic data of maximum and minimum daily temperature and rainfall of the three stations (Bahir Dar, Gonder and Debre Markos) were used. The downscaled data are used in hydrological model to forecast the inflow to the lake. Lake evaporation and lake precipitation are estimated based on the downscaled climate data of Bahir Dar and Gonder stations as well.

The result of downscaling in the baseline period shows maximum temperature and the minimum temperature have better agreement with the observed results than the precipitation. The simulation of precipitation though showed a relatively lesser agreement as compared to the maximum and minimum temperature due to the fact that precipitation is the conditional process. Conditional process like precipitation is dependant on other intermediate processes like on the occurrence of humidity, cloud cover, and wet day occurrence. Unconditional process like temperature; however, are not regulated by other intermediate process. In addition local temperature are largely determined by regional forcing whereas precipitation series display more “noise” arising from local factor. Hence larger differences can be observed in precipitation ensemble members than that of temperature.

The result of downscaling in the future scenario period indicates that the maximum temperature, minimum temperature and precipitation are increasing in the future times. As a result the mean annual lake precipitation, lake evaporation and inflow to the lake in the future period are higher than in the baseline period. But the increase in lake evaporation is obscured by the increase in lake precipitation and inflow, therefore the mean annual net basin supply shows an increasing trend in the future time.

Key words: climate change; downscaling; Lake Tana; net basin supply

Acknowledgements

Above all I thank the living and almighty God for his ever lasting Love and support during my stay in ITC and through out my life time.

I would like to thanks and gratitude the Doctorate of ITC for grating me to study the Master of Science in water resource and environmental management. My sincere gratitude goes to the south water work construction enterprise for providing me leave for the study period.

Very special thanks to my first supervisor Dr. Ir. Christiaan van der Tol and second supervisor Dr. Ir .Tom Rientjes for their guidance, encouragement and critical comment. You are making me to do a nice work. With out your support this work would not be realized.

I would like to thank the program Director Ir. Arno van Lieshout for his valuable support during my stay in ITC and I also thanks and appreciate all the WREM course teachers for your dedication and quality of the lectures.

I would like to thank the Ethiopian Ministry of Water resource and the National meteorological Agency of Ethiopia for giving a long time series hydrological and metrological data for my climate change study.

I would like to thank all my course mates for their contribution for my work and good social interaction.

My sincere appreciation and thanks goes to my wife Wubit Ejigu and my son Gedion Zeryehun for your continuous support and pray to achieve my goal.

Table of contents

List of figures

List of tables

1. Introduction

1.1. Background

Water is the most important natural resource required for the survival of most living species. With respect to the increasing demand of water due to increasing population its availability is limited and it is not equally distributed. Therefore proper water resource management is essential to achieve the current demand and for sustainable utilization. Increase population, rapid urbanization, and climate change causes water resource planning and management becoming difficult in the 21st century. Among these difficulties the impact of climate change on the water resource is a concern to decision makers because of its impact on the water resource. Climate change in a region causes the change in the hydrologic cycle especially the rainfall-runoff relationship and thus could result unexpected flooding and drying of stream flow (Kim and Kaluarachchi, 2008).

A human activity like fossil fuels and land cover change cause atmospheric concentration of green house gases and causes climate change. Some studies indicates that the mean annual global surface temperature has increased by 0.3-0.6 ^{o}C since the late 19th century and it is expected to further increase by 1-3.5 ^{o}C over the next 100 years. Such changes in the climate will have significant impact on local and regional hydrologic regimes, which will in turn affect the ecological, social and economical system. Nevertheless, substantial differences are observed in the regional change in climate compared to global mean change (Dibike and Coulibaly, 2005).

Climate change has already become a global issue, which needs to turn the minds of every one caring for the future. As it is know, climate change have a significant impact on the sea level rise, melting of glaciers and also expected to have adverse impact on the overall air quality, agriculture, forestry and biodiversity. Despite its global impact the climate change has also an impact on the individual nations. In developing countries like Ethiopia the main source of the economy is agriculture. Therefore the variability of the climate has a significant impact on the overall productivity. In addition to this climate variability and shortage of irrigable land causes a recurrent drought in the country. Lake Tana basin is one of the parts of Ethiopia which has shortage of natural resources such as vegetation, soil and water due to increasing demand of irrigable land by increasing population and lack of water shed management. These increasing demand of the natural resources together with climate variability makes the condition challenging. Taking active measure to understand ecohydrological system of the Lake Tana basin and the impact of climate change on the water resource will require detailed study.

1.2. Research problem

In a country like Ethiopia, where agriculture is the main source of the economy as well as ensures the well being of the people, the water resource is quite essential. However, unless the water resource is utilized with a balanced approach of the supply and demand, its sustainability will become in danger. Therefore proper planning of water resources development as well as the utilization based on climate change impact is very essential. Despite the significant importance of Lake Tana and Lake Tana basin for the national income and for the survival of the people around only little is done in this regard.

For Lake Tana basin variation in climate plays a far greater control on lake hydrology than human impact of local forces such as deforestation and diversion of irrigation during the last century. The basin is characterised by limited knowledge on ecohydrology. There is a fluctuation of seasonal and annual flow and in some basins there is a decline in dry season flow across the basin (Kebede et al., 2006). This is mainly driven by impact of erratic and unpredictable changes in climate variables. This unpredictable climate causes famine due to recurrent drought and lack of advanced water structure. Then studying the impact of climate change on the region is very crucial to take adaptation measure.

The Lake Tana basin is exposed and more sensitive to climate variability. At national level, the Ethiopian government is implementing a policy aimed at improving food security which includes greater utilization of the basin water. For this purpose some of the water resource projects are under implementation and the other are under study, but how climate change will affect the situation not clear. When the rainfall increases there may be benefits for crop yields but there may also be balanced by increase variability, soil erosion and siltation of dams due to higher rainfall intensities while a rainfall decrease will cause food security to deteriorate.

1.3. Objective of the study

In this study the general circulation model (GCM) output of HadCM3 to predict the future climate variables and statistical downscaling model (SDSM) to change the coarse resolution of climate variables to the finer scale are used to estimate the future lake water balance.

The general objective of this study is to assess the climate change impact on net basin supply of Lake Tana Water balance.
Specific objectives of this study are:

- To compare the HadCM3 output of maximum air temperature, minimum air temperature and rainfall with observed trends from the weather station records.
- To determine the impact of climate change on the net basin supply of Lake Tana.
- To determine the future lake evaporation.
- To determine the future lake precipitation.

1.4. Research questions

- Is there any trend in maximum temperature, minimum temperature and rainfall between the years 1960 and 2007?
- What is the significance of climate change on lake evaporation?
- How does climate change affect the net basin supply of Lake Tana?
- What is the impact of climate change on lake areal rainfall?

1.5. Research hypothesis

- Due to climate change there is an increasing trend in minimum and maximum temperature.
- The net basin supply of the lake increase due to climate change.
- The GCM and statistical downscaling methods will accurately estimate the impact of climate change on the net basin supply of Lake Tana water balance.

2. Description of the Study area

2.1. General

Lake Tana occupies the largest depression in the Ethiopian plateau. The lake is shallow and fresh water, with weak seasonal stratification. Lake Tana is the source of the Blue Nile River and has a total drainage area of approximately 16000km^2, of which the lake covers 3,060km^2 at an elevation of 1784 m. The maximum depth of the lake is 14 metres and its mean depth is 9 metres. The lake is located in north-west highlands at 12^o 00'N, 37^{o}15'E which is 564 km from the capital Addis Ababa.

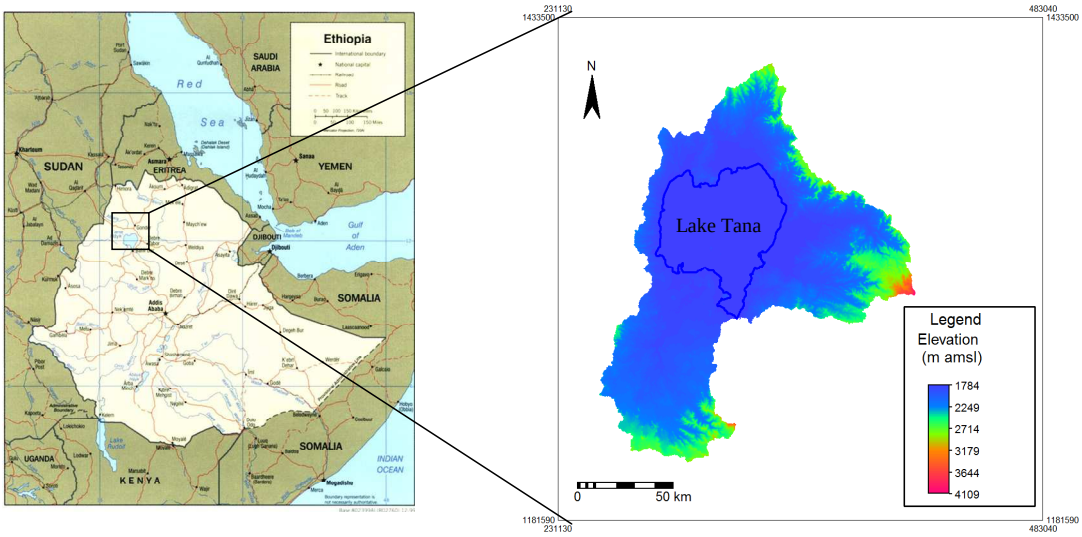

Figure 2-1: Location of the study area (Lake Tana basin)

2.1.1. Topography

The lake catchment has the minimum elevation of 1784 m at Dembia and Fogera flood plain to the North and East side of the Lake Tana respectively and at the north of Gilgel Abbay catchment. The Fogera flood plain is approximately bounded by Lake Tana, the Gumara and Ribb rivers and the Bahir Dar to Gonder road. River flow coming from the surrounding 13 small rivers flows to the flood plain are the main causes of the flooding, in addition to floods caused by the over flow of Ribb and Gumara rivers (SMEC, 2007). Maximum elevation of 4109 m is located in the east of Lake Tana at the boundary of Ribb catchment. The catchment is characterised by undulating topography in the upper parts of the catchment and gentle topography in the lower part. The average elevation of the catchment is 2946 m.

2.1.2. Land cover

The land cover of the Lake Tana catchment is classified in to four major parts namely cropland, urban area, and forest and water body. From the total area 76, 3, 0.14 and 20% are covered by cropland, forest, urban area and water body respectively. This shows that most of the area is covered by the cropland and the percentage of forest is low.

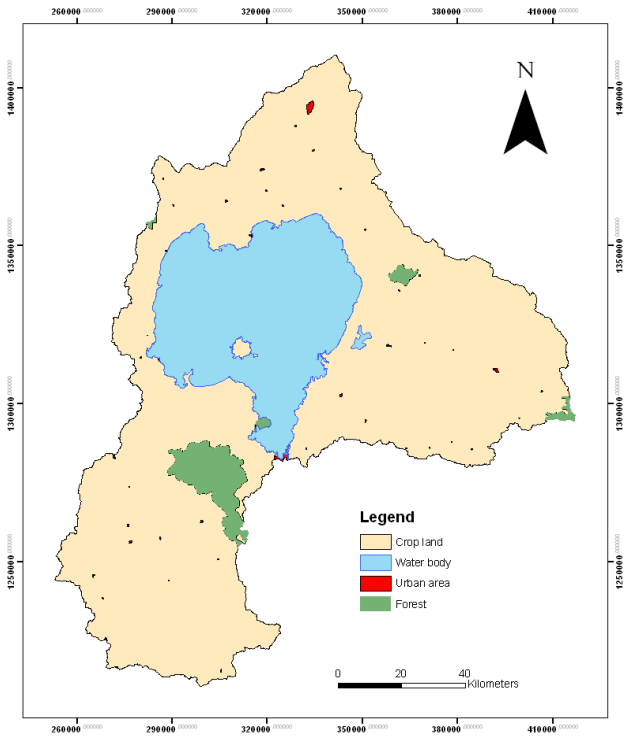

Figure 2-2: Land cover of Lake Tana catchment

2.1.3. Climate

The climate of the study area varies from humid to semi arid. Most precipitation occurs in the wet season (June to September) and the remaining precipitation occurs in the dry seasons (October to February) and in the mild season (March to May).

The annual average daily maximum and minimum temperature of Bahir Dar station (1961-2007) is 26.7 ^{o}C and 11.7 ^{o}C and for Gonder station it is 26.6 ^{o}C and 13.1 ^{o}C respectively. The mean annual relative humidity based on the Bahir Dar station (1997-2007) data is 58 %. The seasonal variation of temperature is between 3 to 6 ^{o}C from the warmest month and the coolest month. In summer, peak temperature is reduced because of rainfall and clouds while the highest temperature normally is expected in (April and May). The range of elevation within the basin is from 1784 to 4109 m and it has the major impact both on the climate and the human activity. On average the temperature falls by 5.8 ^{o}C for every 1000 metres increase in elevation (Conway, 2000).

2.1.4. Hydrology of the basin

Lake Tana has more than 40 tributaries but the major inflows to the lake are Gilgel Abbay, Koga and Kelti from the south, Gumara and Ribb from east and Megech from the north. The total inflow to the Lake Tana is the sum of the guaged and unguaged inflow. The gauged inflow is estimated based on the actual river discharge data that was collected from the Ministry of Water Resource during the field work and the unguaged river discharge is forecasted by conceptual HBV model. The model structure and the input data required to forecast the discharges are described in section 4.5.

The mean annual lake precipitation based on Bahir Dar station from 1961-2007 data is estimated to be 1453 mm and the mean annual surface water inflow from 1997 to 2006 period is 1961 mm. The contribution of gauged rivers is 63 % of the total inflow to the Lake Tana and the rest 37 % is covered by the unguaged catchments (see Table 2-1)

Table 2-1: Inflow of gauged and Ungauged Rivers to Lake Tana water balance (1997-2006)

No	Guaged River	Inflow (mm/year)	No	Unguaged River	Inflow (mm/year)
1	Gilgel Abbay	562	1	Unguaged Gillgel Abbay	388
2	Gumara	367	2	Unguaged Ribb	29
3	Ribb	151	3	Unguaged Megech	19
4	Megech	73	4	Unguaged Gumara	32
5	Koga	51	5	Garno	18
6	Kelti	102	6	Gemero	29
	Total guaged inflow	1313	7	Gelda	59
			8	Tana West	51
			9	Derma	12
			10	Gabi Kura	10
				Total unguaged inflow	648

The water level of Lake Tana is controlled by a weir across the Blue Nile at Chara Chara, approximately one or two km downstream from the point where the river drains from the lake. The construction of weir is completed in 1996 and it is intended to augment the dry season outflow to supply water regularly to the hydropower plant (TisIsat Hydropower).

2.2. Data availability

The data required for both the hydrological model and the climate change studies are collected from Ethiopia National Meteorological Agency (ENMA), Ethiopian Ministry of Water Resource (EMWR) and Bahir Dar Meteorological Agency. The major data collected are the hydrological data, meteorological data and the GPS data for the land cover classification. Hydrological data are the daily discharge records of the gauged rivers while the meteorological data are daily record of rainfall, maximum and minimum temperature, relative humidity, wind speed and sunshine hour data.

2.2.1. Hydrological data

Measurement on the major rivers in Tana basin started around 1959 during the Abbay basin study carried out by USBR (1964). In Lake Tana basin there are around 21 river gauging stations. Some of these stations have only been in operation for a short time, while the others have a long record (SMEC, 2007). The major rivers that have been gauged in Lake Tana are: Gilgel Abbay and Koga near Merawi, Gumara near Bahir Dar, Ribb near Addis Zemen and Megech near Azezo.

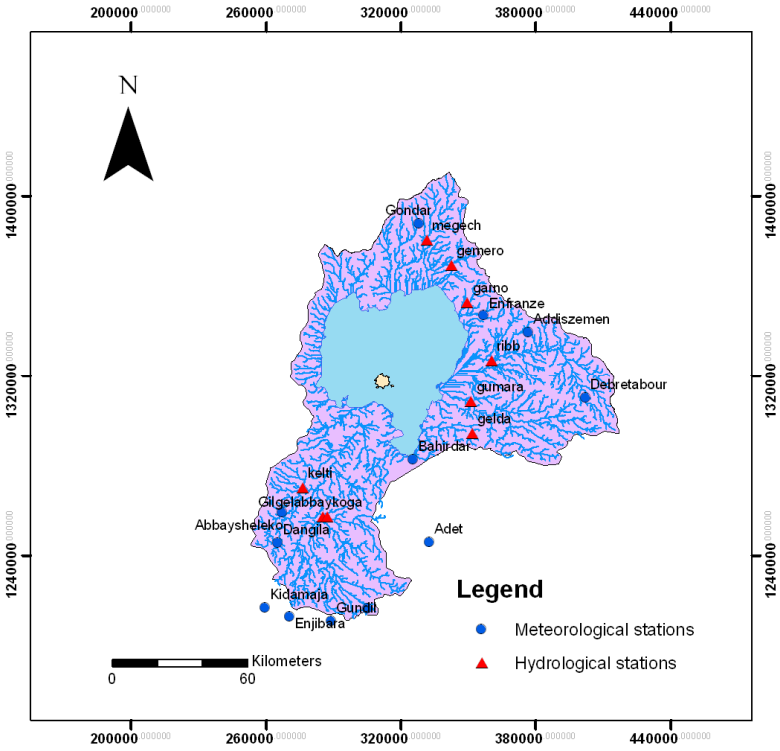

Figure 2-3: Spatial distribution of meteorological and hydrological stations

Most gauging stations have been located near the road in view of their easy accessibility. Sediment accumulation and flooding of the river bank have caused the major problems in the stage discharge relation. Because of these problems some stations show non-homogeneity in the records. In order to observe the homogeneity of the discharge the double mass curve is made for the major rivers (see Appendix D). The double mass curve shows there is inconsistency of flow in Gumara discharge between 2004 and 2007. This is because of some outliers in the records and it is adjusted by correlating the weighted precipitation and the discharge.

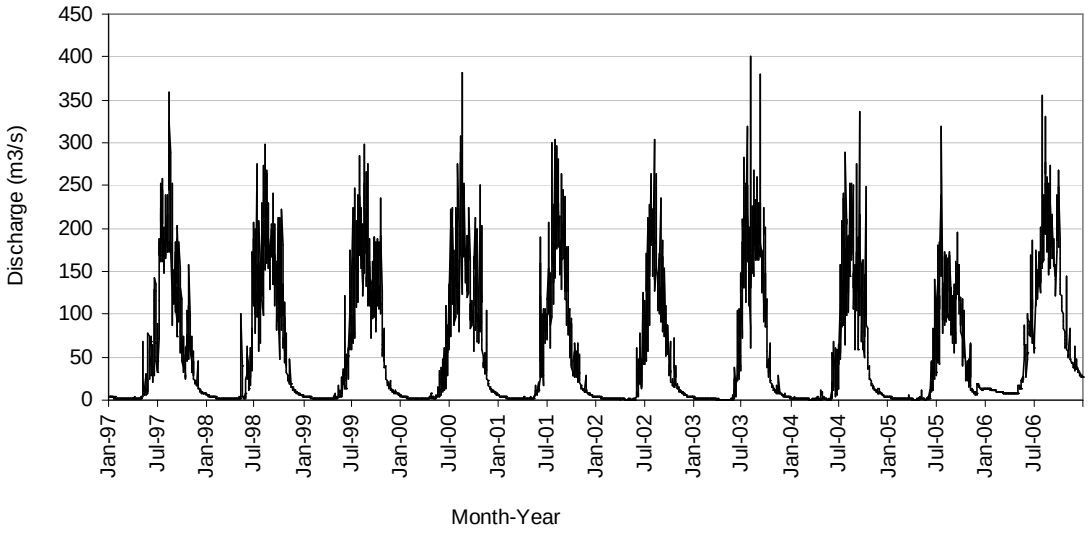

Figure 2-4: Daily Gilgel Abbay river discharge (1997-2006)

The gauging station of Gilgel Abbay is found at Wetet Abbay town near the Bridge of Gilgel Abbay River on the road from Addis Ababa to Bahir Dar. The daily average flow of Gilgel Abbay (1997-2006) is 56.4m ^{3}/s.

2.2.2. Rainfall data

For water balance and climate change studies the rainfall data is collected from 12 meteorological stations. Most stations are distributed around the southern and eastern part of the Lake Tana basin in which major catchments are located. In the western part the spatial distribution is less.

The available records of all meteorological data are visually checked to see the outliers and most of these appeared to be simple typing error. Thereafter consistency checks were carried out using double mass analysis (see Appendix E). The base station used in double mass analysis is Bahir Dar. This station has relatively long and complete records and their data quality is considered acceptable. The consistency check indicates that there is no significant problem in the rainfall records of all the station.

The mean annual rainfall map over the basin is calculated using the annual rainfall depth of the 12 stations (1997-2006) using inverse distance weighting interpolation in ILWIS and it shows that the rainfall distribution is decreases from the south to the north. The mean annual rainfall of the basin is 1624 mm. The maximum annual average rainfall of 2467 mm is observed at Gundil station while the minimum of 1140 mm at Gonder station.

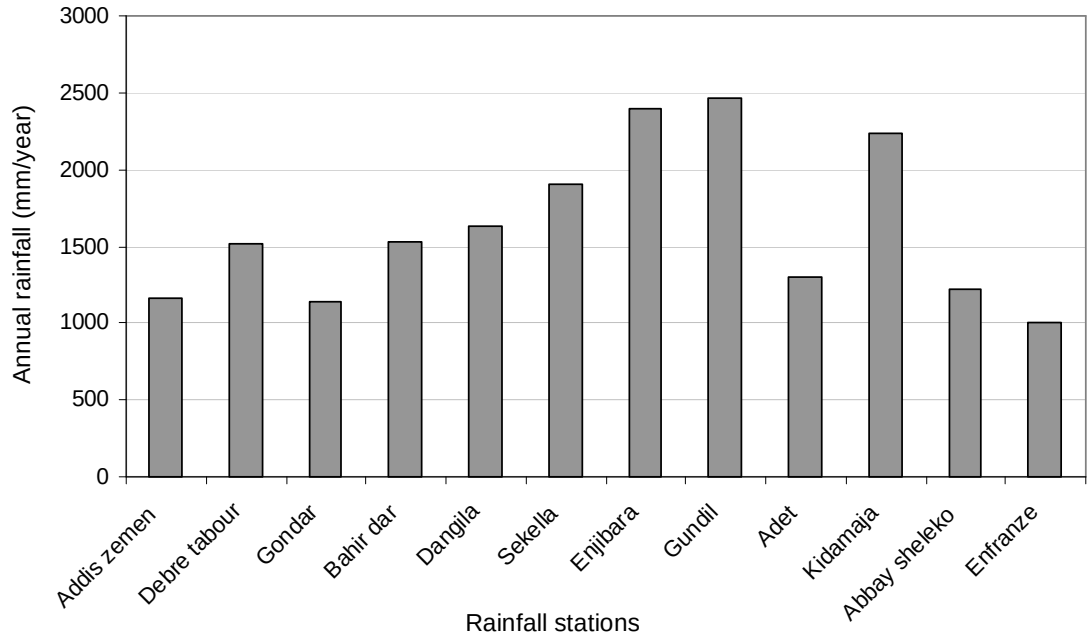

Figure 2-5: Mean annual rainfall distribution (1997-2006)

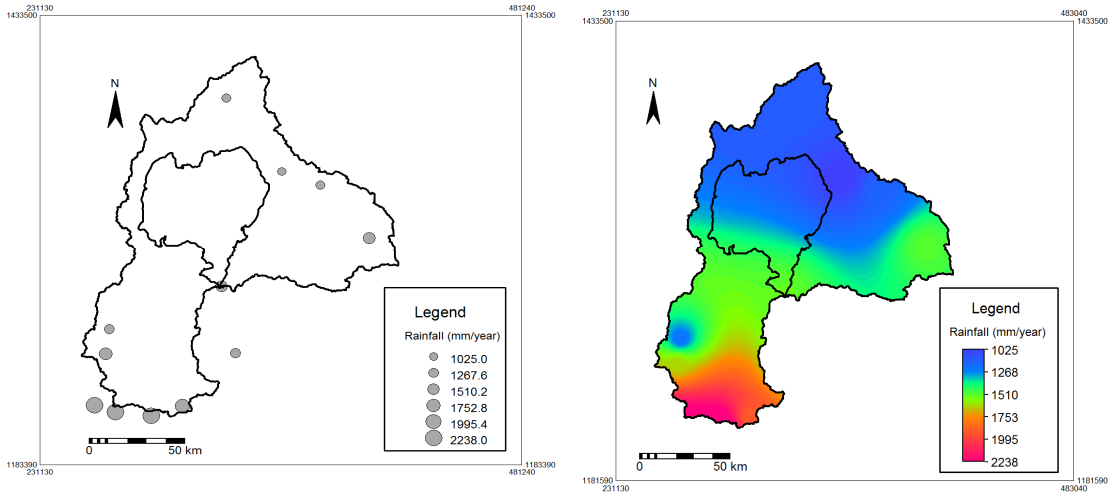

Figure 2-6: mean annual rainfall of the Lake Tana catchment (1997-2006)

2.2.3. Evaporation data

The FAO Penman-Monteith method is found to be suitable for estimation evapotranspiration from the reference surface under any climatic condition as far as sufficient climatic data is available. The reference surface is a hypothetical reference crop with an assumed crop height of 0.12 m, a fixed surface resistance of 70 s m-1 and an albedo of 0.23. The reference surface closely resembles an extensive surface of green grass of uniform height, actively growing, completely shading the ground and with adequate water. The fixed surface resistance of 70 s m^{-1} implies a moderately dry soil surface resulting from about a weekly irrigation frequency (Allen et al., 1998).

This method requires daily records of maximum temperature, minimum temperature, relative humidity, wind speed and sunshine hours. Therefore Bahir Dar, Gonder, Debre Tabour and Dangila stations are selected for this study because of availability of sufficient records from 1997-2006 for estimation of evaporation.

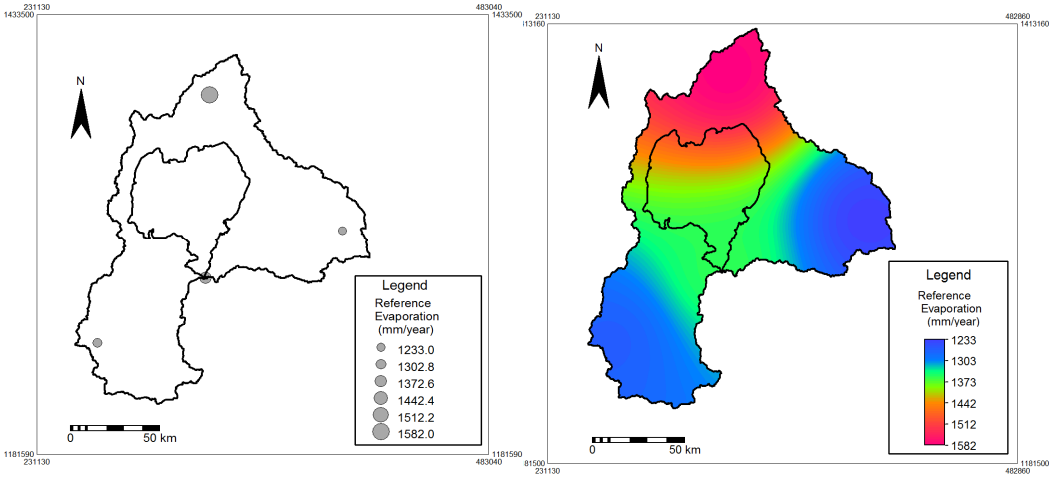

Figure 2-7: mean annual Penman-Monteith reference evaporation of Lake Tana catchment (1997-2006)

The mean annual reference evaporation map of the basin is made using the climate data of the above 4 stations from 1997-2006 using the inverse distance interpolation in ILWIS. The mean annual reference evaporation is low in the southern and eastern part of the Lake Tana basin while the reference evaporation is high in the northern part. The mean yearly reference evaporation within these periods are 1356 mm, 1561 mm, 1265 mm and 1294 mm based on Bahir Dar, Gonder, Debre Tabour and Dangila station respectively. The highest evaporation is estimated at Gonder station while the lowest is estimated at Debre Tabour station.

The average monthly reference evaporation also indicates that the highest evaporation is observed at Gonder stations while at Debre Tabour station the evaporation is low. Seasonally maximum reference evaporation is observed in the March, April and May but in the wet season (June, July and August) the evaporation has the lowest record.

Solar radiation is the main driving force for evaporation. High temperature results an increase of evaporation while low temperature reduces the evaporation despite the wind speed, humidity and other climate factors also have the impact. Topography of the catchment has an influence in the evaporation. At higher elevation the temperature is higher than the lower elevation area. Therefore the evaporation is maximum at high elevation than lower elevation area.

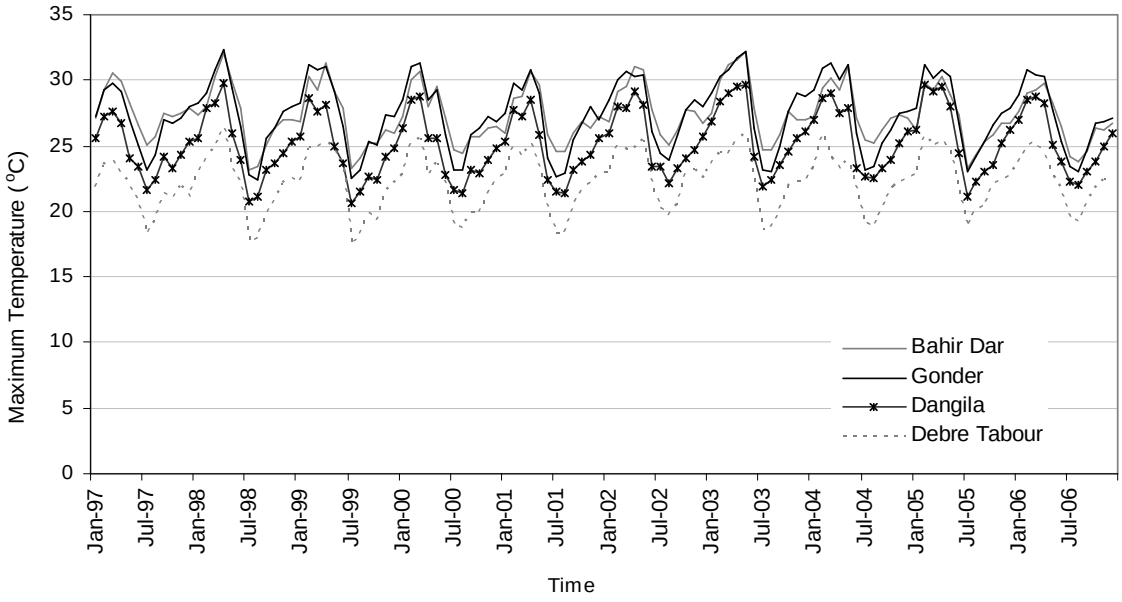

Figure 2-8: Monthly maximum temperature of four satations (1997-2006)

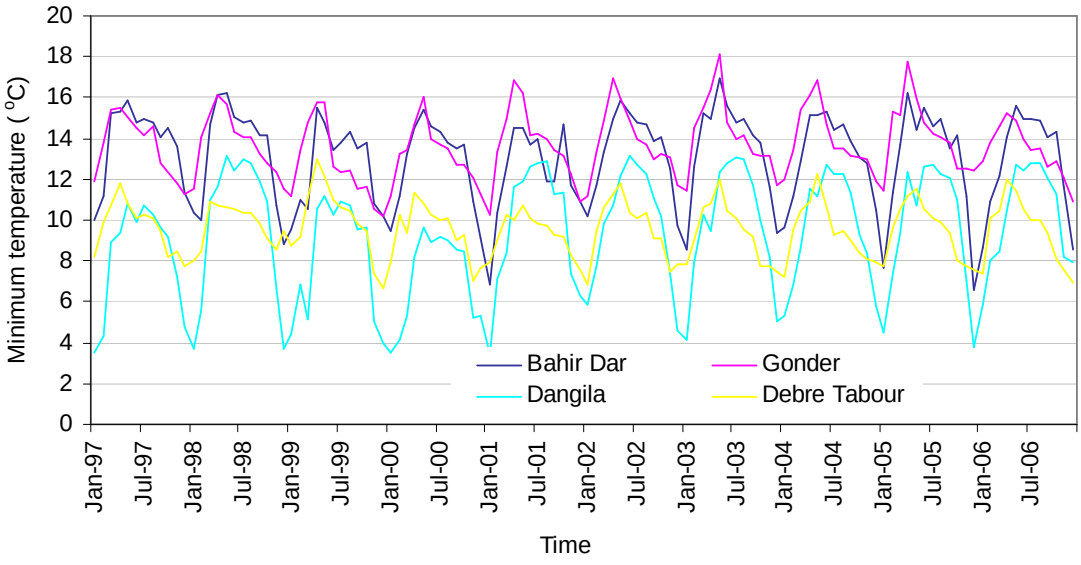

Figure 2-9: Monthly minimum temperature of four stations (1997-2006)

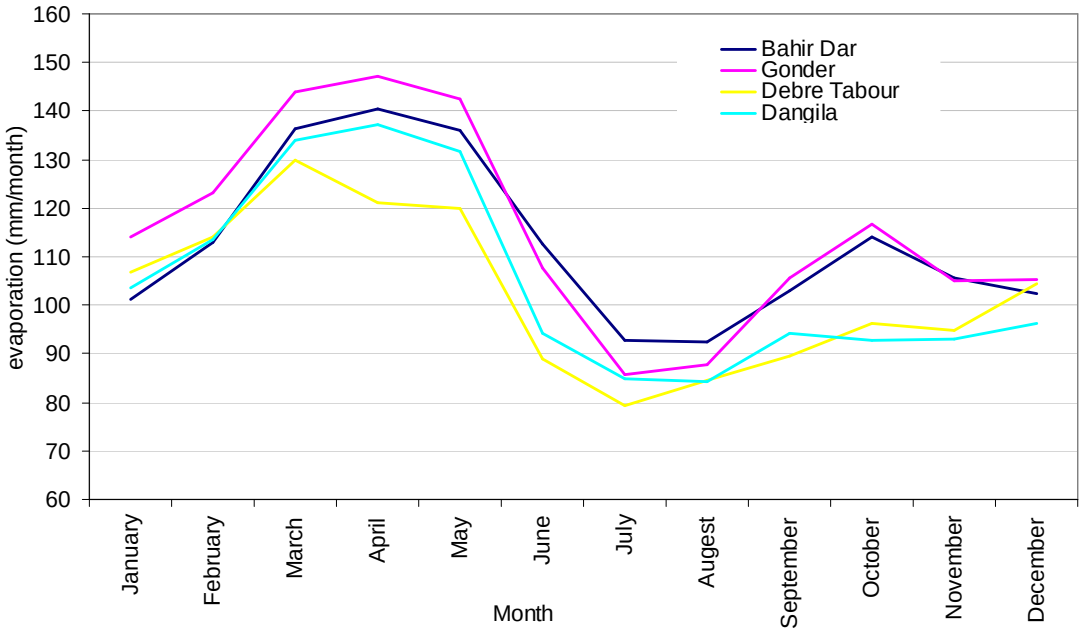

Figure 2-10: Monthly average reference evaporation (1997-2006)

In Lake Tana basin the highest maximum monthly temperature of 32 ^{o}C is observed in May 2003 at Gonder station while the lowest monthly maximum temperature of 17 ^{o}C is observed in July 1999. The mean monthly maximum temperature of 27.3 ^{o}C, 27.4 ^{o}C, 25.2 ^{o}C and 22.2 ^{o}C are observed at Bahir Dar, Gonder, Dangila and Debre Tabour stations respectively. The trend indicates that the highest monthly maximum temperature is observed in March, April and May and the lowest maximum temperature is observed in the wet season of the year (June, July, August and September) because of rainfall, cloudy condition and energy used for evapotranspiration.

The highest monthly minimum temperature of 18 ^{o}C is also observed at Gonder station in May 2003 while the lowest monthly minimum temperature of 3.4 ^{o}C is observed in January 2001 at Dangila station. In March, April and May the minimum temperature shows an increasing trend while in the month of December, January and February, which are part of the dry season, the minimum temperature shows the lowest trend in the analysis period.

3. Literature review

3.1. Climate scenarios

A climate scenario is a reasonable prediction of the future climate change. There are different climate scenarios used for climate change studies, among them synthetic scenario, analogue scenario and scenario based on general circulation model output are the most widely used.

In a synthetic scenario the future temperature and the precipitation is changed by a realistic but arbitrarily chosen value. It is most widely used for exploring system sensitivity prior to the application of more credible, and model based scenario. Analogue scenario is based on identifying recorded climate region which may have the same record of the future climate in a given region. But this scenario has its own drawback for climate change assessment because it is difficult to get climate data in the present which will have the similar record in the future. Scenarios from general circulation model outputs is different from the others since it is a numerical model which represents physical processes in the atmosphere, ocean and land surface by modelling the response of global climate system to increasing green house gas concentrations (Carter, 2007).

For this study the model is selected based on the following criteria:

- The model should be consistent in global projection
- The model should be physically plausible
- The model should be easily available and
- The model should be representative

Most GCM outputs are able to simulate the global and continental climate processes in detail and gives accurate climate prediction in the future (Dibike and Coulibaly, 2005). The GCM is a coarser resolution and correctly model smoothly varying fields such as surface pressure and temperature but unlikely these models properly simulate non smoothing fields such as precipitation (Mujumdar, 2008). The scenario based on the GCM output is selected for this study since it has firm physical bases, easily available and it is physically plausible.

3.2. General circulation model (GCM)

The Intergovernmental Panel on Climate Change (IPCC) data distribution centre (DDC) have seven general circulation modelling centres for getting daily climate variable for climate change studies . Each model has a unique approach to modelling these complex systems, differing in their levels of resolution and degree of specificity. Very recent GCMs are coupled models that include four principal components: atmosphere, ocean, and land surface and sea ice. The GCM uses the future forcing scenarios to produce the range of the climate change. The selection of each model for a particular climate change study depends on time of the model development, the resolution of the model, the validity of the model, the representativeness of the model output and the availability of the model.

Table 3-1: Coupled atmospheric general circulation models for which climate change simulation held by IPCC Data Distribution centre (Carter, 2007).

Modelling centre	Country	models
Common wealth scientific and industrial research organisation(CSIRO)	Australia	CSIRO-MK2
Max Planck Institute for Meteorology	Germany	ECHAM4/OPYC and EPHAM3/LSG
Hadley centre for climate prediction and research	UK	HadCM2&HadCM3
Canadian centre for climate modelling and analysis (CCCMA)	Canada	CGCM1&CGCM2
Geophysical fluid dynamic laboratory(GFDL)	USA	GFDL-R15&GFDL- R30
National centre for atmospheric research(NCAR)	USA	NCAR DOE-PCM
Centre for climate research studies (CCSR) and national institute for environmental studies (NIES)	Japan	CCSR-NIES

HadCM3 is a coupled atmospheric-ocean GCM developed at the Hadley Centre of the United Kingdom National Meteorological Service that studies climate variability and change. The model includes different land cover classification, soil layers and detail evapotranspiration function (Palmer et. al., 2004).

The atmospheric component of the model has 19 levels with a horizontal resolution of 2.5^{o} latitude and 3.75^{o} longitude. The ocean component of the model has 20 levels with horizontal resolution 1.25^{o} latitude and 1.25^{o} longitude.

3.3. Emission scenarios

Emission scenarios are based on prediction of possible population growth, economic development and the available energy utilization in the future world. Its major aim is to identify the future environment related with the production of greenhouse gases. Based on the IPCC Special Report on the Emission Scenarios (SRES) A1, A2, B1 and B2 are the four major emissions to indicate the future increase of green house gases and aerosol concentration.

In A1 scenario the global population become 8.7 billion in the mid-century and reduced to 7 billion by 2100. A1 emission scenarios are further classified in to A1F1, A1T and A1B based on the alternative energy requirement. In A2 emission scenario the population by 2100 become 15 billions and technology become slower than other scenario. In B1 emission scenario the population growth is almost similar to the A1 scenario but the technological change is more on the social service and information. The population growth in B2 emission scenario less than A2 and the there is also

intermediate economic growth as compared to other emission scenarios. In addition to this the scenario focuses on the environmental protection (Carter, 2007).

The IPCC recommends the use of A2 (high emission) and B2 (medium-low emission) for inter-comparison studies because the computing cost of all the scenarios in GCM is too expensive. These two scenarios are the only one that was common to all GCMs. The fact that the inter-model variability higher than the inter-scenario variability also supports the choice of those two scenarios being adequate (Menzel and Bürger, 2002).

3.4. Downscaling methods and tools

GCM were not designed for climate change impact studies and do not provide a direct estimation of hydrological response to climate change. Therefore in climate change impact studies, hydrological models are needed to simulate sub grid scale phenomena. However, such hydrological model requires input data (such as precipitation) at similar sub grid scale, which has to be provided by converting the GCM output into at least a reliable daily rainfall series at the selected watershed scale. The method used to convert GCM output in to local meteorological variables required for reliable hydrological modelling are usually referred to as 'downscaling' techniques (Dibike and Coulibaly, 2005).There are two categories of climate downscaling namely dynamic downscaling and statistical downscaling. They are described in the next sections.

3.4.1. Statistical downscaling

Statistical downscaling is used to relating the large scale atmospheric predictor variables to finer resolution meteorological series which could be used as input to hydrological models (Dibike and Coulibaly, 2005).

Statistical downscaling model requires the availability of long and homogeneous data series but the computational resource needed are small. One of the basic advantages of the model is that they are computationally inexpensive and it can easily apply to different GCM experiment (Wilby et al., 2004). In SDSM the multiple linear relations developed between the predictors and the actual meteorological data (predictand) for the current condition is applicable for future climate that exists under different forcing conditions. The limitation of the SDSM is it requires long time series climate data which may not be readily available in remote or complex topographic regions. The other limitation of the model is that since it is empirical based method then it does not consider any systematic change in the regional forcing conditions or feedback processes.

A diverse range of statistical downscaling techniques have been developed over the past few years and each method lies in one of the three major categories namely, regression method, stochastic weather generator and weather typing scheme.

I. Regression method

In regression downscaling methods the predicators (climate variables) and the predictand (actual data) are correlated with multiple linear regression equation. As compared to other downscaling models the regression method is easy for application and the model is freely available (Dibike and Coulibaly, 2005). In regression downscaling model there is limited correlation between the daily global climate variables and the precipitation then the simulation capability of the model for precipitation is low (Menzel and Bürger, 2002).

II. Stochastic Weather generator

Weather generators are models that replicate the statistical attributes of local climate variables (such as mean and variance) but not the observed sequence of events. These models are based on representation of precipitation occurrence on the Markov chain approach and spell length approach. In Markov chain approach the random process is constructed which determine the day at station as rainy or dry based on the previous day and following the given probability. When the day is wet the amount is determined from the precipitation distribution of that particular month from the previous record or the amount of precipitation on the previous days. In spell length approach instead of simulating rainfall occurrence day by day, the models operates by fitting probability distribution to observed relative frequencies of wet and dry spell length (Dibike and Coulibaly, 2005). In both cases the statistical parameters (mean and variance) extracted from the observed data at a particular station together with some random component are used to generate a similar time series of any length. In stochastic weather generator the secondary variables such as wet day amount, temperature and solar radiation are often modelled conditional on precipitation occurrence (Wilby et al., 2004).

III. Weather typing scheme

Weather typing scheme involves grouping local, meteorological data in relation to prevailing pattern of atmospheric circulation. Climate change scenario are constructed either by re-sampling from the observed data distribution (conditional on the circulation pattern produced by a GCM) or by generating synthetic sequence of weather pattern and then re-sampling from the observed data. The most serious limitation of the approach is that precipitation changes produced by changes in the frequency of the weather patterns are seldom consistent with the changes produced by the host GCM (Dowson & Wilby, 2007).

3.4.2. Dynamic downscaling

As it is discussed in the previous section the statistical downscaling model uses the coarser resolution climate model (GCM) in order to get catchment scale climate variables, while the dynamic downscaling uses a finer resolution of regional climate model (RCM) which has a horizontal resolution of 20-50km. The SDSM is ultimately limited by the assumption of temporal stationary in the empirical relations but dynamic downscaling model does not have such problems. Dynamic downscaling simulations of local climate are more physically based than SDSM and are more

acceptably transferable from the current to the future climate. However, dynamic downscaling simulation of the current climate has not been extensively tested (Hay and Clarck, 2003).

The main advantage of RCMs is that they can resolve small scale atmospheric features such as orographic precipitation better than the GCM. Furthermore, RCMs can be used to explore the relative significance of different external forcing such as terrestrial ecosystem or atmospheric chemistry changes (Dowson & Wilby, 2007). Even though the RCM has the advantage over the GCM in simulating finer resolution climate variables, there also have their own drawback. The basic drawback of RCM is it requires considerable computing resources and it is expensive to run as the GCM (Abdo Kedir, 2008).

3.5. Water balance models

Water balance models are classified as physically based, conceptual and empirical depending on the degree of complexity and physical completeness in the formation of the structure. Models are further classified as lumped, semi distributed and distributed depending on the degree of discretization when describing the terrain in the basin. Today most rainfall runoff models, whether physically based or conceptual are distributed to some degree and larger basins are regularly split into subbasins in model application (Bergström and Graham, 1998).

Distributed model structure accounts for detailed catchment characteristics (e.g. soil and land use), process calculation and highly resolved meteorological variables (e.g. precipitation). The catchment is divided in to a number of subcatchments and each subcatchment is further divided in to a number of grid cells. In the semi distributed model structure, sub division of subcatchment in to a number of different homogeneous zones can be accomplished based on various catchment characteristics (topographic elevation, soil type and land use). Whereas in fully lumped model, the meteorological variables, precipitation, temperature and potential evaporation were assigned to each subcatchment (Das et al., 2008).

Empirical models are based on the mathematical equations which do not take into account the physical processes and therefore are not useful for implementation of the appropriate model components. Physically based model on the other hand incorporate physical laws based on conservation of mass, momentum and energy. In physically based model there is a problem of over parameterization because different combination of parameters giving equally good performance. Besides this over parameterization effect, physically based model generally incorporate too many process and too complex formulation at a too detailed scale on the context of climate change. Conceptual model usually able to capture the dominating hydrological process at the appropriate scale with accompanying formulations. Therefore conceptual model is considered as a nice compromise between the need for simplicity on one hand and the need for firm physical bases on the other hand for climate change study (Booij, 2005).

Sacramento, MIKE-SHE, Topmodel and HBV model are some of the major rainfall runoff model used for the continuous simulation of runoff. Sacramento model approach is a lumped conceptual model used for the continuous stream flow simulation. The model accounts for effective rainfall, evaporation and interception, storage of water in various zones and discharge from these zones and water transport in the drainage system (Rientjes, 2007). Topmodel is classified as conceptual distributed and allows for continuous stream flow simulation. The model domain is fully distributed and the approach is mass conservative but applies relatively simple momentum type equivalency to simulate the stream flow. In Topmodel approach, topography of a catchment is analysed by means of a digital elevation model to represent the topography of the catchment in to a number of rectangular grid element. MIKE-SHE is physical based distributed catchment modelling system that is developed from 1977 onwards by the Danish Hydraulic Institute (DHI), the Institute of Hydrology in the U.K. and the French consulting company SOGREAH (Rientjes, 2007). The model process includes rainfall, canopy interception, evapotranspiration, snow melt, overland flow, channel flow, unsaturated subsurface flow and saturated subsurface flow.

HBV model is a semi distributed conceptual hydrological model for a continuous simulation of runoff. In the model it is possible to forecast the runoff from the individual subcatchment and add the contribution to get the total inflow from the catchment. When the subcatchment has a considerable elevation difference it is divided in to different elevation zone and each elevation zones is further divided in to forest and non forest (SMHI, 2006).

The dominating processes of the HBV model are precipitation, evapotranspiration, subsurface flow and river flow. The different subcatchments and elevation zones are used to obtain appropriate spatial scale and the simulation can be done with different time steps. The process of infiltration, saturation excess overland flow and subsurface storm flow is represented by one component called the runoff generation routine. The advantages of HBV model are (a) it covers most of the important runoff generating process by quite simple and robust structures and does not requires too extensive input data (b) it accounts for topographic conditions by defining elevations zones within the basin or subbasins and (c) the model was successfully tested in different conditions in more than 40 countries (Krysanova et al., 1999).

The other advantage of HBV model compared to other hydrological model for climate change study is because of its availability and firm physical basis for simulating of runoff and its application covers basins of different climataological and geographical regions ranging in size from less than 1 to more than 40,000km^2 area (Booij, 2005).

4. Methodology

4.1. Statistical analysis of observed data

To analyze the trends of observed maximum temperature, minimum temperature and rainfall data of Bahir Dar, Gonder and Debre Markos station, statistical analyses are considered. For this study significance testing using confidence intervals of least square is applied for analyzing the temperature and rainfall change for the time period 1961-2007 for which daily observations are available. First a simple linear regression model of $\hat{y}_i = a + bx_i$ is selected and then it is tested whether b is significantly different from zero. In the linear model a is the constant value of temperature or rainfall and b is the change per year (slope), x_i is a year to which the output is calculated by the model and $\hat{y}_i$ is the estimated rainfall or temperature by the linear model.

The variance is calculated by:

$$\sigma^2 = \frac{\sum\left(y_i - (a + bx_i)\right)^2}{N - 2} \qquad [4\text{-}1]$$

Where σ^2 = variance in $(mm)^2$ for rainfall and $(^oC)^2$ for temperature.

y_i = the observed time series data (mm for rainfall and ^oC for temperature)

$a + bx_i =$ the output of the linear model (mm for rainfall and ^oC for temperature).

N = sum of observation years from 1961 to 2007.

x_i = the observed years from 1967 to 2007

From the above equation it can be shown that the regression coefficient b will have the student-t distribution with variance.

$$\text{var}[b] = \frac{\sigma^2}{\sum\left(x_i - \bar{x}\right)^2} \qquad [4\text{-}2]$$

Based on the variance of b, the t distribution table is used to define the multiplier t for the confidence limits for the regression coefficient under the hypothesis of no climate change.

$$b = \beta \pm t\sqrt{\mathrm{var}(b)} \qquad [4\text{-}3]$$

For t test analysis the slope β is equal to some specified value β_o (often assumed as 0). This is because it has to be tested that there is climate change $(\beta \neq 0)$ and the hypothesis that there is no climate change $(\beta = 0)$. Therefore based on this it is possible to estimate the current climate change with a specified confidence interval.

4.2. General circulation model

Among the different GCMs the HadCM3 model is selected for this study since the model is widely used for climate change impact assessment. Besides this the model is selected due to the availability of the downscaling models called SDSM that is used to downscale the result of HadCM3. For HadCM3 the model result is available for A2 and B2 emission scenario, where A2 is refereed to as medium-high emission scenario and B2 is medium-low emission scenario. For both scenarios the ensemble members a, b, and c are available which refer to a different initial point of climate solution along the reference period (Hanson et al, 2004). But for this study the data is available for the "a" ensembles and hence only the A2a and B2a scenarios are considered.

4.3. Statistical downscaling model (SDSM)

The selected regression based method is the SDSM 4.2 developed by Dowson and Wilbey (2007) and it is downloaded freely from http://www.sdsm.org.uk. It is a decision support tool used to assess local climate change impacts using a statistical downscaling technique. The tool facilitates the rapid development of multiple, low cost, single site scenarios of daily surface weather variables under current and future climate forcing. The model is calibrated and applied at a daily time series even though the output is at monthly basis.

The software manages additional tasks of data quality control and transformation, predicator variable screening, automatic model calibration, statistical analysis and graphing of climate data.

4.3.1. Downloading the predictors

General circulation model (GCM) predictors are freely obtained from the Canadian Climate Impact Scenario Group with web address of: http://www.cics.uvic.ca/scenarios/sdsm/select.cgi/.

The predictor variables of HadCM3 are available on a grid box by grid box basis of size 2.5^o latitude and 3.75^o longitude. The Lake Tana basin found between 36^o 43' 59" E to 38^o 14' 32"E (average 37.488^o E) and 10^{o}56'45"N to 12^{o}45'22"N (average 11.851^{o}N). Hence the nearest grid box which represents the study area to download the HadCM3 data is 12.5^{o}N and 37.5^{o}E (see Figure 4-1). The NCEP_1961-2001 data is downloaded from the specified grid box which represents the Lake Tana

basins. This data is used for calibration of the SDSM with the actual maximum temperature, minimum temperature and precipitation.

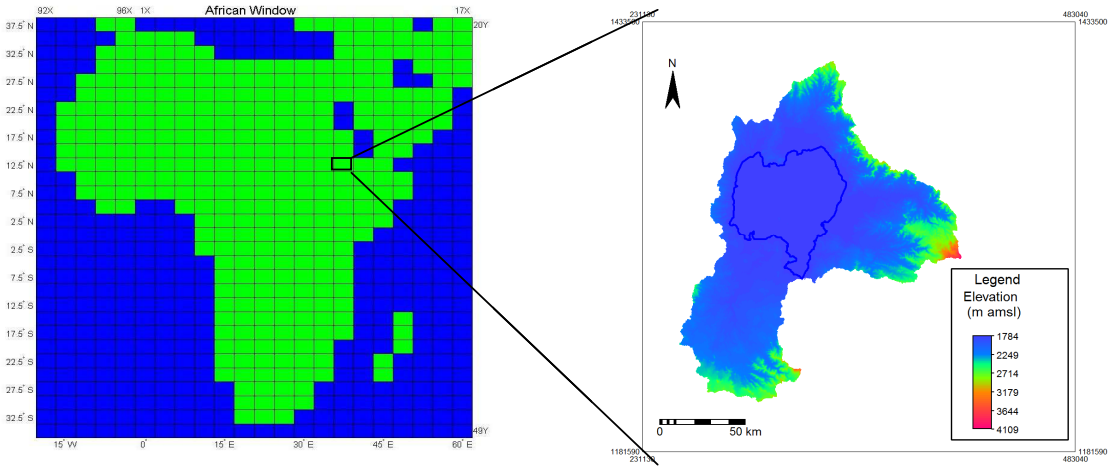

Figure 4-1: Downloading site of Climate variable

Table 4-1: Predictor variables of the climate scenarios (Dawson & Wilby, 2007)

No	Predictor variables	predictor description	No	Predictor variables	predictor description
1	mslpaf	mean sea level pressure	14	p5zhaf	500hpa divergence
2	p_faf	surface air flow strength	15	p8_faf	850hpa air flow strength
3	p_uaf	surface zonal velocity	16	p8_uaf	850 hpa zonal velocity
4	p_vaf	Surface merdional velocity	17	p8_vaf	850 hpa meridional velocity
5	p_zaf	surface vorticity	18	p8_zaf	850 hpa vorticity
6	P_thaf	surface wind direction	19	p850af	850 hpa geopotential
7	p_zhaf	surface divergent	20	p8thaf	850 hpa wind direction
8	p5_faf	500hpa airflow strength	21	p8zhaf	850hpa divergence
9	p5_uaf	500hpa zonal velocity	22	pr500af	Relative humidity at 500hpa
10	p5_vaf	500hpa merdional velocity	23	pr850af	Relative humidity at 850hpa
11	p5_zaf	500hpa vorticity	24	rhumaf	Near surface relative humidity
12	p500af	500hpa geopotential height	25	shumaf	Surface specific humidity
13	p5thaf	500hpa wind direction	26	tempaf	Mean temperature at 2 metre

4.3.2. Preparation of predictands

Maximum temperature, minimum temperature and rainfall records from 1961-1990 of Bahir Dar, Gonder and Debre Markos have been prepared for inputs to the statistical downscaling model. In the time series data there are some outliers, missing data and gap data that should be corrected before it can be used in the model. The outliers are the values that highly deviate from the mean value. The missing data and gap data are less than 1% of the total data available from the meteorological and hydrological stations. In order to fill data the correlation is done with the individual station which has the missing and gap data and the average of the nearby stations which do not have such problem. Then

based on the regression equation the missing and the gap data of the individual station is filled with respect of the available data of the other stations.

4.3.3. Model parameters

In the SDSM before doing any analysis the first step is fixing the model parameters which are basic to the temperature and precipitation simulation. Maximum temperature and minimum temperature are continuous processes while rainfall occurs in events. Therefore to treat less rain days as dry days an event threshold of 0.1 mm/day is used for precipitation while no event threshold is required for temperature. A statistical method is more straightforward than dynamic downscaling but tends to underestimate variance and poorly represent extreme events. Regression method under predict climate variability to varying degrees, since only parts of the regional and local climate variability is related to large scale climate variations . The range of variation of the downscaled and daily weather parameters can be controlled by fixing the variance inflation. This parameter changes the variance by adding /subtracting equal amount applied to regression model estimates of the local process. Then variance inflation of 12 prior to any model transformation produces normal variance inflation for daily temperature values, while for daily precipitation the variance inflation of 18 is added to agree with the observed climate variables.

The choice of statistical method is to some extent determined by the nature of the local predictand. A local variable that is reasonably normally distributed, such as temperature will require nothing more complicated than multiple regression, since the large scale climate predictors are normally distributed and assuming linearity of the relationship. A local variable that is highly heterogeneous and discontinuous in space and time, such as daily precipitation, will require a more complicated non-linear approach or transformation of raw data to be consistent with the large scale predicator variable. Therefore the fourth root transformation is applied to the raw data of the precipitation prior to model calibration.

4.3.4. Screening downscaled predicator variables

Screening is identifying the downscaled predicators which have high correlation with the actual climate variable. The method correlates each predictands (observed maximum and minimum temperature and rainfall) of Bahir Dar, Gonder and Debre Markos with the 26 NCEP downloaded predictors data. The strength of the individual predictors varies on a month by month basis. Therefore most appropriate combination of predictors has to be chosen by looking at the analysis output of the twelve months. The predicators which have significant correlation with each predictands and low correlation with the individual predictors should be selected for calibration.

4.3.5. Model calibration

The calibration of the statistical downscaling model is based on the multiple linear regressions between the screened predictors and the predictand. Twelve multiple linear regression equations for each months are produced automatically between the predictand and the screened predictors. For

model calibration the predictands of daily maximum temperature, minimum temperature and rainfall of the Bahir Dar, Debre Markos and Gonder stations are used. The calibration is done based on the 30 year actual data from 1961-1990 since this period is the baseline period for most climate change impact assessment.

In calibration of the SDSM the process type that identifies the presence of the intermediate process in the predictor-predictand relationship must be defined. In unconditional process there is the direct link between the predicator and the predictand (e.g., maximum and minimum temperature are directly depends on mean temperature at 2 metre height). In conditional process, there is an intermediate process between the predicators and the predictand (e.g., precipitation amount depends on the occurrence of wet day, which in turn depends on predicators of relative humidity).

In unconditional process the predictand and predictors are correlated with automatic calibration method without any intermediate process. But in conditional process like precipitation first the daily probability of non-zero precipitation (a wet day) for a given day is determined with autocorrelation before calibrating the precipitation amount. If the precipitation has occurred the daily precipitation amount is calculated based on the selected screened predictors. Therefore unconditional process is used for maximum and minimum temperature while the conditional process is used for precipitation.

After calibrating the model for each station with the actual data the next step is checking whether the model is able to reproduce the actual data or not. This is done with two methods the first is visual inspection of the modelled value and the actual value from 1961-1990 and the other is by checking the absolute model error and variance of the modelled and the observed data.

4.3.6. Scenario generation

For scenario generation H3A2a-1961-2099 and H3B2a_1961-2099 are downloaded from the same web site as the NCEP data (see section 4.3.1). The predictors are the same type as the NCEP predictors, the difference is that the NCEP predictors used for model calibration while the H3A2a and H3B2a are used for scenario generation. The regression weights produced during the calibration process were applied to the time series outputs of the GCM model. This is based on the assumption that the predictor-predictand relationships under the current condition remain valid under future climate conditions too.

Twenty ensembles of synthetic daily time series data were produced for two of the SERS scenarios for the above future time horizons in order to increase the performance of the model. The final product of the SDSM downscaling method was then found by averaging the twenty independent GCM ensembles. The differences between the 20 ensembles do not reflect the full range of internal variability because only the stochastic component differs in each run. The deterministic component (i.e. controlled by the atmospheric circulation and moisture variables) follows the same evolution in each run because only one source of predictor (i.e. either the NCEP or HadCM3) variables exists in each case (Goodess et al., 2003).

The scenario is generated for three future time horizons, from 2011-2039, 2040-2069 and 2070-2099 and for the baseline period 1961-1990 based on HadCM3A2a and HadCM3B2a.

Table 4-2: Scenario periods

Run	Start date	End date
1st run	1961	1990
2nd run	2010	2039
3ndrun	2040	2069
4th run	2070	2099

Once the scenario data is computed in the future period, the monthly change of temperature and rainfall from the baseline period for Bahir Dar, Gonder and Debre Markos stations is calculated. These changes in temperature and relative change in precipitation are superimposed up on 30 years climate records and used as input for hydrological model. The change observed in one month is added to every day record of the same months in the 30 years climate data. The 30 years climate data are the actual data of maximum temperature, minimum temperature and rainfall of the above three station used for statistical downscaling model.

4.4. Lake evaporation

Open water evaporation is important for computation of the net basin supply of Lake Tana water balance from 2010-2099 in future time period and from 1961-1990 in baseline period. Open water evaporation can be calculated with modified Penman method based on the observation of wind speed, sunshine hours and relative humidity and temperature. But only the 1997-2006 climate data are available from the meteorological office required for Penman evaporation estimation. Therefore to estimate the lake evaporation in the future time periods temperature index methods are required of which the Hargreaves is best known method. The Hargreaves method is as follows:

$$ET_O = 0.0023(T_{\max} - T_{\min})^{0.5}(T_{mean} + 17.8)R_a \qquad [4\text{-}4]$$

Where all temperatures are in ^oC and ET is evaporation in mm/day. The mean temperature is calculated as $0.5(T_{max}+T_{min})$. R_a is the extraterrestrial short wave radiation in mm/day.

In order to check the accuracy of the Hargreaves method for open water evaporation estimation other methods are considered and the result is compared with the Hargreaves method with 1997-200 climate data. The Penman combination equation of (Maidment, 1993) is one of the methods for estimation of lake evaporation provided that sufficient climatic data available. The Penman combination equation is as follow:

$$E_p = \frac{\Delta}{\Delta+\gamma} * (R_n + A_h) + \frac{\gamma}{\Delta+\gamma} * \frac{6.43 * (1 + 0.536 U_2) * D}{\lambda} \quad [4\text{-}5]$$

Where: E_p is potential evaporation from the lake surface (mm/day), R_n is the net radiation exchange for the free water surface (mm/day), A_h is energy advected to the water body (mm/day), U_2 is the wind speed measured at 2 m (m s^{-1}), D is the average vapour pressure deficit (kPa), λ is the latent heat of vaporization (MJ kg^{-1}), γ is psychometric constant (kPa $^oC^{-1}$) and Δ is the slop of saturation vapour pressure curve (kPa $^oC^{-1}$).

The mean annual lake evaporation based on this method is 2084.9 mm. It is over estimated compared to the lake evaporation obtained from different studies at the same area (see Table 5-9). The reason is that Maidment (1993) modify the original Penman equation for small open water bodies and it over estimate for large lake like Lake Tana.

The modified Penman combination of (Vallet-Coulomb et al., 2001) is also tested for Lake Tana evaporation estimation. The equation is described below:

$$E = R_n \frac{\Delta}{\Delta+\gamma} + Ea \frac{\gamma}{\Delta+\gamma} \quad [4\text{-}6]$$

Where E is the daily evaporation rate (mm day^{-1}), the net radiation R_n expressed as equivalent evaporation rate (mm day^{-1}), Δ is the slope of the saturated vapour pressure curve at the air temperature, γ is the psychometric constant , and Ea is the drying power of the air given as a daily rate (mm day^{-1}) by:

$$Ea = 0.26(1 - 0.54 U_2)(e_w - e) \quad [4\text{-}7]$$

Where U_2 is the wind speed measurement at two metre high (m s^{-1}), $(e_w - e)$ is the saturation deficit, difference between the saturated (e_w) and the actual (e) vapour pressure (kPa).

Both methods are the same except that the weight of wind function for estimation of the evaporation with (Maidman, 1993) is larger than the (Vallet-Coulomb et al., 2001). The mean annual lake evaporation based on this method is 1729 mm. The method estimates of the Lake Tana evaporation compared to the above method. The mean yearly lake evaporation with Hargreaves method is 1708 mm. Then it is possible to conclude that the Hargreaves method also gives good result for Lake Tana evaporation. (Gieske et al., 2008) also indicates that the Hargreaves method which is based on the temperature measurement of Gonder and Bahir Dar station provide good approximate values for open water evaporation of Lake Tana.

The lake energy balance method is one the best method for inferring lake evaporation (Vallet-Coulmb et al, 2001). The method does not require wind speed data. The general expression for energy balance is:

$$Rn = H + \lambda E + \Delta S \quad [4\text{-}8]$$

Where Rn is the net radiation, λE is the latent heat flux (λ the latent heat of vaporization in J kg^{-1}, and E the evaporation rate in kg s^{-1} m^{-2}), H the sensible heat flux, and ΔS the change of energy storage in the lake (all terms expressed in W m^{-2}). The net radiation (Rn) results from the balance short wave and long wave radiation:

$$Rn = R_s(1-\alpha) - R_1 \quad [4\text{-}9]$$

Where Rs the net short is wave radiation, R_1 is net long wave radiation (W m^{-2}) and α is the surface albedo. In the absence of direct radiation measurement, daily short wave radiation can be calculated with the Angstrom formula, which relates solar radiation to the extraterrestrial radiation and relative sunshine duration. The Angstrom formula is as follow:

$$R_s = \left(a_s + b_s \frac{n}{N}\right) R_a \quad [4\text{-}10]$$

Where R_a is the solar radiation at the top of the atmosphere (Wm^{-2}), n is the actual sunshine hours (hours), N is the maximum possible sunshine hours (hours), a_s and b_s are the regression constants.

Where no actual solar radiation data are available and no calibration has been carried out to improve a_s and b_s parameters, the values a_s = 0.25 and b_s = 0.50 are usually recommended.

Lake Tana is the shallow lake and there is weak seasonal variation in temperature therefore change in storage (ΔS) coulde be neglected. Therefore the equation 4-8 can be can be simplified by introducing bown ratio (β) to the general energy balance equation.

$$E = \frac{R_n - G}{\lambda(\beta + 1)} \quad [4\text{-}11]$$

$$\beta = \frac{H}{\lambda E} = \gamma \frac{[T_2 - T_1 + \Gamma(z_2 - z_1)]}{e_2 - e_1} \quad [4\text{-}12]$$

Where T_1[K] and e_1[mbar] are air temperature and vapour pressure at height z_1 [m] and T_2[K] and e_2[mbar] are the temperature and vapour pressure at height z_2[m], γ is the psychometric constant [mbar K^{-1}] and Γ is adiabatic lapse rate, generally taken as 0.0065Km^{-1}. Γ can be neglected if the distance between the Bown ratio measurement heights is less than 2m. So the final equation for the bown ration from field measurement is:

$$\beta = \frac{H}{\lambda E} = \gamma \frac{[T_2 - T_1]}{e_2 - e_1} \quad [4\text{-}13]$$

Since I do not have sufficient water surface temperature data of the Lake Tana it is difficult to calculate the evaporation with the energy balance method. But the annual Lake evaporation estimated

by Alebachw (2009) by energy balance method considering different albedo for each month is 1818.08mm/ year. This result also comparable to the lake evaporation estimated by the Hargreaves method earlier.

Therefore the evaporation from 2010-2039, 2040-2069 and 2070-2099 is calculated using Hargreaves by the downscaled maximum and minimum temperature for Bahir Dar and Gonder station while the 1961-1990 evaporation is calculated by the observed data. The weight of each station for lake evaporation is computed by inverse distance weighting method. Bahir Dar has a weight of 0.60 and Gonder has a weight of 0.4 for the estimation lake evaporation. Then the lake evaporation is calculated by multiplying the evaporation of each station with the weight calculated by inverse distance interpolation method.

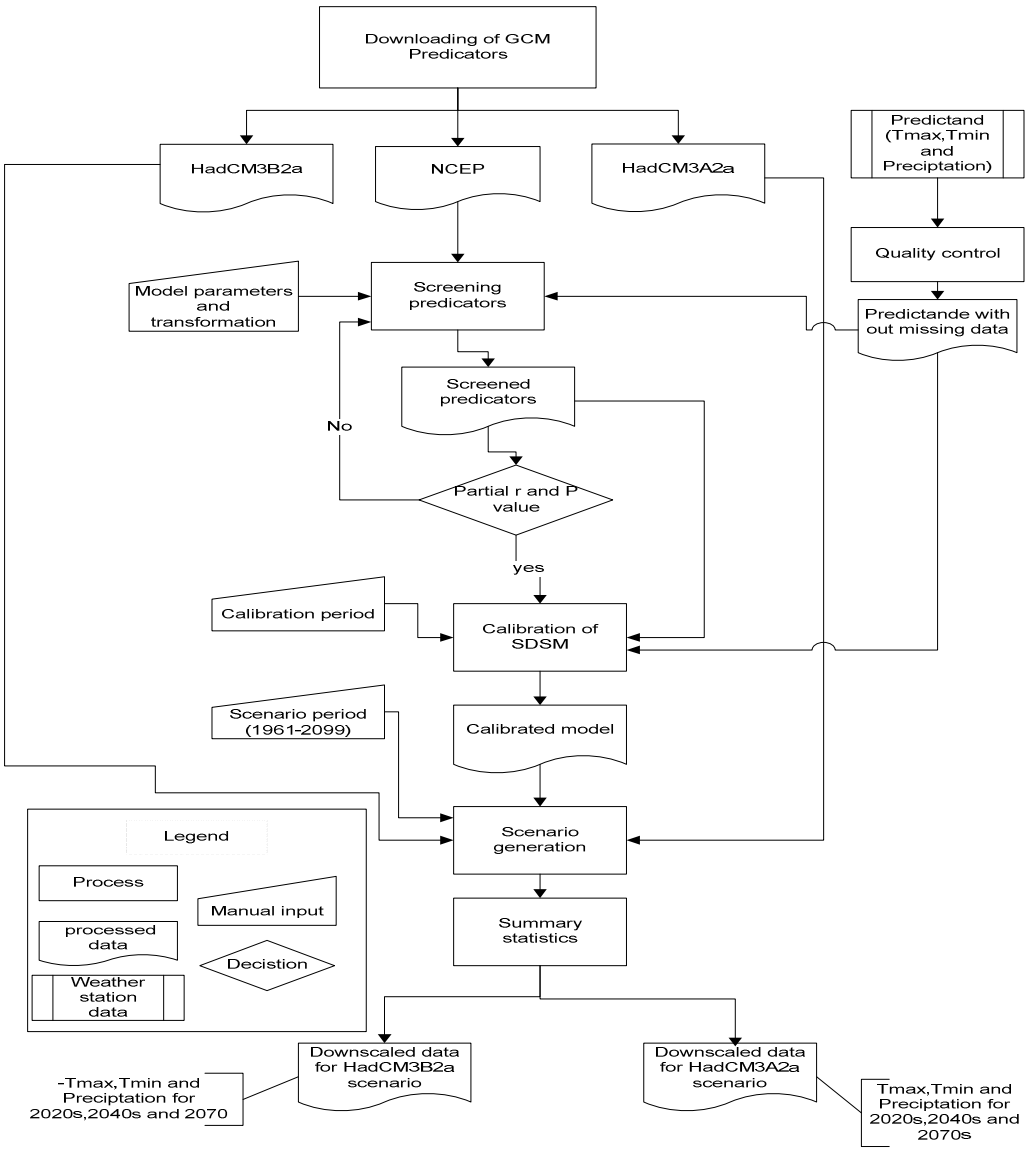

Figure 4-2: Methodology of statistical downscaling model

4.5. HBV model

4.5.1. HBV model structure

Among different hydrological models HBV-96 model is selected since it is applicable for climate change impact assessment. The model is semi distributed conceptual hydrological model which simulates runoff based on daily precipitation, daily mean temperature and a long term monthly potential evapotranspiration.

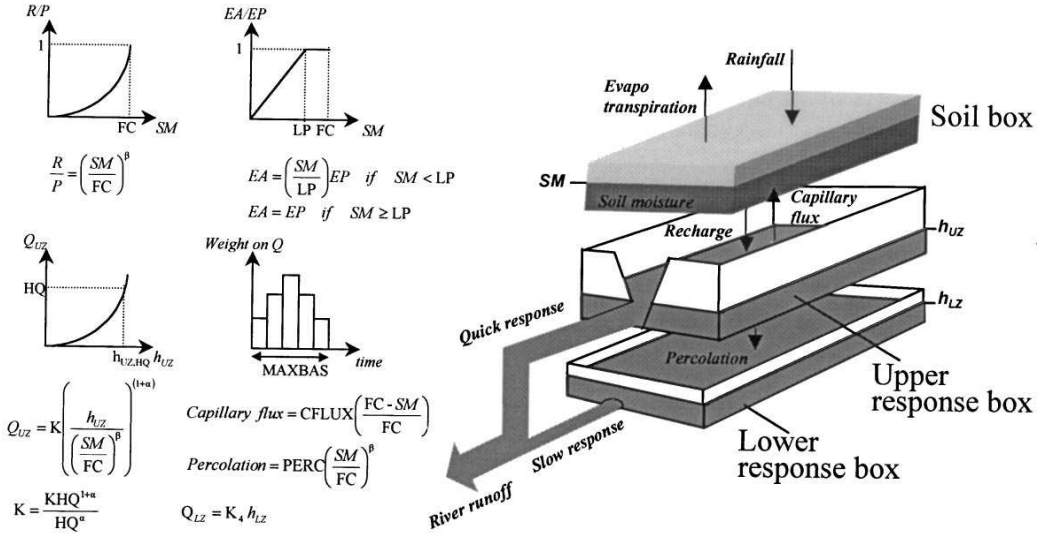

$\frac{R}{P} = \left(\frac{SM}{FC}\right)^{\beta}$

$EA = \left(\frac{SM}{LP}\right) EP \quad if \quad SM < LP$

$EA = EP \quad if \quad SM \geq LP$

$Q_{UZ} = K\left(\frac{h_{UZ}}{\left(\frac{SM}{FC}\right)^{\beta}}\right)^{(1+\alpha)}$

$K = \frac{KHQ^{1+\alpha}}{HQ^{\alpha}}$

$Capillary\ flux = CFLUX\left(\frac{FC - SM}{FC}\right)$

$Percolation = PERC\left(\frac{SM}{FC}\right)^{\beta}$

$Q_{LZ} = K_4 h_{LZ}$

VARIABLES

R	Recharge
P	Rainfall
SM	Soil moisture storage
EP	Potential evapotranspiration
EA	Actual evapotranspiration
h_{UZ}	Storage in upper response box
h_{LZ}	Storage in lower response box
Q_{UZ}	Runoff from upper response box
Q_{LZ}	Runoff from lower response box
Q	River runoff

PARAMETERS

FC	Maximum soil moisture storage
LP	Limit for potential evapotranspiration
β	Soil routine parameter
KHQ	Recession at HQ
HQ	Half of mean annual flood
α,K_4	Recession parameters
$h_{UZ,HQ}$	h_{UZ} level at HQ
PERC	Percolation rate
CFLUX	Capillary flux rate
MAXBAS	Routing parameter

Figure 4-3: Schematic representation of HBV-96 model (Seibert, 2002)

The Lake Tana basin is divided into 10 major subbasins and each subbasin is further divided in different elevation zones in order to consider the effect of elevation on temperature and rainfall estimation. The HBV model have precipitation and snow routine, the soil moisture accounting routine, the runoff generation routines and the transformation function.

Actual evapotranspiration (EA) was computed as a function of soil moisture condition and potential evapotranspiration (EP). When the soil moisture exceeded the storage threshold (LP), water would evaporate at the potential rate. At the lower soil moisture value a linear relationship between the ratio EP/EA and the soil moisture was used. The general storage variable (S) was formed by soil moisture storage (SM) and the storage in the upper and lower response boxes respectively, (h_{UZ} and h_{LZ}). Recharge to ground water was calculated through a non linear relationship between the ratio R/P and

the soil moisture. The runoff generation routine of the catchment was described by the outflow from the upper non linear reservoir (Q_{UZ}) while the base flow (Q_{LZ}) was governed from the lower response box which is filled by the percolation from the upper response box. Runoff from the catchment (Q) was given by the sum of the outflow from the two response boxes.

4.5.2. HBV model inputs

The inputs for HBV model consists of daily rainfall, temperature, estimates of potential evapotranspiration and catchment characteristics of the area.

I. Areal rainfall

12 stations in and around the Lake Tana basin (see Figure 2-3) are selected for the computation of the areal rainfall for the each subbasins. The areal rainfall is computed by multiplying rainfall in each station by a weight which is computed by inverse distance weighting. This method was chosen because it takes in to account the rainfall distribution of every rainfall station. The rainfall stations nearer to the interpolated point have the greater weight than the stations farther apart. The inverse distance weighting method is given byequation [4-14].

$$\overline{P} = \frac{\sum_{i=1}^{n} \frac{1}{d_i^{\,m}} * P_s}{\sum_{i=1}^{n} \frac{1}{d_i^{\,m}}} \qquad [4\text{-}14]$$

Where:

$\overline{p}$ = estimated areal average rainfall

P_s= rainfall at the station

d_i= distance of the station from the region centre

m= distance weight

n= number of meteorological stations.

II. Catchment data

The HBV model is a semi distributed model. Therefore a digital elevation map of the area was prepared from SRTM with the resolution of 90 m for the delineation of the lake catchment. The catchment area and the drainage network of the catchment are extracted with the DEM hydro processing tool in the Integrated Land and Water Information System (ILWIS) software. The catchment area is divided in to 10 major subcatchments and it is further divided in to different elevation zones of 100 metre interval. Among the subcatchments Gilgel Abbay, Ribb, Gumra, Garno, Gumero, Megech and Gelda are partly gauged while Gabi Kura, Derma and Tana West are unguaged catchments. The unguaged catchments contribute 40 % of the total area of the catchment and the rest is covered by gauged catchments. The Gilgel Abbay catchment includes the main Gilgel Abbay and a number of tributaries such as Koga and Kelti. The Koga confluences with the Gilgel Abbay downstream of Merawi and the Kelti confluences further downstream.

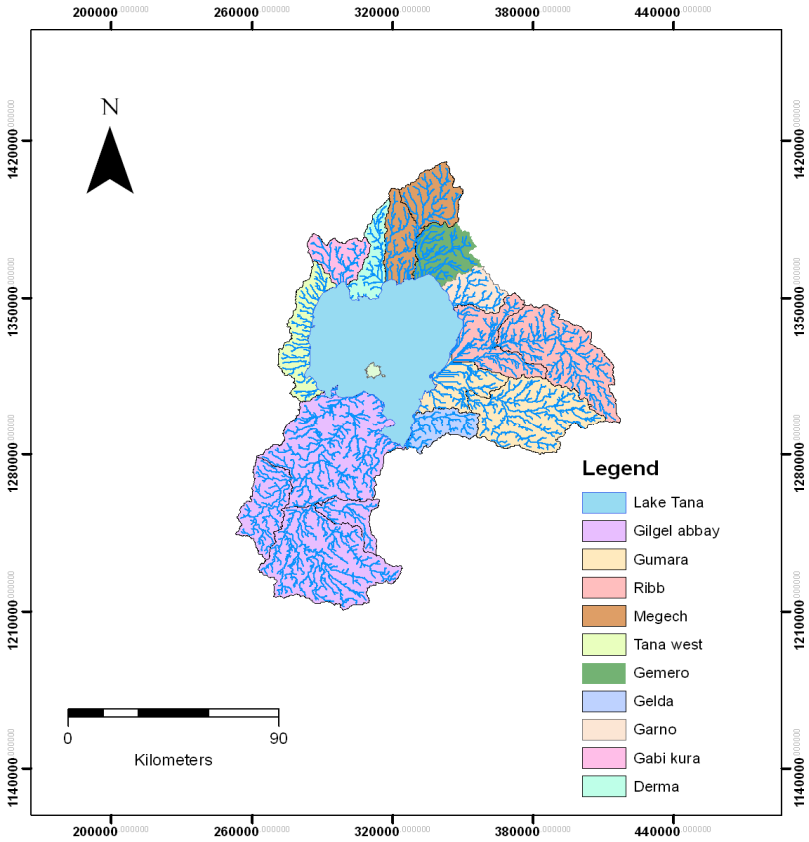

Projection: UTM, Datum: Adinidan, Ellipsoid: Clarke 1880

Figure 4-4: Major subcatchments of Lake Tana basin

Table 4-3: Catchment area of Lake Tana basin

Sub catchment	Gauging location	Gauged area (km^2)	Unguaged area (km^2)	Total area of the catchment (km^2)
Gilgel Abbay	Near Merawi	2562.7	1991	4553.7
Gumara	Near Bahirdar	1280.6	517.3	1797.9
Ribb	Near Addis Zemen	1301.8	711.5	2013.3
Megech	Near Azezo	513.3	462.3	975.6
Garno	Near Enfranze	97.4	256.5	353.9
Gemero	Near Maksegnit	165.1	389.9	555
Gelda	Near Ambesame	27	356.1	383.1
Tana West	Unguaged		610.6	610.6
Gabi Kura	Unguaged		382.5	382.5
Derma	Unguaged		376	376

III. Evapotranspiration

The model uses monthly potential evapotranspiration as input. Therefore the data of Bahir Dar, Gonder, Debre Tabour and Dangila are selected for estimation of evapotranspiration due to the availability of sufficient climatic data. The FAO Penman-Monteith method is applied for estimation of reference evapotranspiration since sufficient climate data are available from the above stations. The weighted evapotranspiration in each basin is estimated by multiplying the evapotranspiration with the weight of the station computed by inverse distance weighting.

$$ET_O = \frac{0.408\Delta(R_n - G) + \gamma \frac{900}{T+273} u_2 (e_s - e_a)}{\Delta + \gamma(1 + 0.34u_2)} \quad [4\text{-}15]$$

Where:

ET_O = reference evapotranspiration [mm day^{-1}]

R_n = net radiation [MJ m^{-2} day^{-1}]

G = soil heat flux [MJ m^{-2} day^{-1}]

T = mean air temperature [^{o}C]

u_2 = wind speed at 2 metre height [ms^{-1}]

e_a = actual vapour pressure [kpa]

e_s = saturation vapour pressure [kpa]

$e_s - e_a$ = saturation vapour pressure deficit [kpa]

Δ = slope vapour pressure curve [kpa^{o}C^{-1}]

γ = psychometric constant [kpa^{o}C^{-1}]

Table 4-4: Monthly reference evapotranspiration (mm/month)

Moths	Bahir Dar	Gonder	Debre Tabour	Dangila
January	101.3	114.0	106.7	103.5
February	113.0	123.2	114.2	113.4
March	136.2	144.0	130.0	133.8
April	140.5	147.0	121.0	137.3
May	136.1	142.6	119.9	131.5
June	112.5	107.8	88.9	94.2
July	92.9	85.7	79.2	84.9
August	92.3	87.7	84.5	84.3
September	102.9	105.5	89.5	94.3
October	114.2	116.6	96.4	92.6
November	105.7	105.0	94.9	93.0
December	102.4	105.4	104.4	96.3

IV. Land cover data

The land cover is further reclassified for each elevation zone according to the type required by the HBV model. The HBV model requires forest, non forest, glaciers and lake. But in this study only forest and non forest are considered because the glacier and the water bodies are almost negligible in the elevation zones of the subcatchments. Based on the land cover data and the Penman-Monteith reference evaporation, the HBV model calculates the potential evaporation of the catchment. The actual evaporation is then calculated based on the potential evapotranspiration, the parameter called limit of potential evaporation and the moisture content of the soil.

4.5.3. Objective function

The goodness of fit of the model to the observed discharge is estimated by two methods, relative volume error and Nash-Sutcliffe coefficient which are represented by equation [4.10] and [4.11] respectively.

The relative volume error of 0 indicates as there is no change between the observed and simulated discharge. But it is difficult to conclude the performance of the model by estimating relative volume error only because there may be a small value of relative volume error with wrong distribution of the observed and simulated discharge. Therefore another performance indicator is essential together with the relative volume error in order to accurately determine the model performance. The relative error less than +5 % or -5% indicates that the model performs well and a relative volume error between +5 % to +10 % and -5 % to -10 % indicates the model is within reasonable performance.

$$RVE = \frac{\sum_{i=1}^{n} Q_{sim} - \sum_{i}^{n} Q_{obs}}{\sum_{i}^{n} Q_{obs}} \times 100 \qquad [4\text{-}16]$$

Where: RVE = relative volume error, Q_{sim} = simulated flow and Q_{obs} = observed flow

Nash-Sutcliffe coefficient is the other performance indicator used to assess the predictive power of the hydrological model.

$$R^2 = \frac{\sum\left(Q_{obs} - \overline{Q_{obs}}\right)^2 - \sum\left(Q_{sim} - Q_{obs}\right)^2}{\sum\left(Q_{obs} - \overline{Q_{obs}}\right)^2} \qquad [4\text{-}17]$$

Where: R^2= Nash-Sutcliffe coefficient Q_{obs} = the observed discharge, $\overline{Q_{obs}}$ = mean of observed discharge and Q_{sim} is the simulated discharge.

The perfect model would result in an R^2 equal to 1. However, normally R^2 ends up somewhere between 0.8 and 0.95, this is only the case when good quality input data is available (SMHI, 2006).

4.5.4. Validation

For this study the calibrated parameters of gauged catchment are taken from Abeyou (2008). But the hydrological model should be validated against independent data set which is not used during calibration period to test the model simulation capability. For validation of the model 12 rainfall stations and 4 evaporation and temperature stations data are used. The model is validated with the daily discharge data (2004-2007) of Gilgel abbay, Koga, Megech, Gumara and Rib.

Table 4-5: Calibrated model parameters of gauged catchment (Abeyou, 2008)

Parameters	Ribb	Gumara	Gilgel Abbay	Koga	Megech	Kelti
Alfa	0.5	0.5	1	0.5	0.9	1
Beta	1.8	1	2	1	1	1
Fc	150	100	200	1000	800	1100
Hq	2.64	6.76	7.33	5.96	4.57	4.55
K4	0.006	0.02	0.02	0.007	0.01	0.002
KHQ	0.62	1	0.95	0.42	0.38	0.24
LP	0.62	1	0.95	0.42	0.38	0.24
PERC	0.26	0.65	0.52	1	0.1	0.4

4.5.5. Parameterization of unguaged catchment

Several methods are available to determine the model parameters of unguaged catchments. These include the application of the spatial proximity, the area ratio and the regional calibration method. The regional calibration method developed by Abeyou (2008) for Lake Tana unguaged catchments is adapted for this study since the method is most reliable and widely used for estimation of unguaged catchment model parameters. The method correlates the calibrated model parameters and the catchment characteristic of the gauged catchments. Using those catchment characteristics which are highly correlated with the model parameters of gauged catchments, the multiple linear regression models are established. Therefore the model parameters of the unguaged catchments are determined using the established linear regression model based on catchment characteristics. The catchments characteristics of unguaged catchments and the regression models are available in the Appendix C and D.

Table 4-6: Model parameters of Unguaged catchments (after Abeyou, 2008)

catchment	Alfa	Beta	FC	Hq	K4	KHQ	LP	PERC
Unguaged Gilgel Abbay	1.29	2.60	432	8.21	0.013	0.076	1.00	0.550
Unguaged Megech	1.00	1.27	1408	4.98	0.004	0.103	0.32	0.234
Unguaged Ribb	0.74	1.36	1101	3.80	0.025	0.093	0.27	0.086
Unguaged Gumara	1.00	1.28	1401	4.32	0.004	0.126	0.29	0.414
Gumero	0.83	1.18	1163	2.03	0.018	0.102	0.20	0.157
Garno	0.86	0.89	1143	2.98	0.07	0.100	0.16	0.06
Gelda	0.9	1.00	800	3.00	0.01	0.100	0.38	0.100
Derma	0.98	1.10	1381	2.20	0.02	0.103	0.13	0.120
Gabikura	1.11	1.26	1572	3.02	0.003	0.106	0.166	0.16
Tana West	0.63	1.14	977	3.49	0.037	0.114	0.317	0.344

4.6. Net basin supply of Lake Tana water balance

The net basin supply (N) is the major part of the Lake Tana water balance and it is estimated by the lake precipitation, lake evaporation and the inflow to the lake (see equation 4.12).

$$N = P - E + \frac{Q_{in}}{A_o} \qquad [4\text{-}18]$$

Where:

P = precipitation of the Lake Tana (mm/day)

E = evaporation of the Lake Tana (mm/day)

Q_{in} = the inflow to Lake Tana (m^3/s)

A_o = surface area of the lake (km^2)

No lake outflow data is used for the computation of the net basin supply because it is estimated only by the lake precipitation; lake evaporation and the inflow to the lake. The unit of inflow component should be consistent with the precipitation and the evaporation. Therefore the inflow to the lake is multiplied by the factor 86.4 to convert m^3/s to mm/day.

The net basin supply is calculated for the baseline period (1961-1990) and three future periods each covering non overlapping 30 years. These periods are 2010-2039, 2040-2069 and 2070-2099. The calibrated and validated HBV model is used for forecasting the inflow to the lake. The inputs of the model are the downscaled maximum temperature, minimum temperature and precipitation. The evaporation used for the model is also calculated from the downscaled temperature. The total inflow to the lake is the sum of the inflows from each subcatchment. The inflow from each subcatchment is computed based on the Bahir Dar, Gonder and Debre Markos precipitation, temperature and

evapotranspiration. The weight of each station to the catchment is calculated by the inverse distance weighting method. The lake evaporation and lake precipitation is calculated by the Bahir Dar and Gonder climatic data as well.

It is very essential to estimate the lake surface area for computation of the net inflow to the lake. To estimate the lake area it is necessary to analyse the changes with respect to volume of the lake and elevation of the lake. For this purpose the bathymetric survey done by Kaba Ayana (2007) is considered to get the relation of the lake surface area and lake elevation with the volume of the lake. The Bathymetry done by Kaba Ayana (2007) is further developed by Abeyou (2008) by increasing additional data set in the lake not covered by Kaba Ayana (2007) to increase the accuracy of the interpolation. The interpolation result of bathymetric survey is as follow:

Polynomial fitted bathymetry by Abeyou (2008)

$$E = 1.21*10^{-13}V^3 - 1.02*10^{-8}V^2 + 6.2*10^{-4}V + 1774.63 \quad [4\text{-}19]$$

$$A = 7.93*10^{-11}V^3 - 5.81*10^{-6}V^2 + 1.65*10^{-1}V + 1147.51 \quad [4\text{-}20]$$

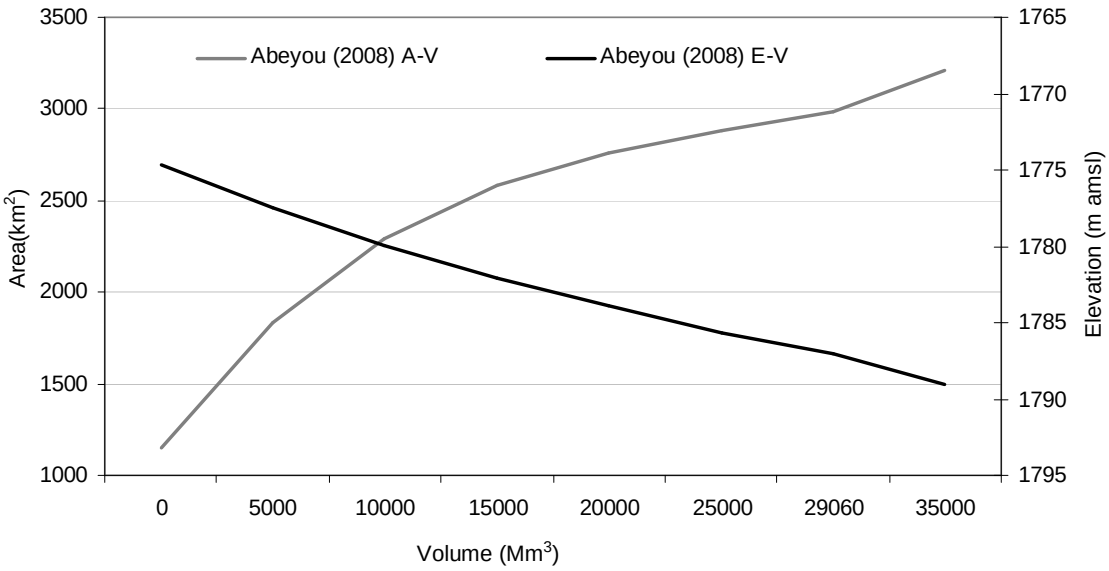

Figure 4-5: Elevation-volume and area-volume relation of Lake Tana

Based on the Elevation-volume and area-volume relationship the elevation-area relation of the Lake Tana is derived which is very essential to know the relation of the lake area with change in depth.

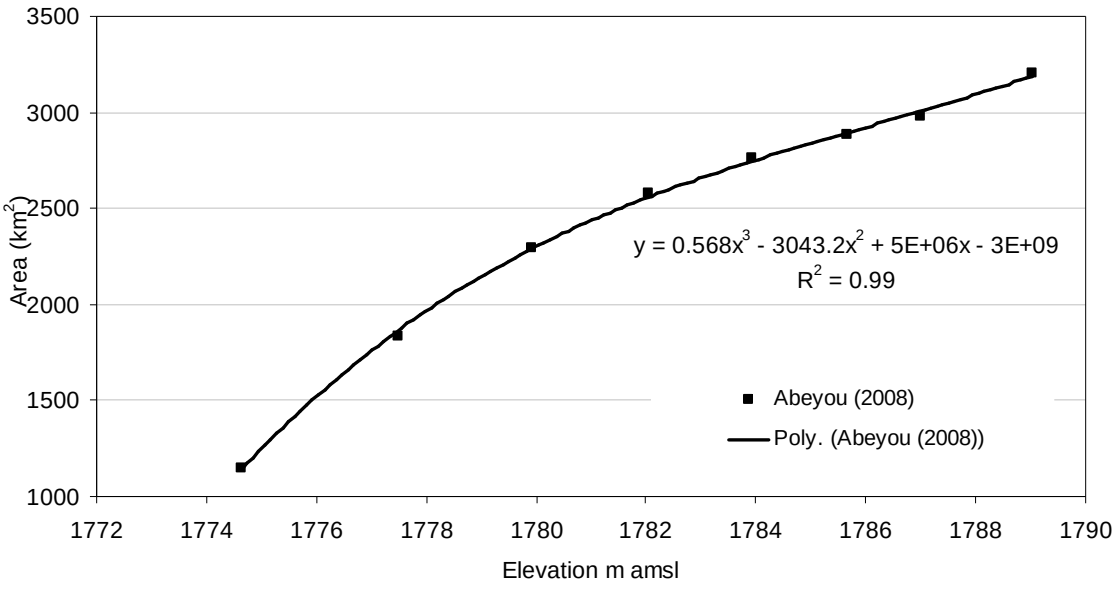

Figure 4-6: Elevation-area ratio of Lake Tana

The elevation-area relation indicates that the surface area of the lake in general is increased by 145 km^2 with 1 m increase in depth which is negligible compared to the total area of the lake. Therefore it is reasonable to take a constant area of 3060 km^2 for the computation of the net basin supply of Lake Tana water balance. (Kebede et al., 2006) also consider constant surface area of Lake Tana for the computation of the net basin supply since the change of lake surface area with change in depth is not significant for the net basin supply computation.

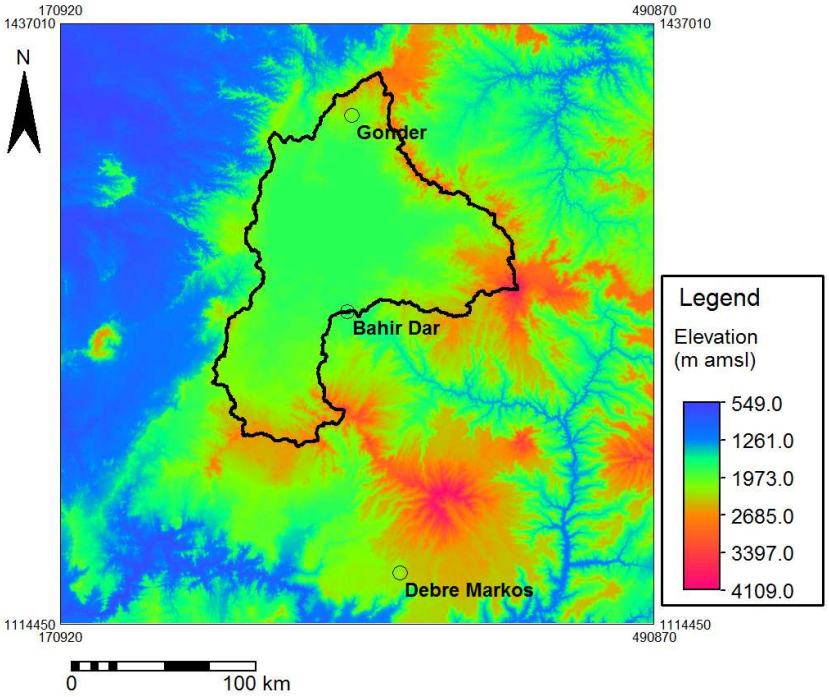

Figure 4-7: Station used for downscaling of the climate variables

Table 4-7: Weight of precipitation, temperature and evaporation stations using inverse distance weighting for net basin supply computation

Catchments	Bahir Dar	Gonder	Debre Markos	Catchments	Bahir Dar	Gonder
Gilgel Abbay	0.22	0.78		Unguaged Ribb	0.53	0.47
Koga	0.9		0.1	Unguaged Megech	0.03	0.97
Kelti	0.82		0.18	Gelda	0.96	0.04
Gumara	0.76	0.24		Garno	0.25	0.75
Ribb	0.59	0.41		Gemero	0.06	0.94
Megech	0.02	0.98		Tana West	0.53	0.47
Unguaged Gilgel Abbay	0.93	0.07		Gabi Kura	0.15	0.85
Unguaged Gumara	0.82	0.18		Derma	0.1	0.9

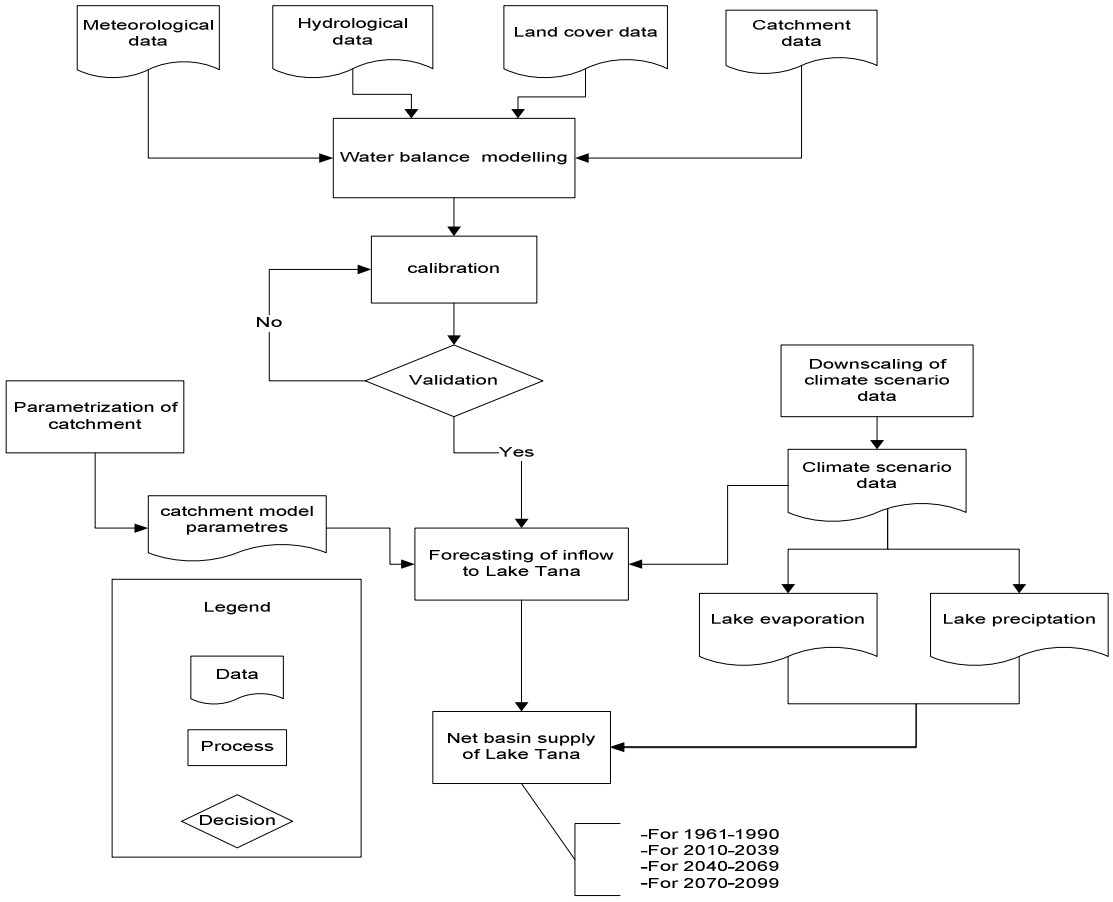

Figure 4-8: Methodology on the net basin supply computation

5. Result and discussion

5.1. Statistical analysis of observed data

The observed maximum temperature, minimum temperature and rainfall of Bahir Dar, Gonder and Debre Markos stations are analysed with the significance test analysis to know the trends. This trend analysis is very essential to identify the impact of climate change on the observed data and to compare this result with the future climate variables. For the trend analysis the observed daily climate variables of 47 years (1961-2007) of three stations are applied. Besides the above climate variables the mean temperature which is the average of maximum and minimum temperature are also considered in this significance test analysis. The analysis result of Bahir Dar station is described below and the others are presented in Appendix F.

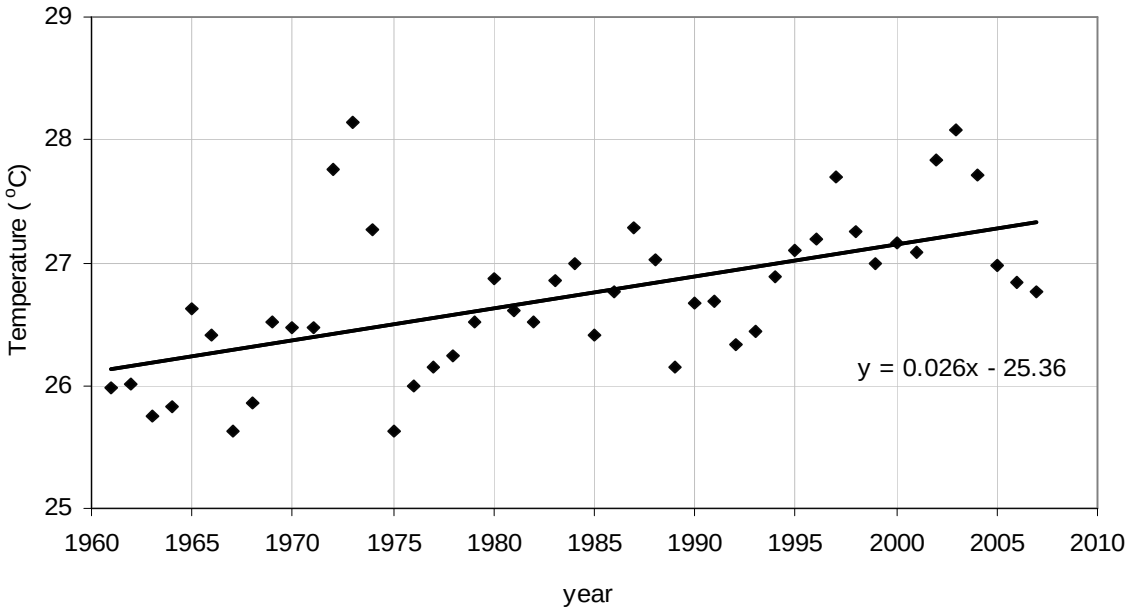

Figure 5-1: Bahir Dar yearly average of daily maximum temperature (1961-2007)

The highest yearly average daily maximum temperature of 28.14 ^{o}C is observed in 1973. This year was a very dry year for Lake Tana area with only little rainfall. The lowest yearly maximum temperature of 25.62 ^{o}C is observed in 1967 and the average maximum temperature is 26.73 ^{o}C.

Based on the significance test analysis of the yearly average maximum temperature from 1961-2007, $\sigma^2 = 0.39$, var (b) = $4.45*10^{-5}$ and t = 3.93, then from t-distribution table the confidence interval for increasing temperature is 99 %. Therefore the maximum temperature of Bahir Dar station has increased with 0.026 ^{o}C per year from 1961-2007 with 99 % confidence interval.

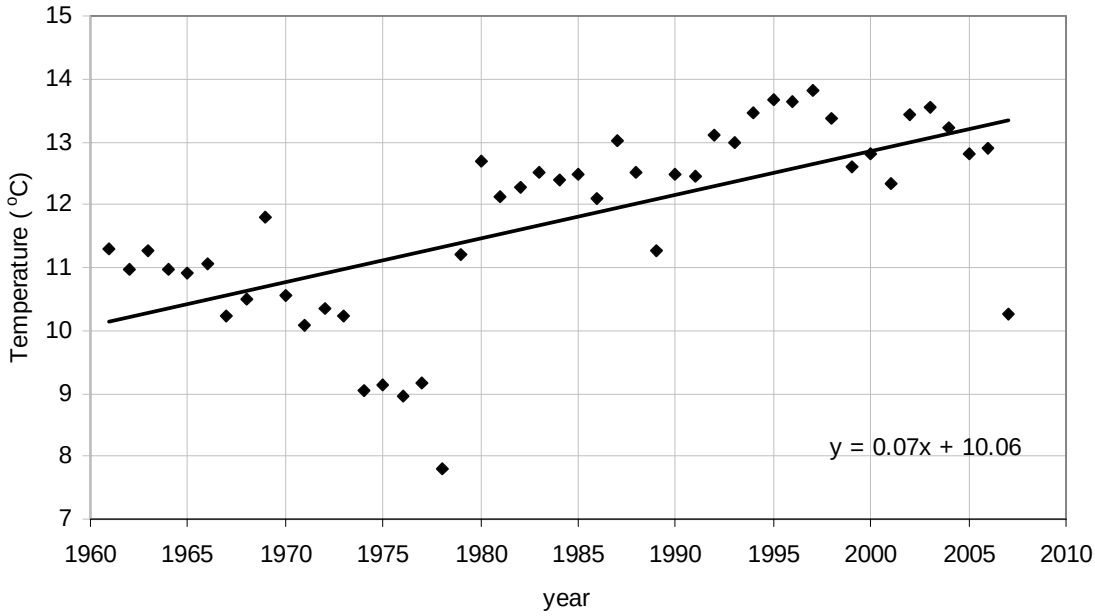

Figure 5-2: Bahir Dar yearly average of daily minimum temperature (1961-2007)

The highest yearly minimum temperature of 13.81 °C is observed in 1997 while the lowest minimum temperature of 7.81°C is observed in 1978. The average minimum temperature from 1961-2007 is 11.74 °C.

Based on the significance analysis of yearly minimum temperature $\sigma^2 = 1.32$, var (b) = 0.0002 and t = 5.66. Then from t-distribution table the confidence level for increasing the minimum temperature is 99 %. Therefore the minimum temperature of Bahir Dar is increasing with 0.07 °C every year from 1961-2007.

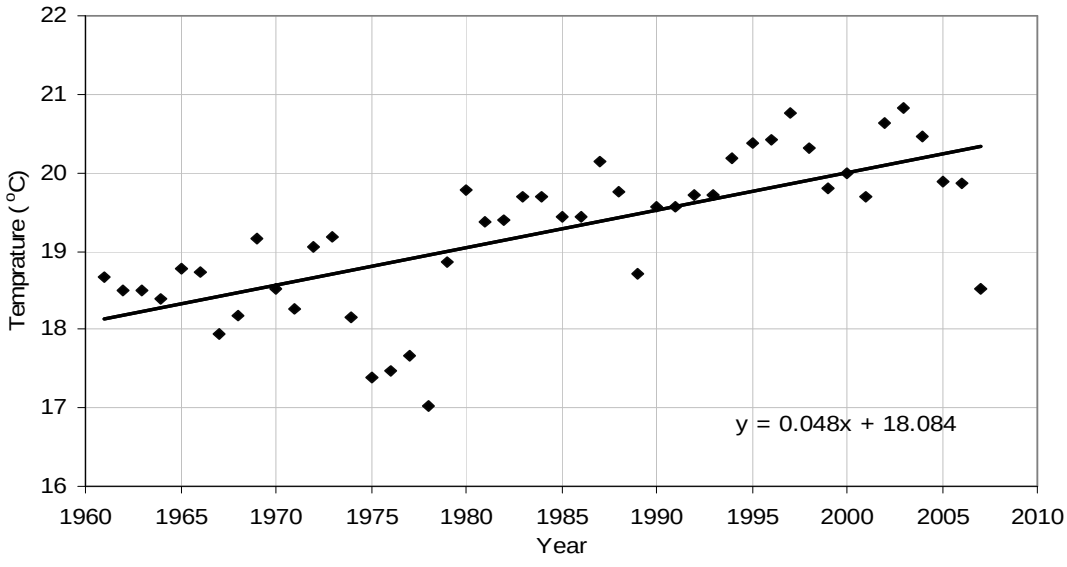

Figure 5-3: Bahir Dar yearly average of daily mean temperature (1961-2007)

The highest yearly mean temperature of 20.81 ^{o}C is observed in 2003 while the lowest mean temperature of 17.02 ^{o}C is observed in 1978. The average mean temperature from 1961-2007 is 19.23 ^{o}C.

Based on the significance test analysis of yearly mean temperature $\sigma^2 = 0.87$, var (b) = 0.0001 and t = 4.79.Then from t-distribution table the confidence level for increasing mean temperature is 99 %. Therefore the mean temperature of Bahir Dar is also increasing with 0.05 ^{o}C per year.

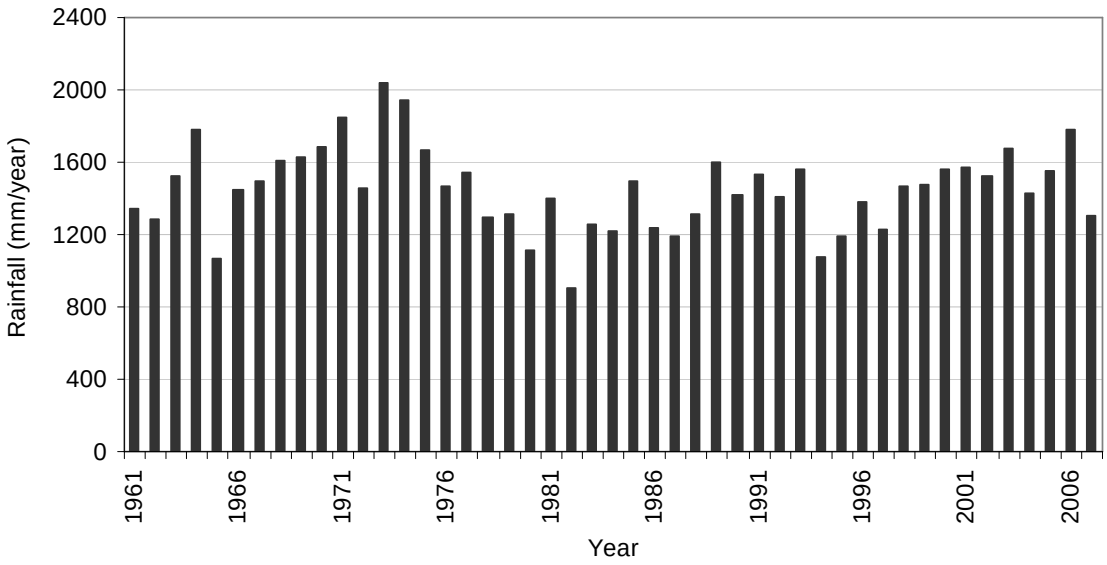

Figure 5-4: Bahir Dar annual rainfall (1961-2007)

The significant analysis indicates that the annual precipitation does not show consistent increase or decrease in the analysis period (1961-2007). But there is a decrease of rainfall is observed from the mid 1970s to the mid 1980s and after that the annual rainfall shows an increasing trend up to the 1990. The lowest yearly rainfall of 901 mm is recorded in1982 and the maximum yearly rainfall of 2036 mm is observed in 1973. (Kebede et al., 2006) also indicate that in Lake Tana basin regional consistent variation in hydrologic parameters is observed between the years 1975 and 1986. This period shows a decline in annual precipitation in the basin.

The evaporation of Bahir Dar from 1961-2007 is also analysed based on the maximum temperature and minimum temperature the Bahir Dar station. As it is indicated in Figure 5-5 the maximum yearly evaporation is 1864 mm in 1973 while the lowest yearly evaporation is 1633mm in 1992. The mean evaporation in the analysis period is 1708 mm/year.

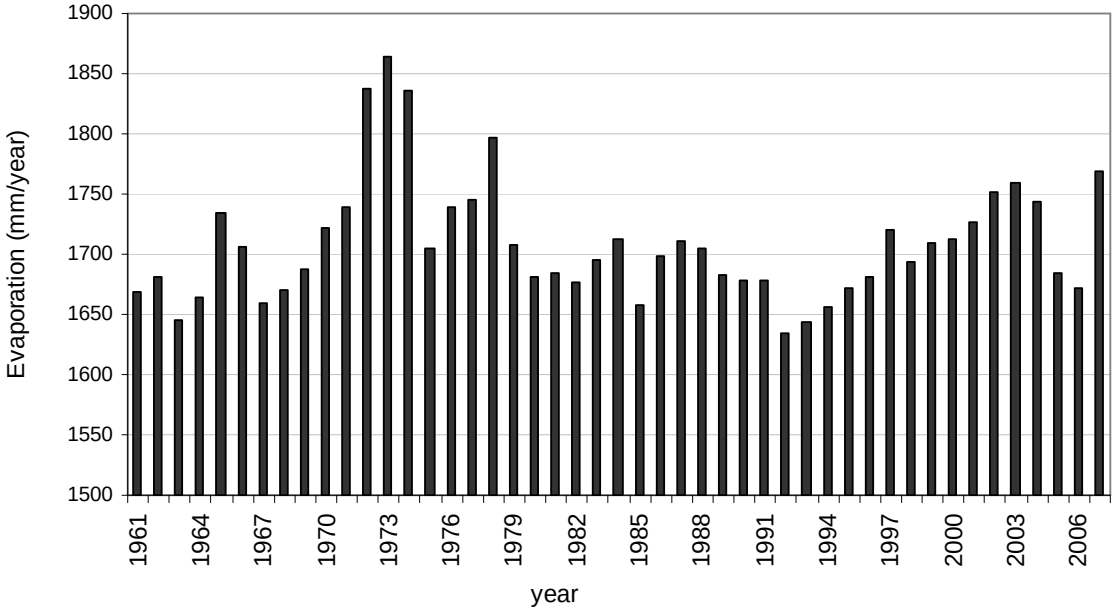

Figure 5-5: Bahir Dar yearly evaporation

Table 5-1: Yearly increase of temperature using significance test from 1961-2007

Station name	Maximum Temperature (^{o}C)	Minimum Temperature (^{o}C)	Mean Temperature (^{o}C)
Bahir Dar	0.07	0.026	0.05
Gonder	0.03	0.026	0.03
Debre Markos	0.05	0.016	0.04

The significance level of maximum, minimum and mean temperature for all the station is greater than 90 %. Therefore it is confident that the maximum and the minimum temperature of the present are higher than the past periods.

5.2. Climate model output

5.2.1. Selected predictor variables

The selected predictor variables should be physically and conceptually sensible, strongly and consistently correlated with the predictand and realistically modelled by GCMs. For precipitation downscaling it is also recommended that the selected predictors contain variables describing atmospheric circulation, thickness and stability and moisture content (Dawson and Wilbey, 2007). Considering the above criteria daily data of surface divergent (ncepp_zhaf), 500hpa geo potential height (ncepp500af) and mean temperature at 2 meter height (nceptemp) are selected for downscaling of maximum and minimum temperature for all station used in the SDSM. For precipitation the Surface divergent (ncepp_zhaf) and relative humidity at 500hpa (ncepr_500af) are selected.

Large scale convection over the warmer tropical ocean provides an important portion of the driving energy for the general circulation of the atmosphere. The analysis of regional associations between ocean temperature, surface wind divergence and convection produces two important phenomena. The convergence zone is promoted by warm (> 28 ^{o}C) equatorial sea surface temperature (SST) while the divergence zone is a result of subdued convection caused by colder SST (< 24 ^{o}C). The intertropical convergent zone (ITCZ), which forms the zonal belt a few degrees to the north and south of the equator, is best example of atmospheric convergences which drive the Hadley circulation. The position of these zones (convergent and divergent) migrates seasonally and they exhibit inter annual variation, which have a major effect on local precipitations (Luis and Pandey, 2005).

The predictor variables selected for each downscaling process conducted in this study are summarized in Table 5-2, Table 5-3 and Table 5-4.

Table 5-2: List of predictor variables that give good correlation with Bahir Dar climate data

Maximum temperature			Minimum temperature			Rainfall		
predictors	Partial r	P value	predictors	Partial r	P value	predictors	Partial r	P value
ncepp_zhaf	-0.367	0.00	ncepp_zhaf	0.542	0.00	ncepp_zhaf	0.251	0.00
ncepp500af	0.305	0.00	ncepp_500af	0.243	0.00	ncepr_500af	0.122	0.00
nceptemp	0.56	0.00	ncepp_temp	0.195	0.00			

Table 5-3: List of predictor variables that give good correlation with Gonder climate data

Maximum temperature			Minimum temperature			Rainfall		
predictors	Partial r	P value	predictors	Partial r	P value	predictors	Partial r	P value
ncepp_zhaf	-0.566	0.00	ncepp_zhaf	0.249	0.00	ncepp_zhaf	0.278	0.00
ncepp500af	-0.257	0.42	ncepp500af	0.131	0.00	ncepr_500af	0.101	0.00
nceptemp	0.545	0.00	ncepp_temp	0.381	0.00			

Table 5-4: List of predictor variables that give good correlation with Debre Markos climate data

Maximum temperature			Minimum temperature			Rainfall		
predictors	Partial r	P value	predictors	Partial r	P value	predictors	Partial r	P value
ncepp_zhaf	-0.548	0.00	ncepp_zhaf	0.334	0.00	ncepp_zhaf	0.261	0.00
ncepp500af	-0.357	0.00	ncepp500af	0.204	0.00	ncepr_500af	0.157	0.00
nceptemp	0.576	0.00	ncepp_temp	0.322	0.00			

Where: The partial r is the correlation of the predicators with the predictand and P value is the correlation of the predicators between each others.

5.2.2. Scenario developed for the baseline period

The IPCC recommends the 1961-1990 years as climatological baseline period in impact assessment. Therefore the downscaling is done from 1961-1990 with A2 and B2 scenario outputs and the result is compared to observed data of maximum temperature, minimum temperature and rainfall. The monthly, the seasonal and the annual simulation for the baseline period is computed to compare the result with the actual data. The wet season is from June to September and the dry season is from October to February. The downscaling result for Gonder station is discussed below:

I. Maximum temperature

The actual and modelled result of maximum temperature indicates that the lowest monthly maximum temperature is observed in July and August while the highest is observed in March and April. The wet season has low maximum temperature than the dry season of the year because of rainfall and cloud cover.

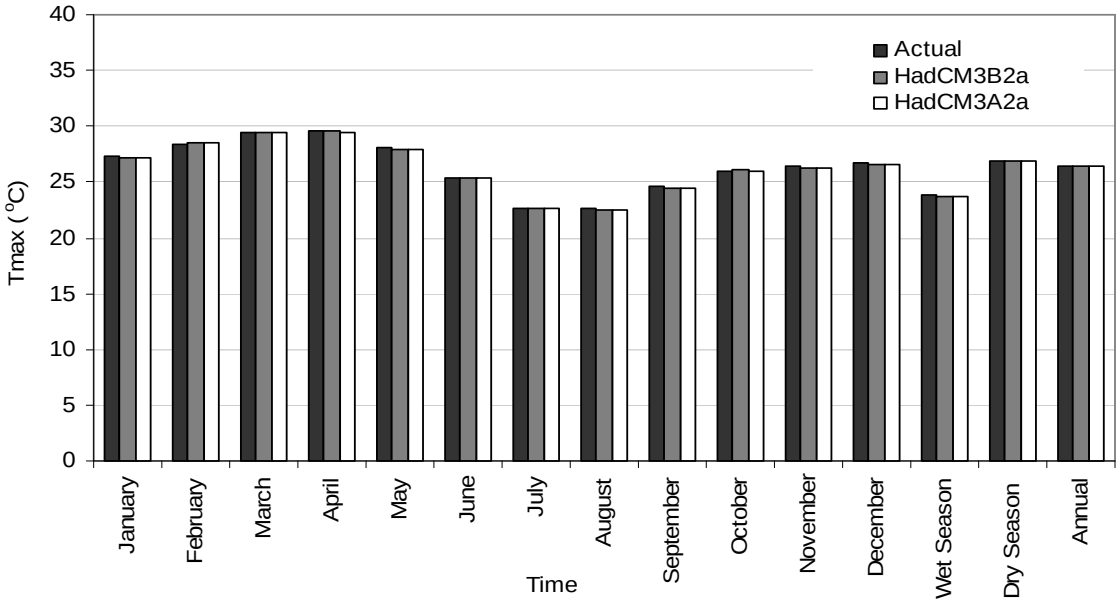

Figure 5-6: Observed and simulated maximum temperature for Gonder station (1961-1990).

As indicated in Figure 5-6 the downscaling result of maximum temperature with HadCM3A2a and HadCM3B2a scenario output do not show much difference in the actual and modelled result. The model error which is the difference of the observed and the simulated maximum temperature indicates that the maximum absolute error is 0.24 ^{o}C in the month of September with HadCM3B2a scenario output and the minimum is 0.03 ^{o}C in the month of April. Seasonally high model error is observed in the wet season than dry seasons .The seasonal model error is general less than the monthly model error. Generally no significant model error is observe in both scenario output for the whole months in the analysis period then it is possible to conclude that the SDSM is able to simulate the maximum temperature.

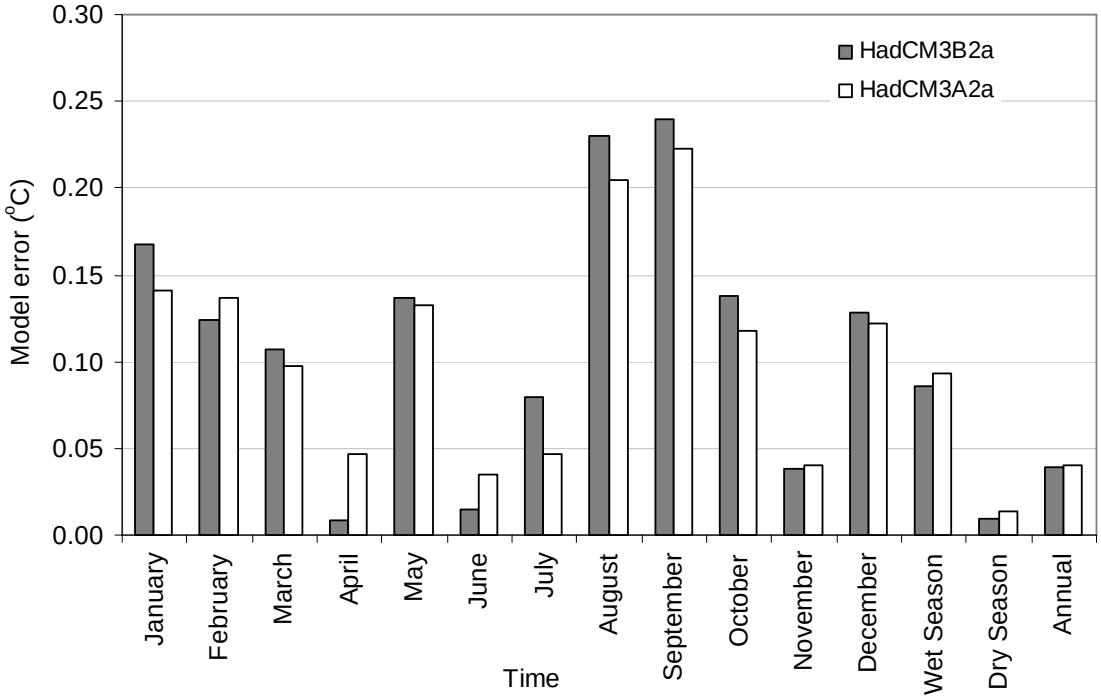

Figure 5-7: Absolute model error of maximum temperature (1961-199)

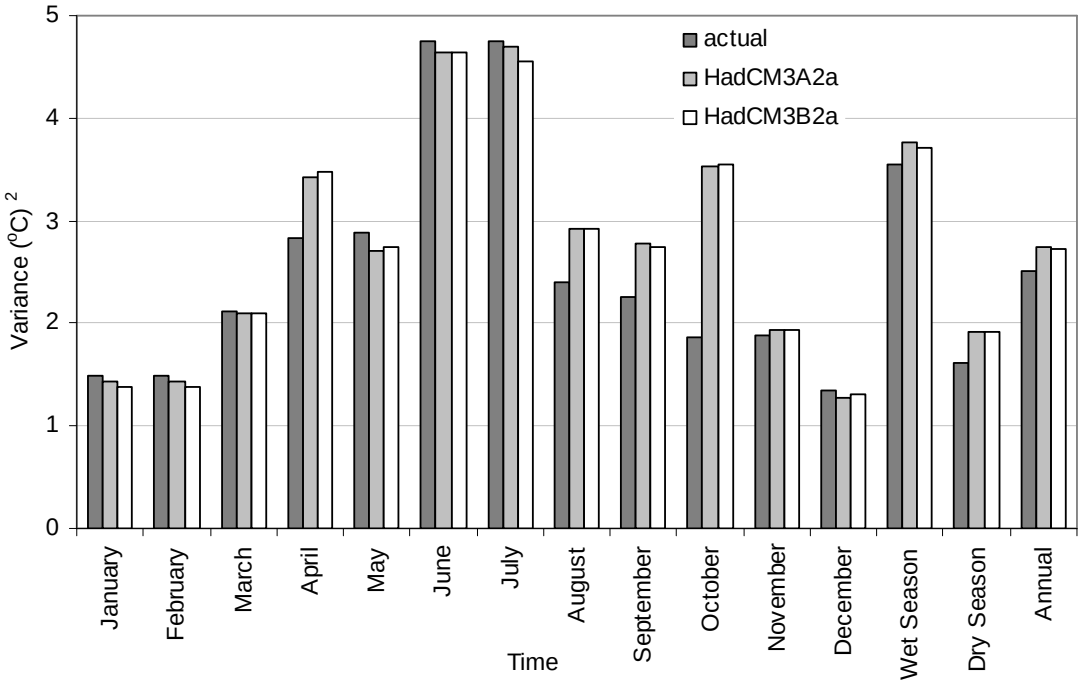

Figure 5-8: Variance of downscaled and actual maximum temperature (1961-1990)

Figure 5-8 also shows that the monthly and seasonal variability of maximum temperature for both scenario output is almost similar to the observed variability of maximum temperature except a little

deviation from August to September and April. This indicates the model result follows the trend of the actual maximum temperature.

II. Minimum temperature

Like maximum temperature the statistical downscaling model is able to reproduce the actual minimum temperature except for a slight underestimation in the month of February and March. The model error indicated in Figure 5-10 shows that the error in minimum temperature is less as compared to the maximum temperature. Maximum error is observed in February, May and September while the error in October is almost negligible for both scenario outputs.

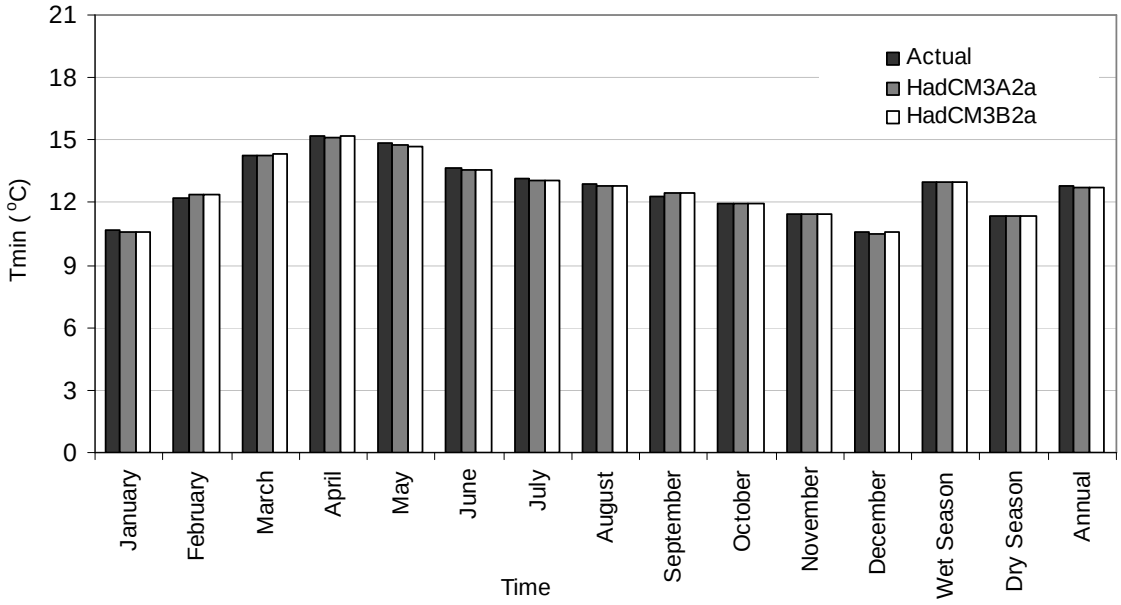

Figure 5-9: Observed and simulated minimum temperature for Gonder station (1961-1990).

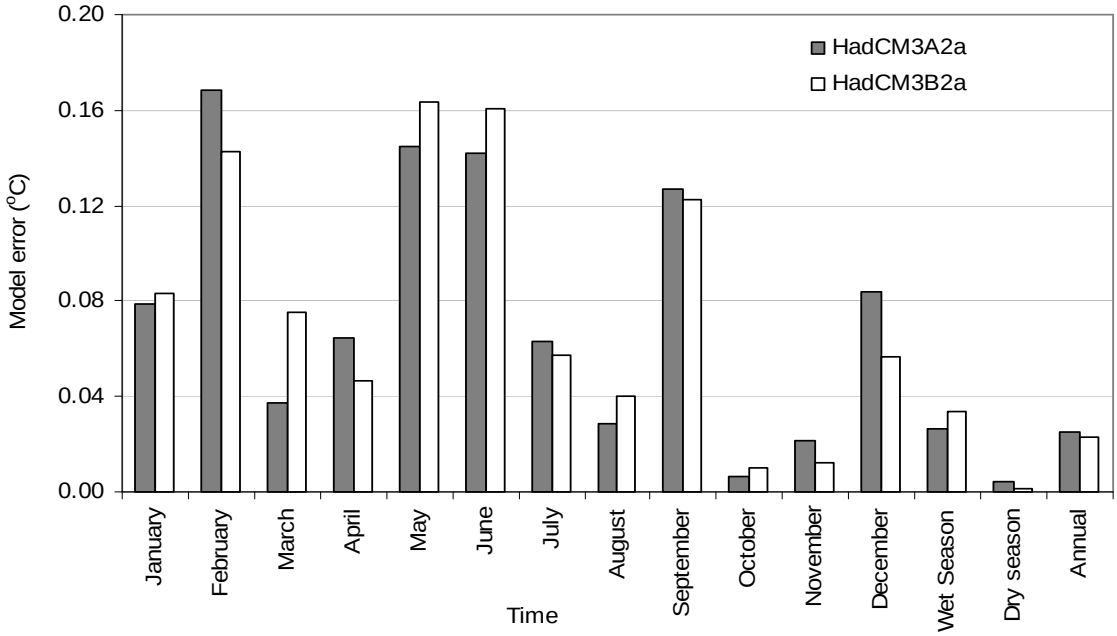

Figure 5-10: Absolute model error of minimum temperature

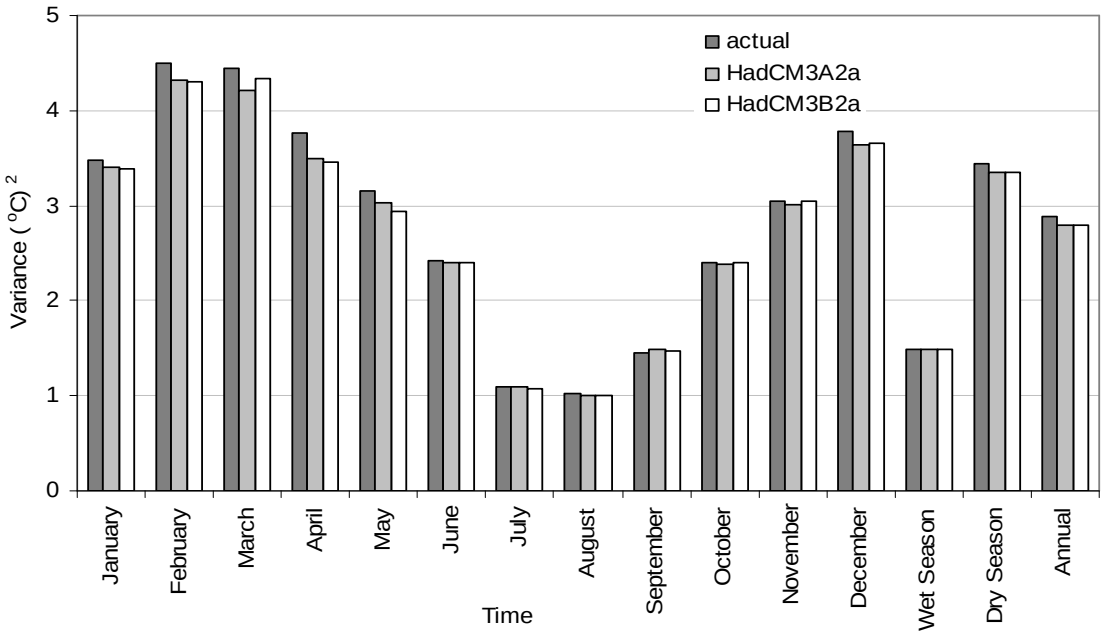

Figure 5-11: Variance of downscaled and actual minimum temperature

Like the maximum temperature the monthly and seasonal variably of the actual and modelled minimum temperature is similar. High variance in minimum temperature exists in February and March while in July and August the variance has the lowest value.

III. Precipitation

As it is shown in Figure 5-12 the statistical downscaling model is able to simulate the actual precipitation except for a slight over estimation in September, October and May and a slight under

estimation on the month of July and June. But the simulation result of precipitation with the statistical downscaling model is less accurate as compared to the maximum and minimum temperature. The average monthly model error is 8.47 and 9.01 mm and the annual model error is 46 mm and 50 mm for HadCM3A2a and HadCM3B2a scenario output respectively. High model error occurred in wet season than the dry season of the year. Even though some difference between the observed and the simulated precipitation, the monthly and seasonal variability is in good agreement and SDSM able to replicate the precipitation in acceptable limit.

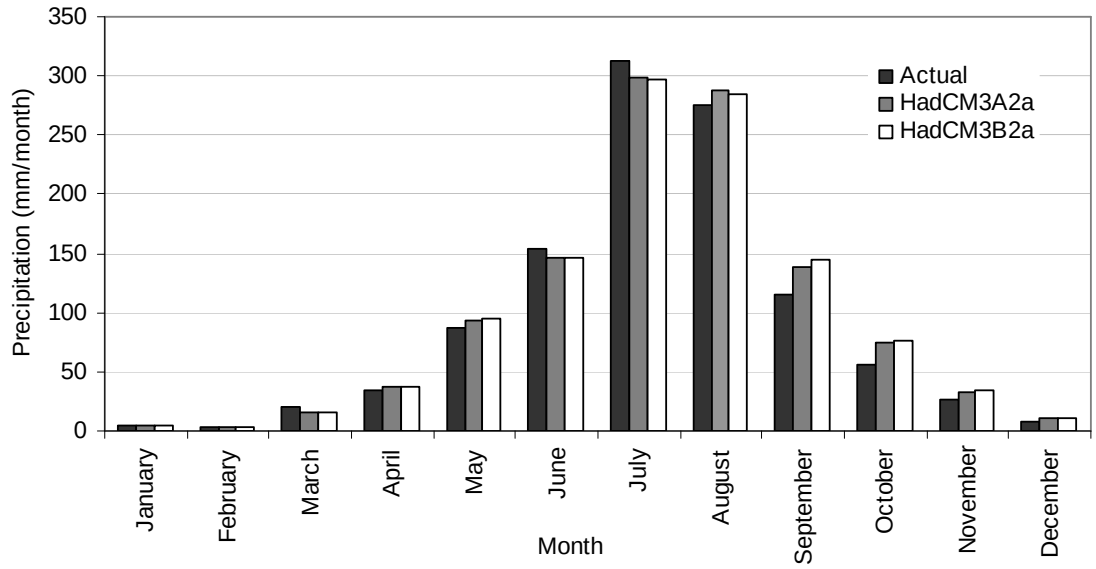

Figure 5-12: Observed and simulated precipitation for Gonder station (1961-1990)

Seasonally as shown in the Figure 5-13 the precipitation amount in wet and dry seasons are slightly over estimated compared to the actual. Therefore the annual precipitation with both HadCM3A2a and HadCM3B2a scenario output is higher than the actual precipitation.

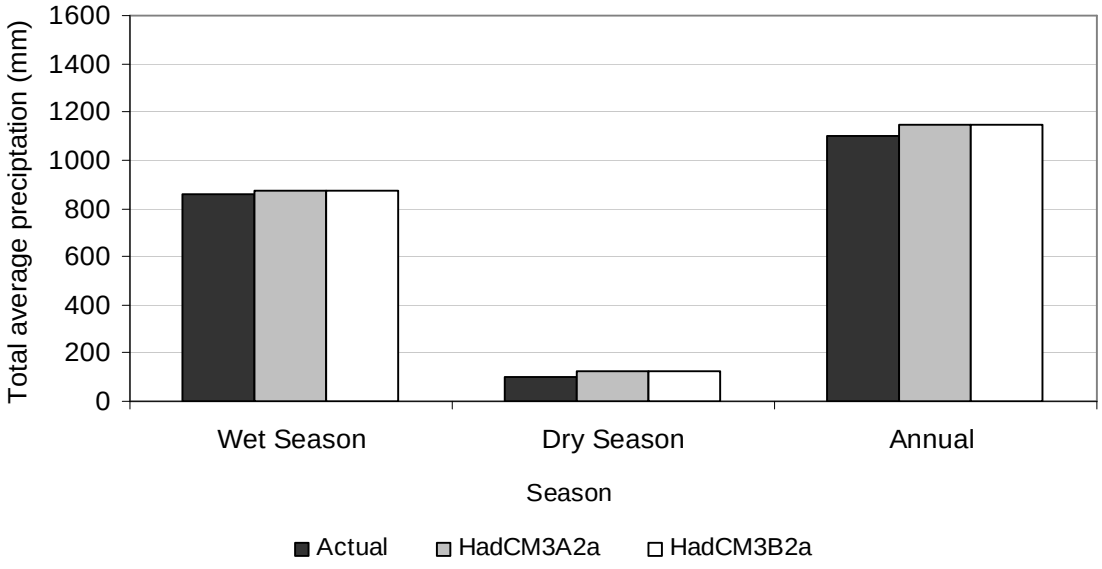

Figure 5-13: Average seasonal precipitation of Gonder station (1961-1990)

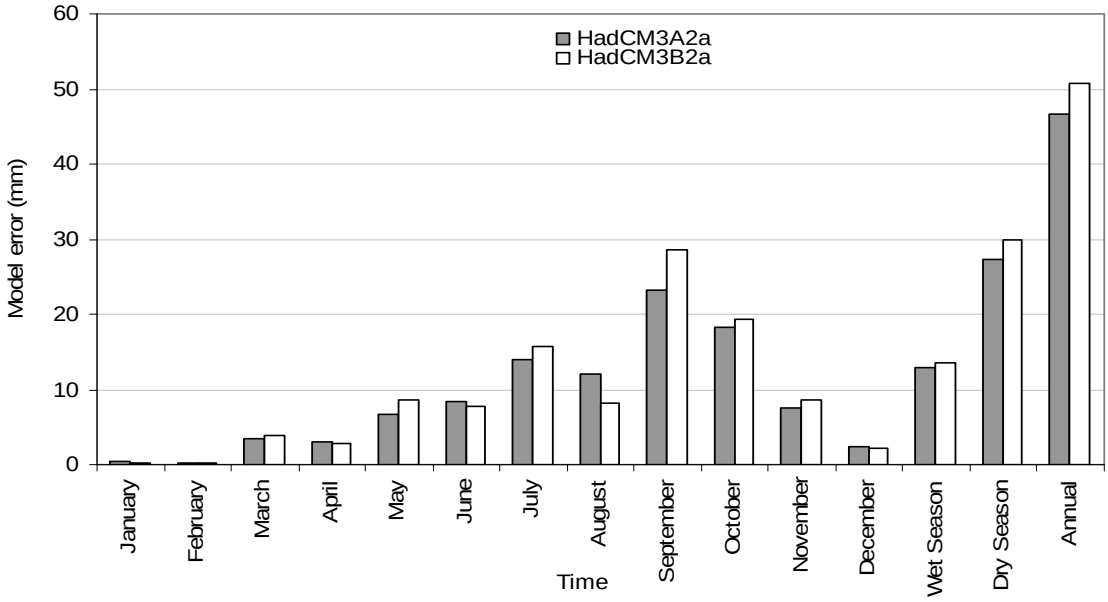

Figure 5-14: Absolute model error of precipitation (1961-1990)

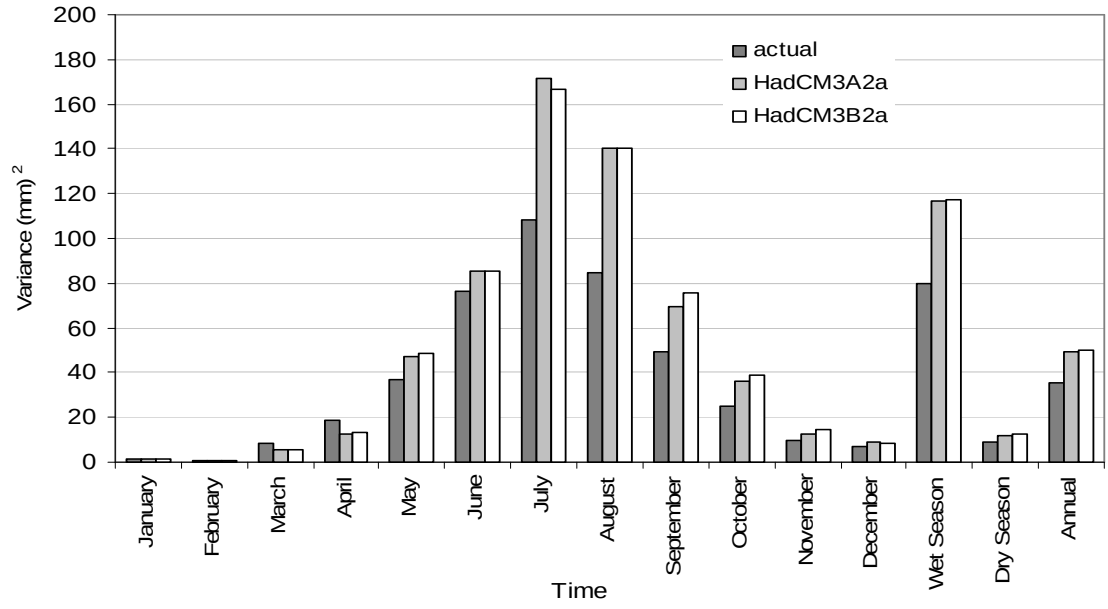

Figure 5-15: Variance of downscaled and actual precipitation (1961-1990)

The simulation result of the maximum temperature, minimum temperature and precipitation of Bahir Dar and Debre Markos stations for the baseline period with HadCM3A2a and HadCM3B2a scenario output is also well. Like the result obtained for Gonder station the SDSM well simulate the maximum temperature and minimum temperature than precipitation for the other stations.

Generally maximum temperature and the minimum temperature have better agreement with the observed result than the precipitation. The simulation of precipitation though showed a relatively lesser agreement as compared to the maximum and minimum temperature, but the result is acceptable

due to the fact that precipitation is the conditional process. As discussed before, conditional process like precipitation are dependant on other intermediate processes like on the occurrence of humidity, cloud cover, and wet day occurrence. Unconditional process like temperature; however, are not regulated by other intermediate process. In addition, as indicated in the SDSM manual (Wilby & Dawson 2007), local temperature are largely determined by regional forcing whereas precipitation series display more "noise" arising from local factor. Hence larger differences can be observed in precipitation ensemble members than that of temperature.

5.2.3. Downscaling of GCM for future period

Once the downscaling model has been setup the next step is to use the SDSM to downscale for the future period based on the HadCM3A2a and HadCM3B2a scenario outputs. The Precipitation and temperature downscaling is done for each of the three periods 2020s (2010-2039), 2040s (2040-2069) and 2070s (2070-2099). The respective average monthly, seasonal and annual change from the baseline period for both A2 and B2 scenarios were calculated for maximum and minimum temperature. For precipitation the monthly, seasonal and annual precipitation amount for the baseline and future scenario period is calculated. The change in temperature and the precipitation amount for Gonder station is discussed below. The result obtained for Bahir Dar and Debre Markos station are presented in the Appendix F.

I. Maximum temperature

The downscaling of maximum temperature in the future period as it is indicated in Figure 5-17 and Figure 5-17 shows that the average increase of temperature in 2020s is 0.4 ^{o}C and in 2040s it is further increases to 0.7 ^{o}C and 0.8 ^{o}C for A2 and B2 scenario respectively. In 2070s the increase is 1.15 ^{o}C and 1.47 ^{o}C for A2 and B2 scenario. The 2070s increase is higher than for both 2020s and 2040s increase. This shows the maximum temperature has an increase trend in the future period. The change in maximum temperature from the baseline period is high in wet season for both scenarios. Seasonally high maximum temperature change occurred in the wet season while the maximum temperature change in dry season shows minor increment.

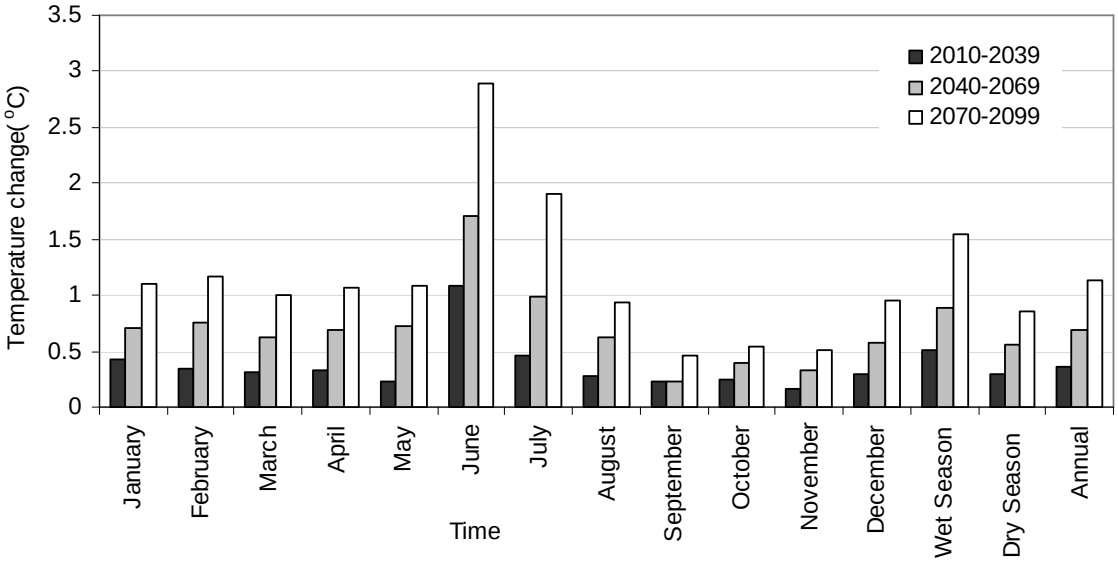

Figure 5-16: Average monthly Maximum temperature change from the baseline period with HadCM3B2a scenario output (Gonder station)

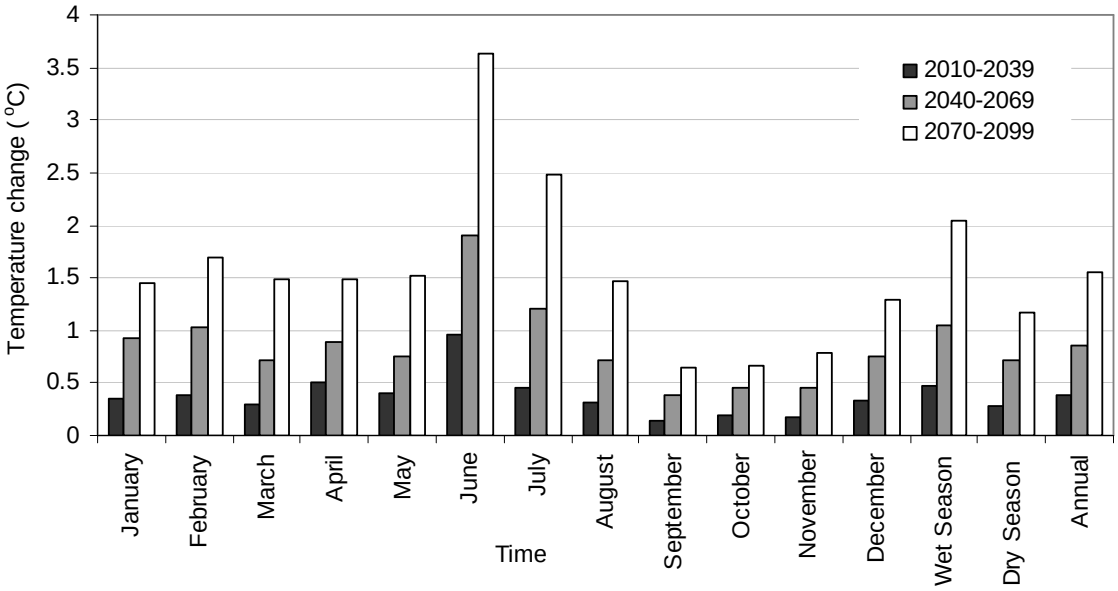

Figure 5-17: Average monthly maximum temperature change from the baseline period for HadCM3A2a scenario outputs (Gonder station)

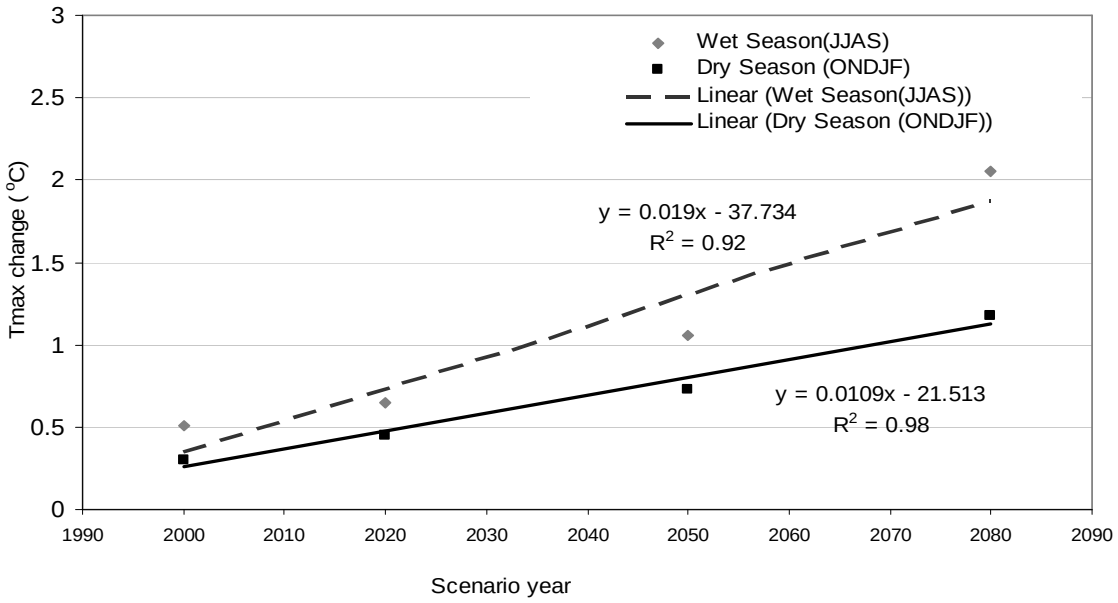

Figure 5-18: Seasonal maximum temperature change in the current and future time for Gonder station (HadCM3A2a)

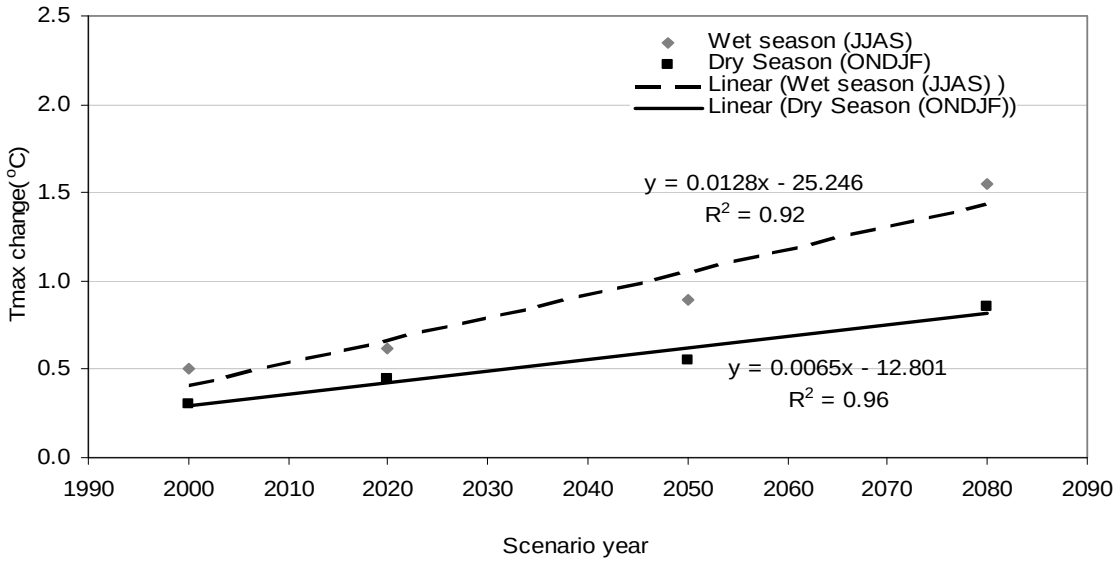

Figure 5-19: Seasonal maximum temperature change in the current and future time for Gonder station (HadCM3B2a)

In Figure 5-19 and Figure 5-19 the scenario year 2000, 2020, 2050 and 2080 indicates 1991-2007, 2010-2039, 2040-2069 and 2070-2099 year respectively. The 2000 (1991-2007) seasonally changes for minimum temperature, maximum temperature and rainfall is calculated with the observed data. Based on monthly average maximum temperature of the above scenario years the seasonal changes with respect to the baseline period is computed. The result indicates that both scenario outputs have a high maximum temperature changes in the wet season than in the dry season. But the overall increase

in maximum temperature is higher with HadCM3A2a scenario output than the output from HadCM3B2a scenario.

II. Minimum temperature

Like the average monthly maximum temperature the average monthly minimum temperature also shows an increment in all months of the year. Figure 5-21 and Figure 5-21 indicates that the increase in minimum temperature in 2020s is 0.20 ^{o}C and 0.24 ^{o}C for B2 and A2 scenario respectively. This change increases to 0.41^{o}C and 0.50 ^{o}C in 2040s and it is further increases to 0.61^{o}C and 0.84 ^{o}C in 2070s for B2 and A2 scenario respectively .High minimum temperature change is observed in month of February, March and December. Seasonally contrary to the average maximum temperature change high minimum temperature change occurred in dry season of the year while the minimum temperature change in the wet season shows small increment.

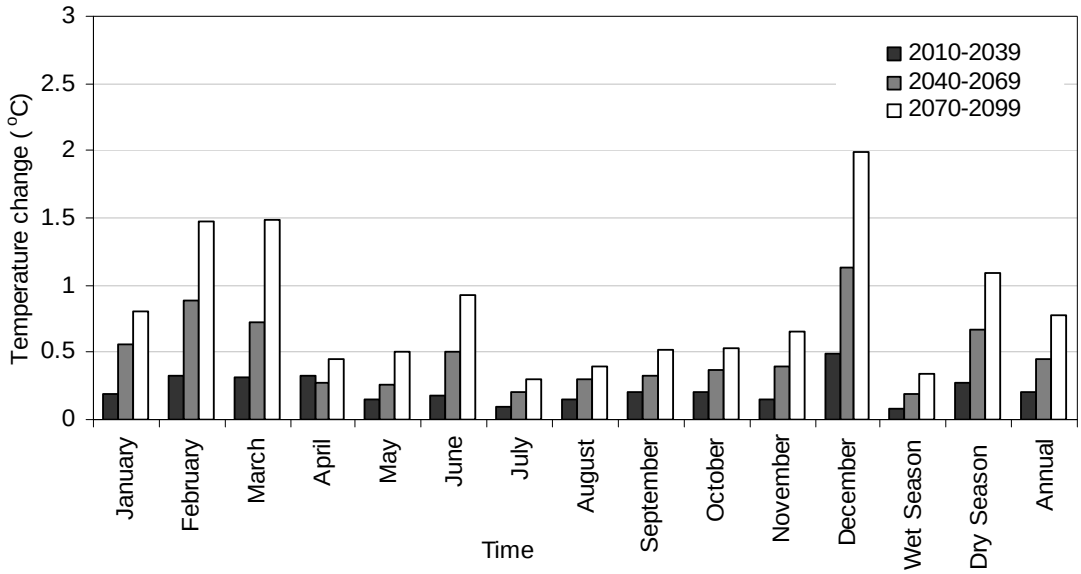

Figure 5-20: Average minimum temperature change from the baseline period for HadCM3A2a scenario output (Gonder station)

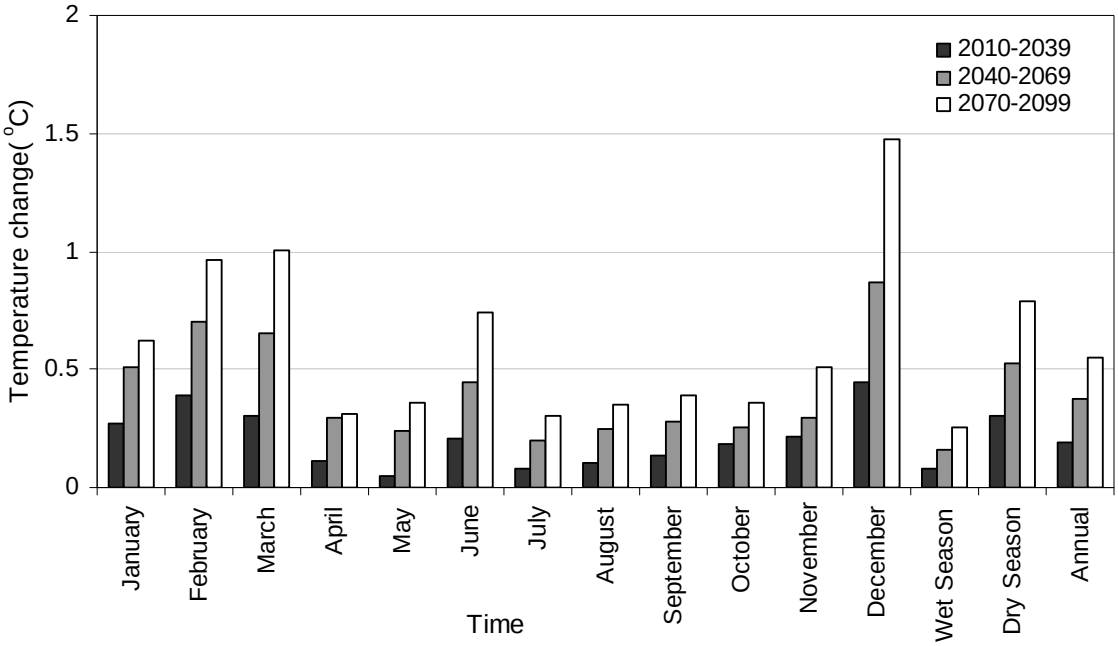

Figure 5-21: Average minimum temperature change from the baseline period for HadCM3B2a scenario output (Gonder station).

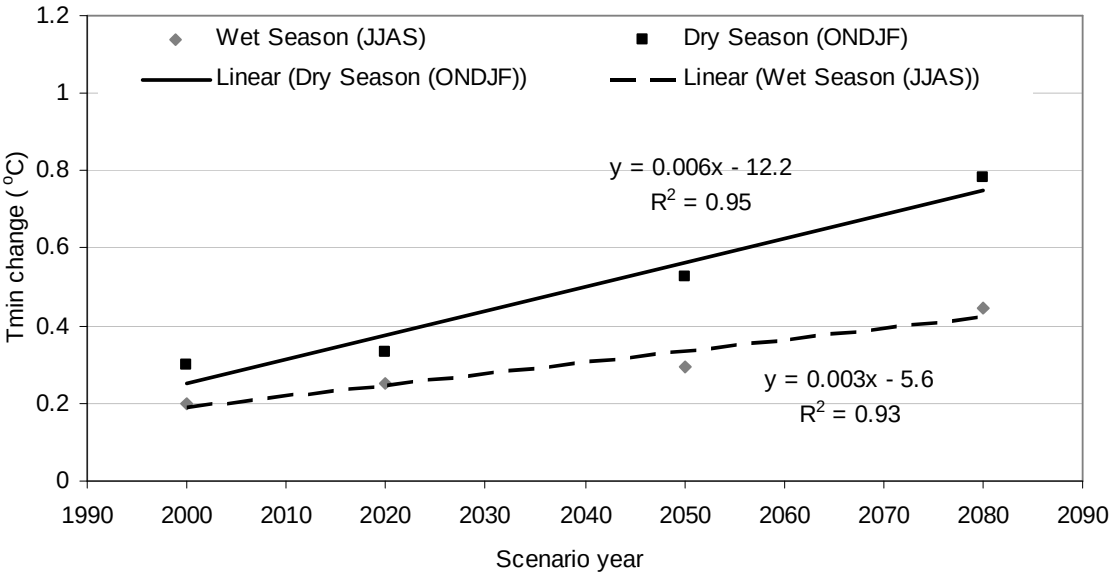

Figure 5-22: Seasonal minimum temperature change in the current and future time for Gonder station (HadCM3B2a)

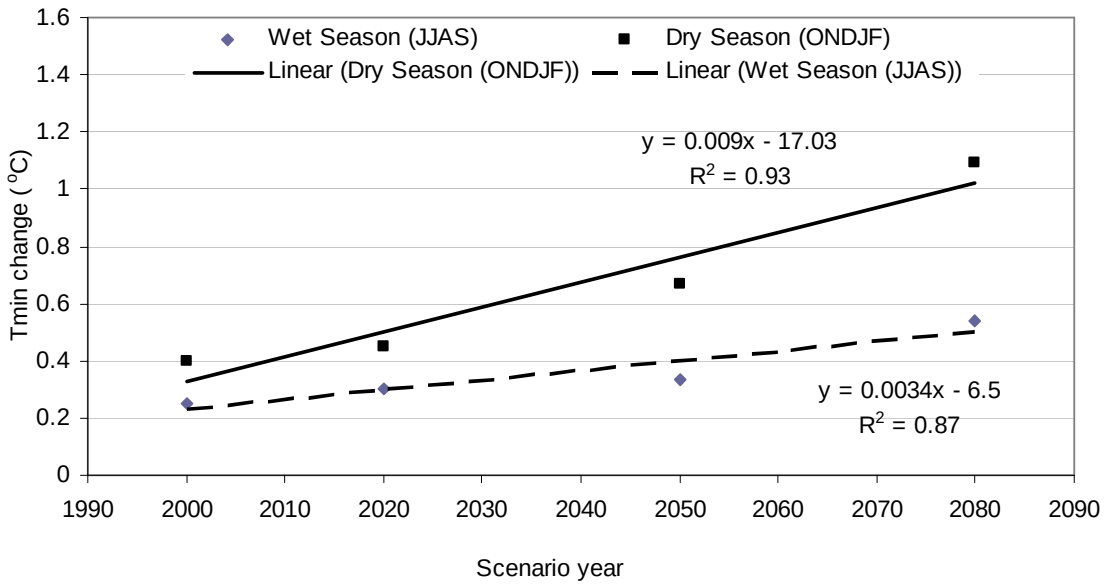

Figure 5-23: Seasonal minimum temperature change in the current and future time for Gonder station (HadCM3A2a)

As it is observed in Figure 5-23 and Figure 5-3 the minimum temperature change in dry season is higher than the wet season for all scenario years. The increase of minimum temperature with both scenario output shows an increasing trend as compared to the baseline period for both dry season and wet season.

III. Evaporation

The evaporation of Gonder is computed with the maximum and minimum temperature for the analysis period. Hargreaves method is applicable for the evaporation estimation since no sufficient climate data are available for the other methods. The increase in maximum and minimum temperature with both scenario output results in an increase in evaporation of the catchment. As it is observed in Figure 5-24 the evaporation shows an increasing trend as compared to the baseline period. But the evaporation with HadCM3A2a scenario output is higher than HadCM3B2a scenario output. The annual mean evaporation is 1660 mm, 1681mm and 1711mm for the period of 2010-2039, 2040-2069 and 2070-2099 respectively with HadCM3B2a scenario output. The mean annual evaporation with HadCM3A2a scenario output is 1658 mm, 1691 mm and 1739 mm for the period of 2010-2039, 2040-2069 and 2070-2099 respectively. The baseline period and the 1991-2007 annual mean evaporation are calculated by the observed data with Hargreaves method and it is estimated to be 1636mm and 1648mm respectively.

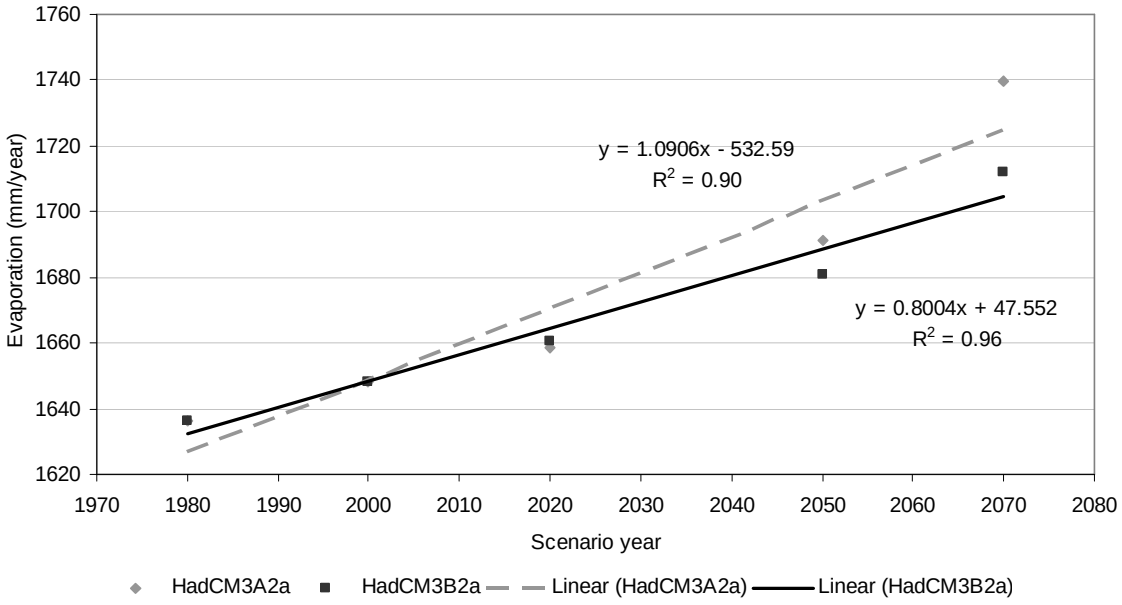

Figure 5-24: Annual average evaporation for Gonder station

IV. Precipitation

The monthly average precipitation is increasing by 4.8 % and 7.4% in 2020s for A2 and B2 scenarios with reference to the baseline period precipitation. The average increase of monthly precipitation is 7.2 % and 7.8 % in 2040s and 9.4 % and 8.9 % in 2070s for A2 and B2 scenario respectively.

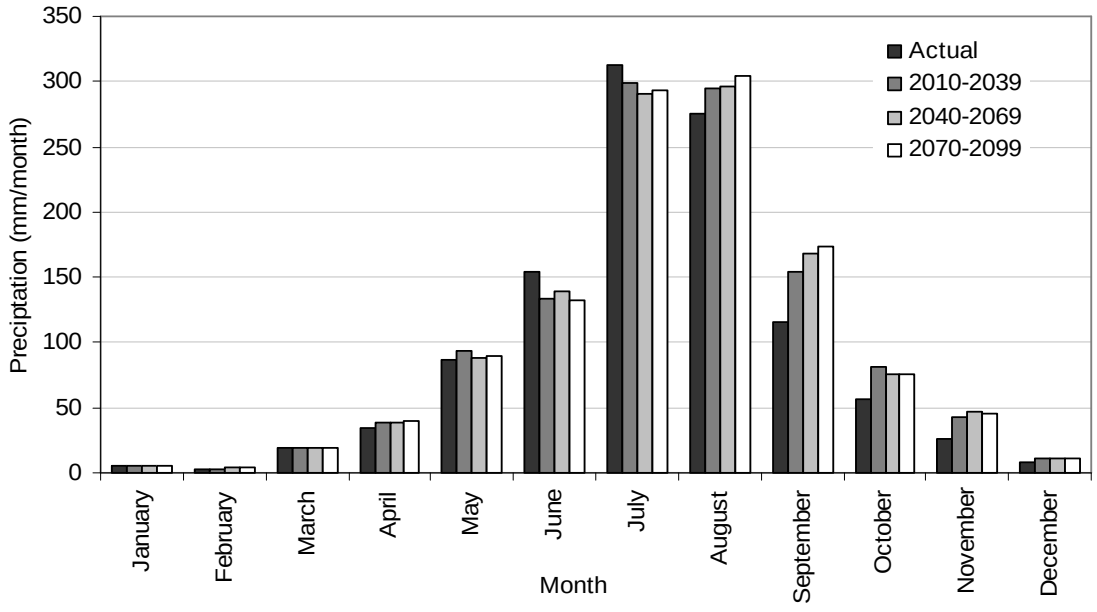

Figure 5-25: Monthly average precipitation downscaled from HadCM3B2a scenario output (Gonder station)

A higher increase in precipitation is occurred on the month of August and September which are the part of the wet season. As it is observed in Figure 5-29 and Figure 5-28 for both HadCM3A2a and

HadCM3B2a scenario outputs the wet season shows an increasing trend for all future periods. The wet season has 75% contribution for the annual rainfall in the Lake Tana basin therefore the annual rainfall also shows an increasing trend in the future period. But the increase in precipitation for HadCM3A2a scenario output is slightly higher than the precipitation obtained from HadCM3B2a scenario.

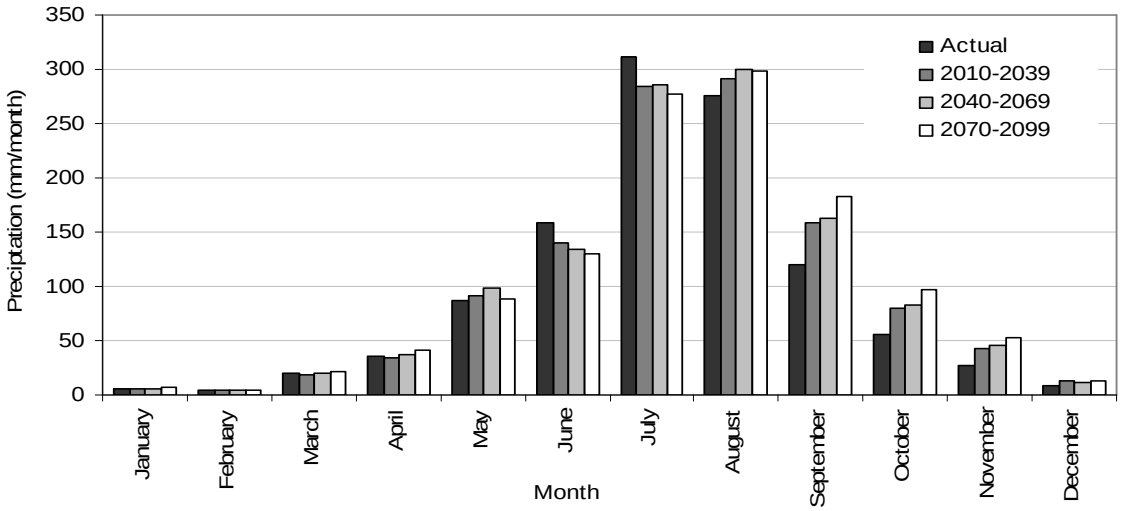

Figure 5-26: Monthly average precipitation downscaled from HadCM3A2a scenario output (Gonder station)

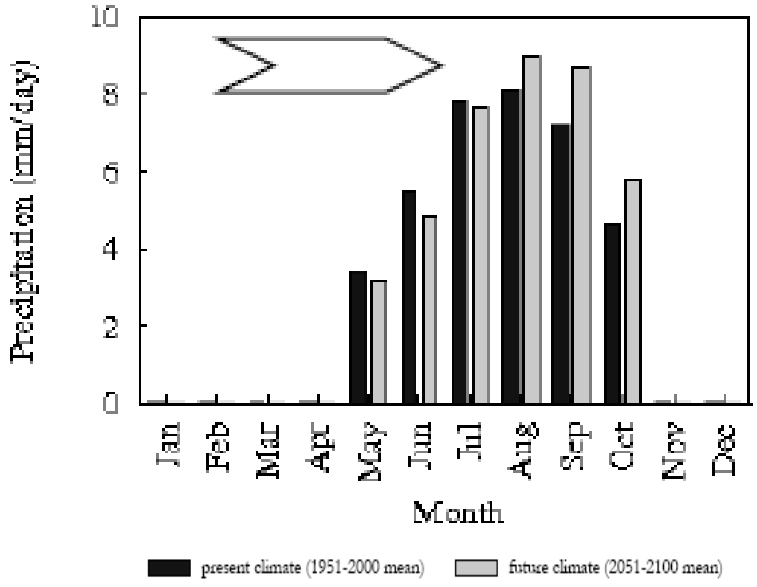

Figure 5-27: Mean daily precipitation in Ethiopian Highland under the present and future period (deBoer, 2007)

The climate change and impact study in the Blue Nile region by deBoer (2007) indicates that there is a shift of the rainy season towards the end of the year and there is an increase of total precipitation in

the future as compared to the present time in the Northern Ethiopian highland that also includes the Lake Tana catchments. An ensemble of 17 models run with different initial conditions of GCM is used for the climate change impact study. The result of deBoer (2007) supports the forecast of precipitation with HadCM3A2a and HadCM3B2a scenario output of this study. Both studies indicate that there is an increase of precipitation in the future period compared to the present precipitation in the Lake Tana catchments.

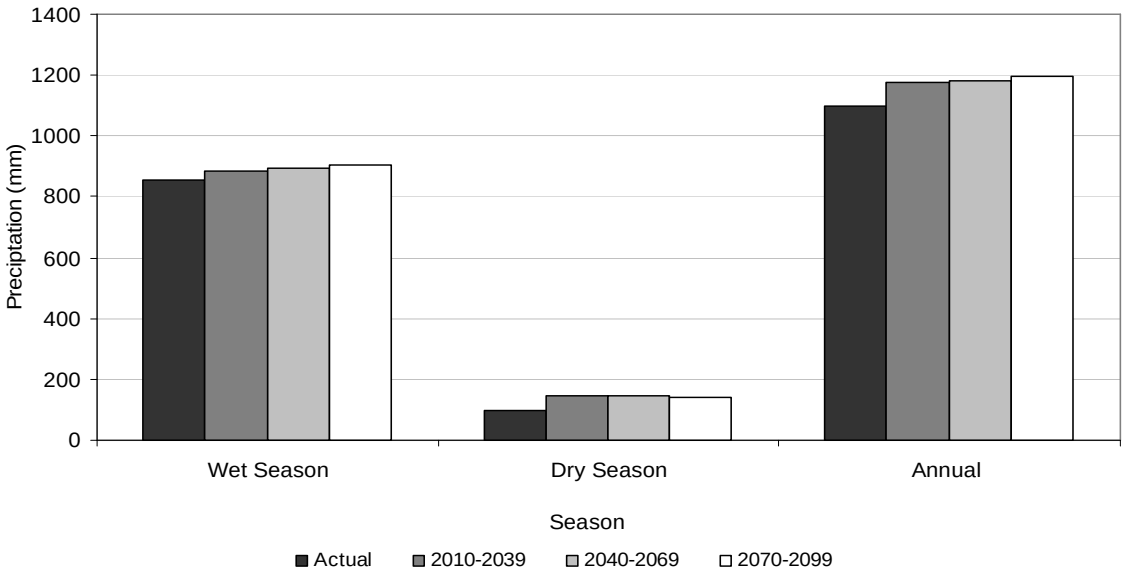

Figure 5-28: Simulated precipitation with HadCM3B2a scenario out put

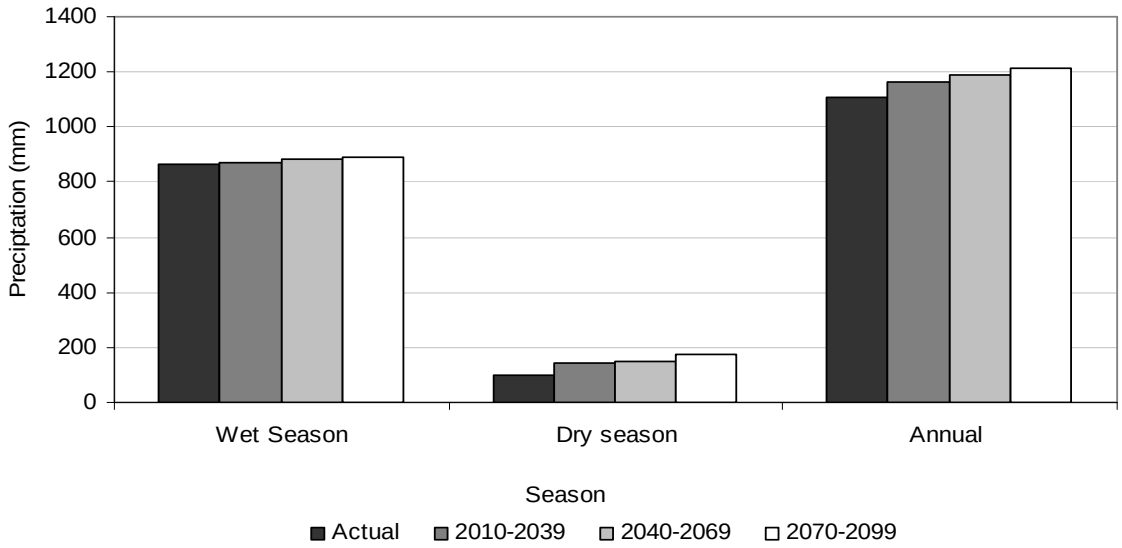

Figure 5-29: Simulated precipitation with HadCM3A2a scenario output

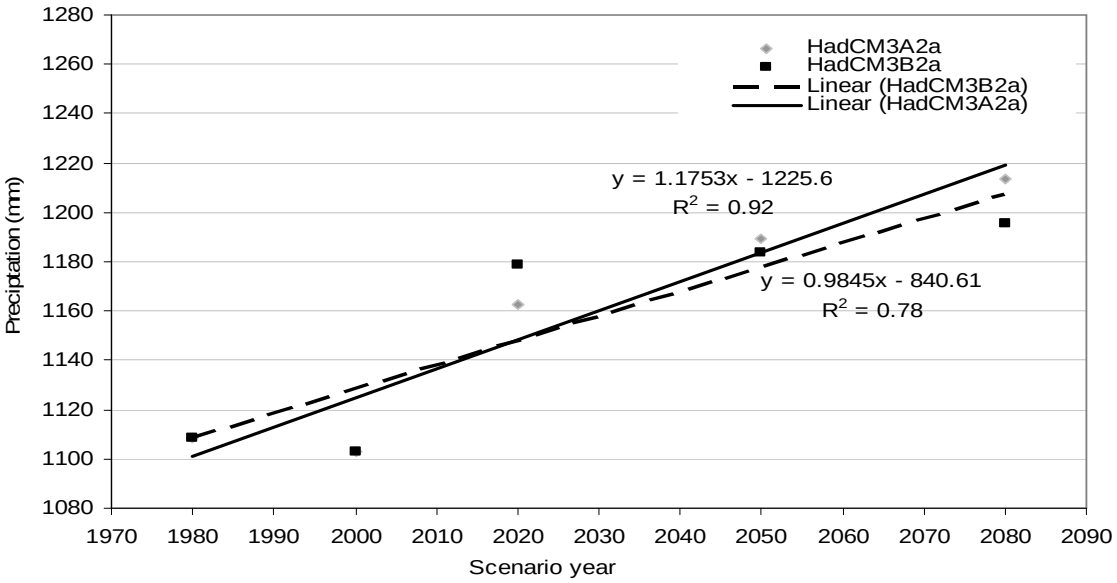

Figure 5-30: Annual average precipitation for Gonder station

The annual mean precipitation for both scenarios indicates that there is an increase in precipitation in future scenario period mainly due to an increasing of precipitation in the wet season. As it is observed in Figure 5-30 the annual average precipitation in 2050 (2040-2069) and 2080 (2070-2099) for HadCM3A2a scenario output is higher than the HadCM3B2a scenario output while in 2020 (2010-2039) the precipitation of HadCMEB2a scenario is higher than the HadCM3A2a scenario. As it is observed in Figure 5-31 the observed annual and seasonal mean of precipitation in 2000 (1991-2007) is less compared to mean of the baseline and future scenario year precipitation. But the forecasted precipitation in the future scenario period is higher than the observed precipitation.

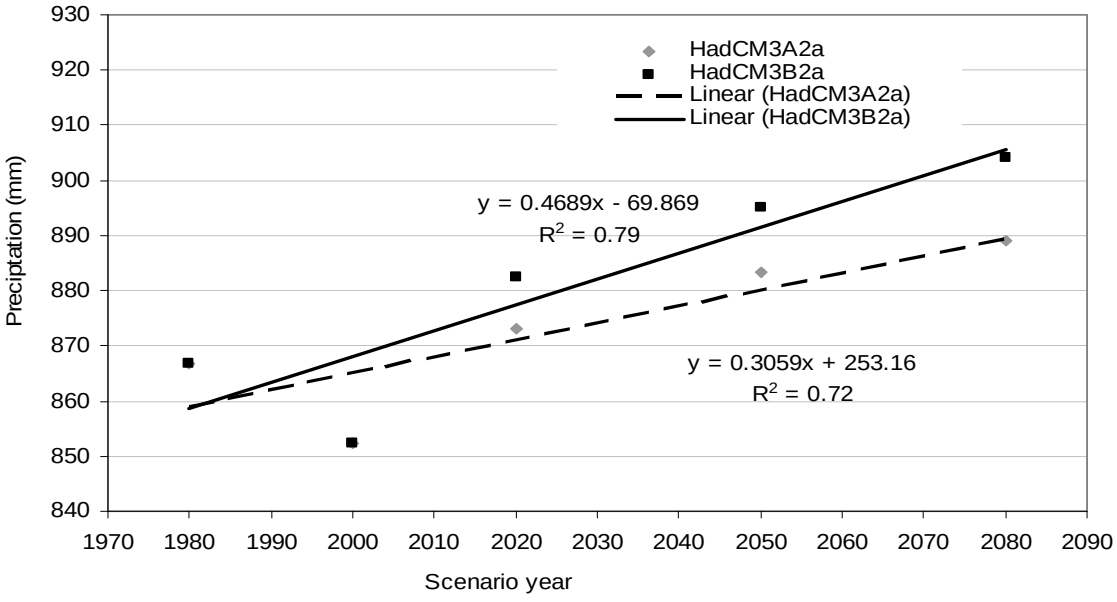

Figure 5-31: Wet Season precipitation for Gonder station

5.3. Validation of the water balance model

For this study the calibrated HBV model with 1993-2000 data for the Lake Tana catchments of (Abeyou, 2008) is applied. The calibration is done for Ribb, Gumara, Megech, Koga, Kelti and Gilgel Abbay daily river discharge. But the model has to be validated with independent data set in order to check the performance of the calibrated model. Therefore validation is done with independent data of 2004-2007. For validation 12 rainfall stations and 4 temperature and evaporation stations are selected because of the availably of the sufficient records. The areal rainfall, mean temperature and evaporation which are required for the HBV model to simulate the discharge are estimated by the multiplying the station daily records with the weight computed by inverse distance interpolation. The weight of rainfall and evaporation station for each catchment is indicated in Table 5-5 and Table 5-6.

Table 5-5: Weight of rainfall station by inverse distance

Stations	Gilgel Abbay	Kelti	Koga	Megech	Ribb	Gumara	Gumero	Garno	Gelda
Addis zemen					0.16	0.18		0.06	0.07
Dangial	0.2	0.19	0.15						
Gonder				0.93			0.6	0.02	
Bahirdar			0.17			0.09			0.76
Enfranze				0.07		0.1	0.4	0.92	
Engibara	0.18								
Gundil	0.3								
Abbay sheleko		0.79							
Adet			0.42						0.11
Kidamaja		0.02							
Sekela	0.32		0.26						
Debre tabour					0.84	0.63			0.06

Table 5-6: Weight of evaporation station by inverse distance weighting

catchment	Bahir Dar	Gonder	Debre Tabour	Dangila
Gilgel abbay	0.18	0.02	0.03	0.77
Kelti	0.02	0.00	0.01	0.97
Koga	0.49	0.04	0.06	0.41
Megech	0.01	0.97	0.01	0.01
Ribb	0.02	0.01	0.96	0.01
Gumara	0.12	0.04	0.82	0.02
Gemero	0.06	0.86	0.06	0.02
Garno	0.17	0.53	0.25	0.05
Gelda	0.86	0.03	0.07	0.04
Tana west	0.36	0.32	0.11	0.21
Gabikura	0.13	0.73	0.07	0.07
Derma	0.09	0.82	0.05	0.04
Unguaged ribb	0.29	0.27	0.38	0.06
Unguaged megech	0.02	0.95	0.02	0.01
Unguaged gilgelabby	0.66	0.05	0.24	0.05
Unguaged gumara	0.56	0.13	0.24	0.07

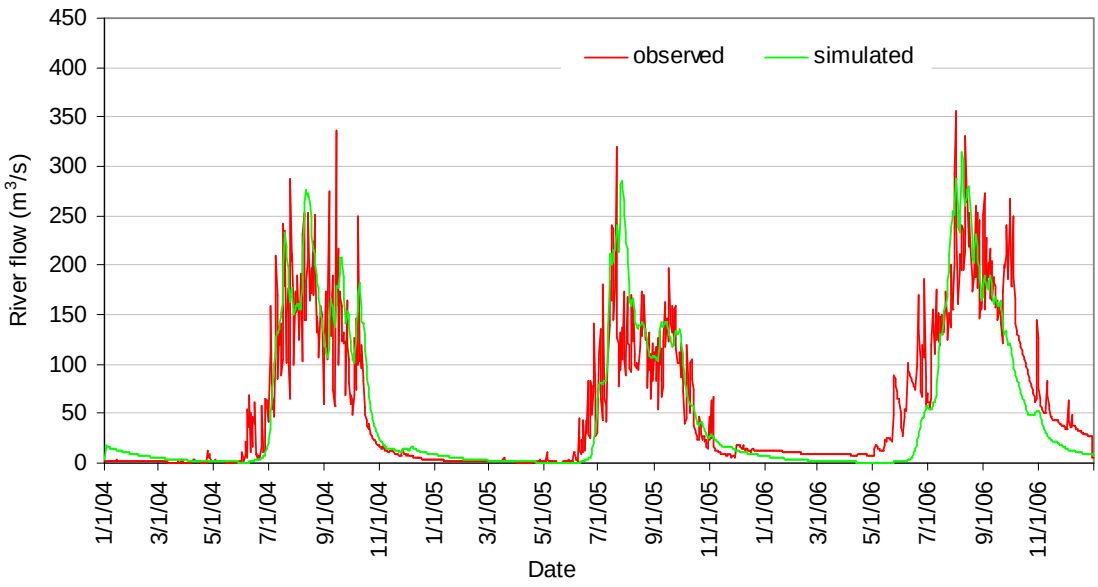

Figure 5-32: Validation result of Gilgel Abbay discharge (2004-2006)

The validation result of Gilgel Abbay indicates that R^2 = 0.83 and RVE = -3.58% .This shows the validation is very good and there is no need for recalibration of the model for this subcatchment.

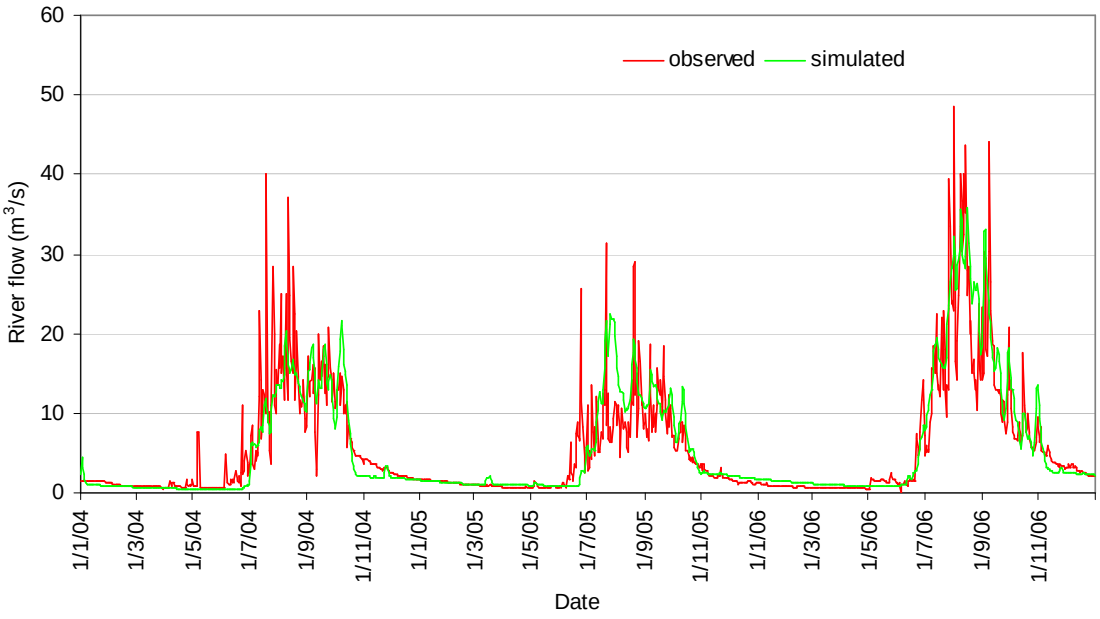

Figure 5-33: validation result of Koga discharge (2004-2007

The validation result of Koga subcatchment also shows R^2 = 0.85 and RVE = -3.44%. This indicates that the model performance is very well like Gilgel Abbay subcatchment. The result of the other gauged subcatchments also shows R^2 above 70 % while RVE is less than -10% and 10%, then no need for recalibration for all subcatchments.

5.4. Lake evaporation

The evaporation is computed with Hargreaves for 1961-1990, 2010-2039, 2040-2069 and 2070-2099 periods. The Bahir Dar and Gonder meteorological data are used for estimation of lake evaporation with this method. Due to increase in maximum and minimum temperature in the future time as compared to the baseline climate the lake evaporation also shows an increasing trend. As it is indicated in Figure 5-35 and Figure 5-35 the yearly average lake evaporation is 1674, 1685, 1706 and 1741 mm for the period of 1961-1990, 2010-2039, 2040-2069 and 2070-2099 respectively with HadCM3A2a scenario output. This shows the mean annual lake evaporation is increasing by 1%, 2% and 4% in 2020s ,2040s and 2070s as compared to the reference period evaporation. Like HadCM3A2a scenario output the lake evaporation with HadCM3B2 scenario output also shows an increasing trend. The average yearly evaporation with this scenario output is 1682, 1715, 1716 mm in 2020s, 2040s and 2070s respectively.

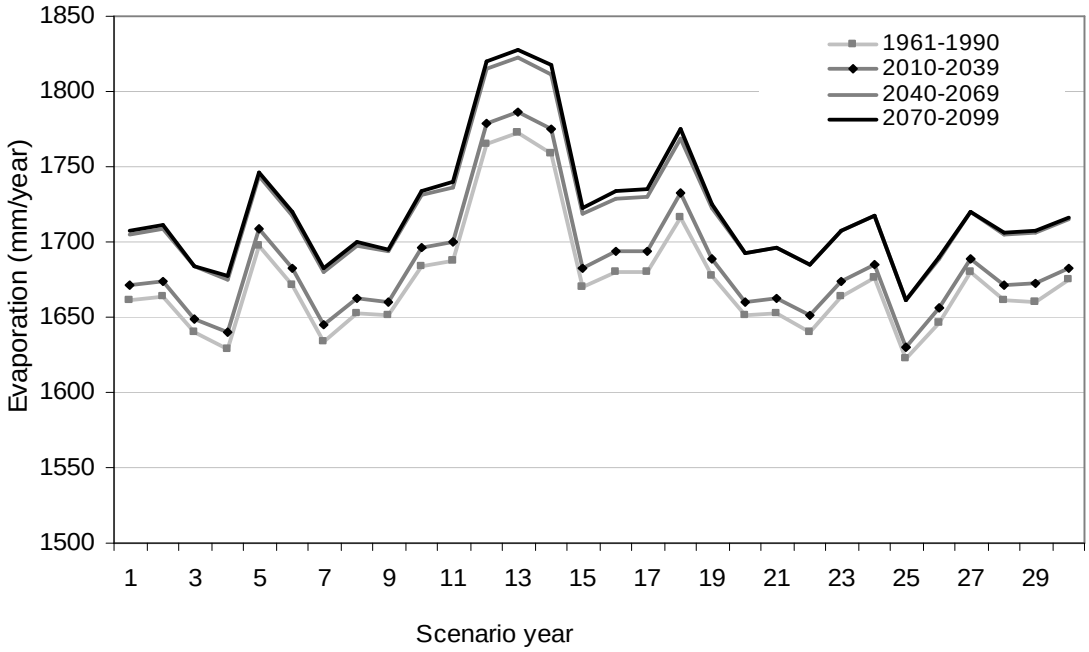

Figure 5-34: Lake Tana yearly evaporation with HadCM3B2a scenario output

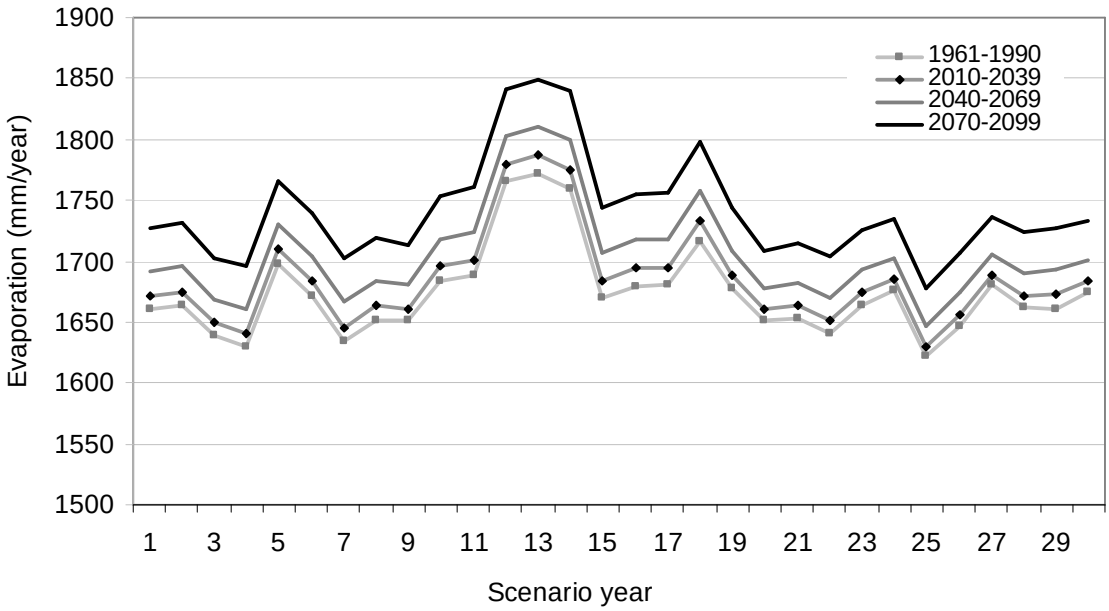

Figure 5-35: Lake Tana yearly evaporation with HadCM3A2a scenario output

5.5. Lake precipitation

Lake Tana precipitation is one of the major components of the net basin supply and it is calculated based on the Bahir Dar and Gonder stations. Both stations are relatively near to the lake and they have sufficient data for downscaling of precipitation in the future scenario period then they are selected for estimation of the lake precipitation for the current and future time period.

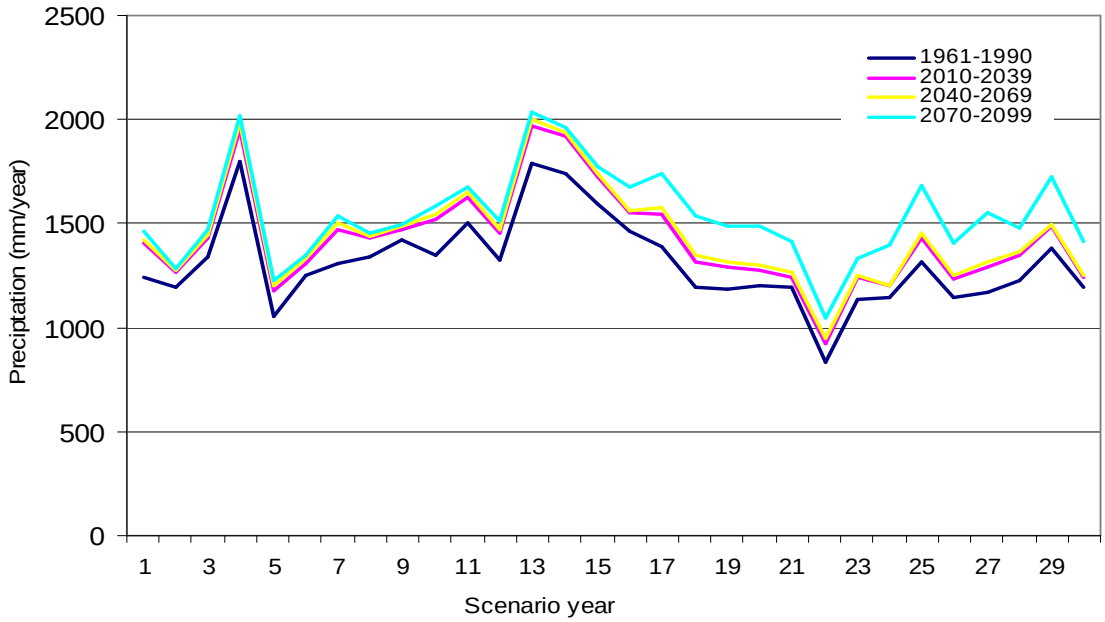

Figure 5-36: Annual Precipitation of Lake Tana with HadCM3A2a scenario output

The annual lake precipitation is computed for HadCM3A2a and HadCM3B2a scenario outputs for the three future time horizons and the result is compared to the baseline period in order to determine the change. The result indicates that the mean annual lake precipitation is increasing by 8.54 %, 10.02 % and 17.27 % for the 2020s, 2040s and 2070s as compared to the baseline period with HadCM3A2a scenario output. The mean annual lake precipitation for the baseline period is 1312 mm/year.

Figure 5-37: Annual lake precipitation with HadCM3B2a scenario output

The lake precipitation also computed with HadCM3B2a scenario output and the result indicates that the mean annual precipitation increases by 3.68, 3.65 and 3.2 % respectively for 202s, 2040s and

2070s periods as compared to the 1961-1990 periods. The increase in precipitation with HadCM3B2a scenario output is less as compared to the HadCM3A2a scenario output. This is because the Bahir Dar and Gonder precipitation in the future period with HadCM3A2a scenario output is higher than that of HadCM3B2a scenario output.

An increase in surface temperature in the future period leads to higher evaporation rates and enable the atmosphere to transport higher amount of water vapour. Therefore the global hydrological cycle will be accelerated (Menzel and Bürger, 2002). According to the Intergovrernmental Panel on Climate Change (IPCC, 2001) an increasing in preciptation is likely to happen large contenintal area in the tropics and at higher latitudes.

5.6. Net basin supply of Lake Tana water balance

After validation of the HBV model the next step is forecasting of the inflow to the Lake Tana based on the observed and downscaled precipitation, temperature and evaporation of the three stations. The net basin supply is then calculated based on the lake precipitation , lake evaporation and inflow to the lake for baseline period and the other three future time periods 2020s (2101-2039), 2040s (2040-2069) and 2070s (2070-2099).

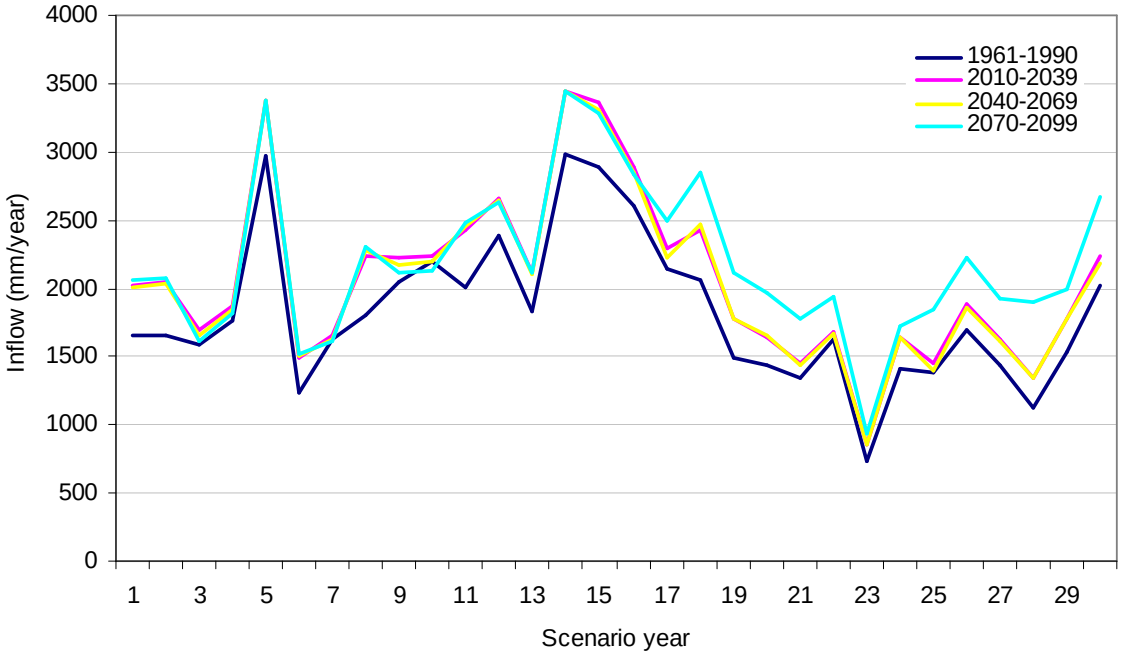

Figure 5-38: Annual Lake Tana inflow with HadCM3A2a scenario output

The increase of inflow to the lake is due to increase in precipitation. As it is indicated in Figure 5-38 the minimum annual inflows are observed between 1979-1988 while the maximum inflows are observed between 1973-1976 and 1963-1965 with HadCM3A2a scenario output.

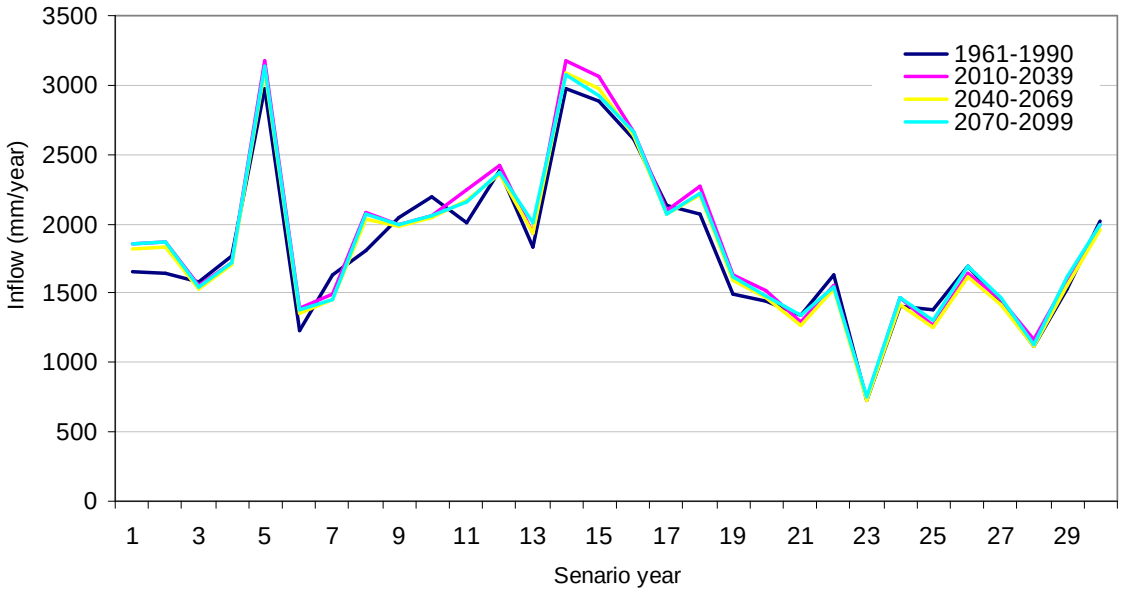

Figure 5-39: Annual lake inflow with HadCM3B2a scenario output

The annual inflow to the lake with HadCM3B2a scenario output also shows an increasing trend but as compared to the HadCM3A2a scenario output the increase is less. This less inflow is due to the decrease of downscaled precipitation of Bahir Dar, Gonder and Debre Markos with HadCM3B2a scenario output than HadCM3A2a. The average annual inflows are increasing by 3.1, 1.1 and 2.5% for 2020s, 2040s and 2070s periods respectively as compared to the baseline period.

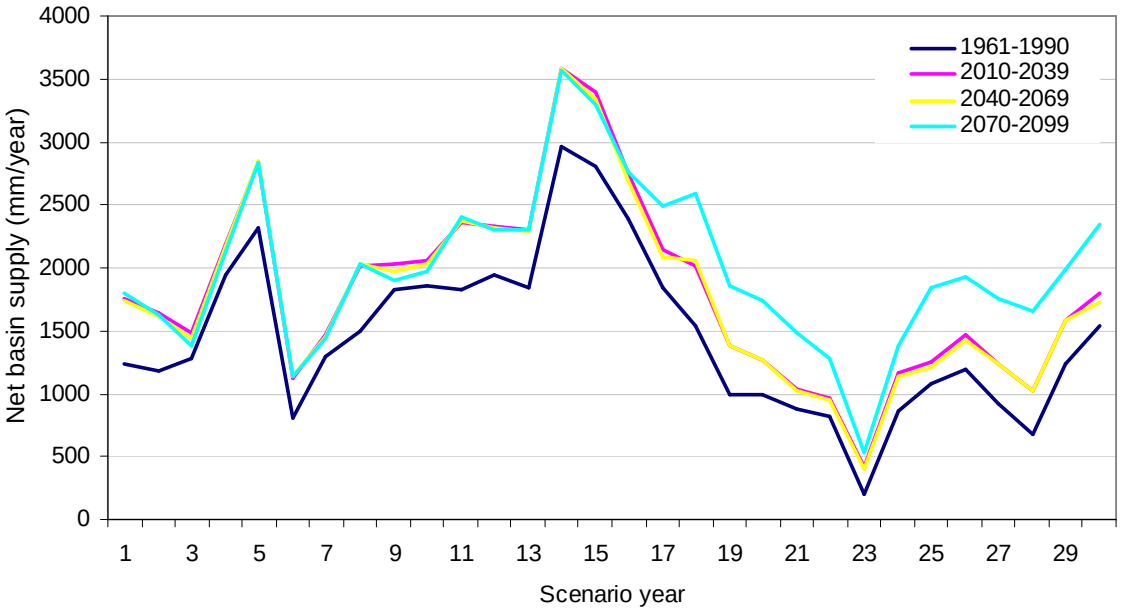

Figure 5-40: Net basin supply of Lake Tana water balance with HadCM3A2a scenario output

The net basin supply of Lake Tana shows an increasing trend from the baseline period of 1961-1990. The average annual net basin supply is 1801, 1783 and 1991mm/year for the period of 2010-2039,

2040-2069 and 2070-2099 respectively with HadCM3A2a scenario output and the baseline period net basin supply is 1459 mm/year. The analysis of hydrology and water resources in on the Upper Blue Nile river basin under climate change by Kim and Kaluaranchchi (2008) also indicates that there is increasing of precipitation and runoff in Northern Amhara (North Ethiopia) which covers the Lake Tana catchment, in the future scenario periods as compared to the base line period. Therefore both result shows increase of precipitation and inflow in the Lake Tana basin for the future scenario periods.

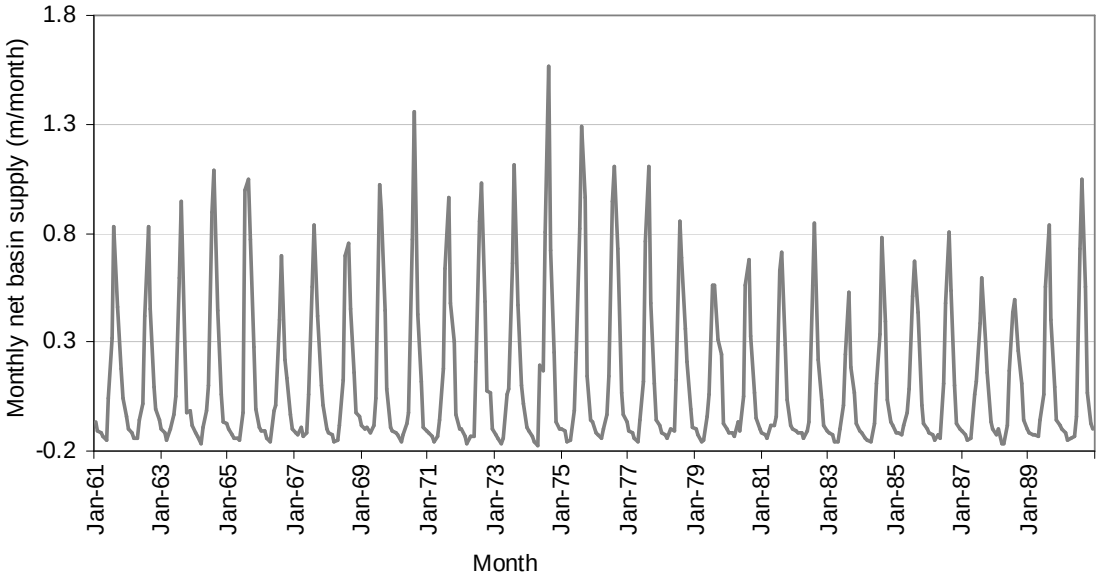

Figure 5-41: Monthly Net basin supply with HadCM3A2a scenario output

The monthly net basin supply with HadCM3A2a scenario output indicates that the net basin supply is high in the wet season from July to October while in the dry seasons from January to May it shows the lowest value. During dry months the net basin supply becomes negative since lake evaporation is higher than the sum of inflow to the lake and lake precipitation.

As it is shown in Figure 5-42 the net basin supply with HadCM3B2a scenario also indicates an increasing trend like the HadCM3A2a scenario output compared to the baseline period. The mean annual net basin supply is 1554, 1481, and 1530 mm/year for the period of 2010-2039, 2040-2069 and 2070-2099 respectively. But the increase in mean annual net basin supply is generally less as compared to HadCM3A2a model because of decrease of the annual lake precipitation and lake inflow.

In A2 scenario the future world becomes warmer than the B2 scenario because of increasing CO_2 concentration and hydrological cycle is likely to become more affected. Therefore the precipitation in A2 scenario is higher than B2 scenario. This increase in precipitation causes an increase in stream flow in future time periods and consequently the net basin supply become increase with A2 scenario than B2 scenario.

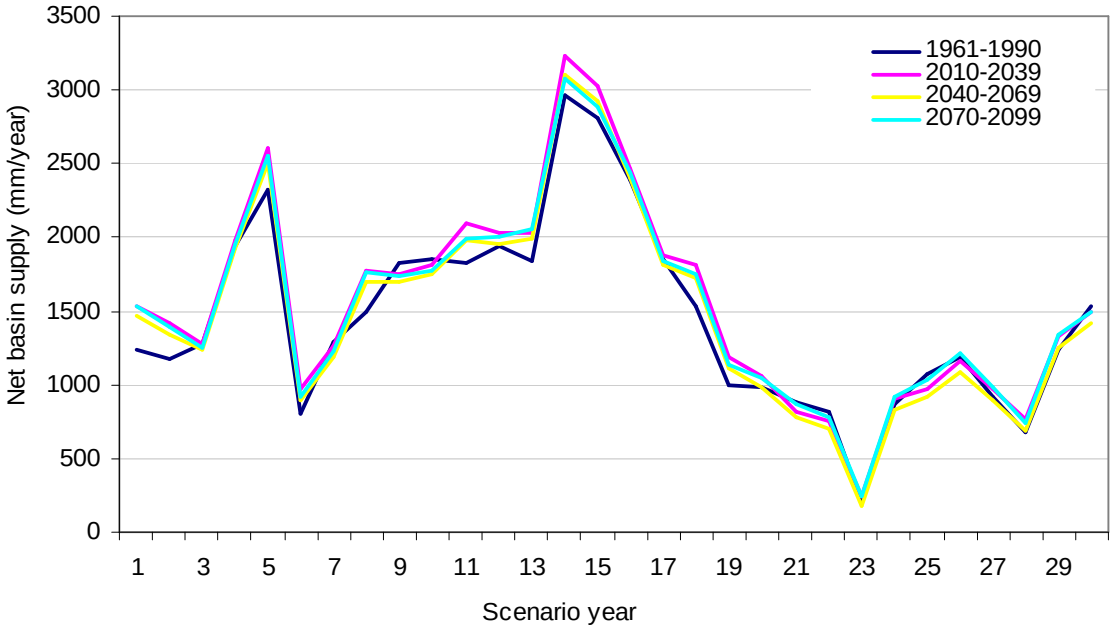

Figure 5-42: Annual net basin supply with HadCM3B2a scenario output

To analyse the effect of climate change on the net basin supply the mean monthly net basin supply for both scenario out put is made beside the annual net basin supply. As it is indicated in Figure 5-43 and Figure 5-44 the mean monthly net basin supply is 121.6, 129.5, 123.5 and 127.6 mm/ month for 1961-190, 2010-2039, 2040-2069 and 2070-2099 with HadCM3B2a scenario output. Like the mean annual net basin supply with this scenario the highest mean monthly net basin supply is observed in 2020s. The mean monthly net basin supply with HadCMEA2a scenario output is 121.6, 150.1, 148.6 and 166 mm for the period of 1961-1990, 2010-2039, 2040-2069 and 2070-2099 respectively. For both scenario output the mean monthly net basin supply shows an increasing trend as compared to the baseline period.

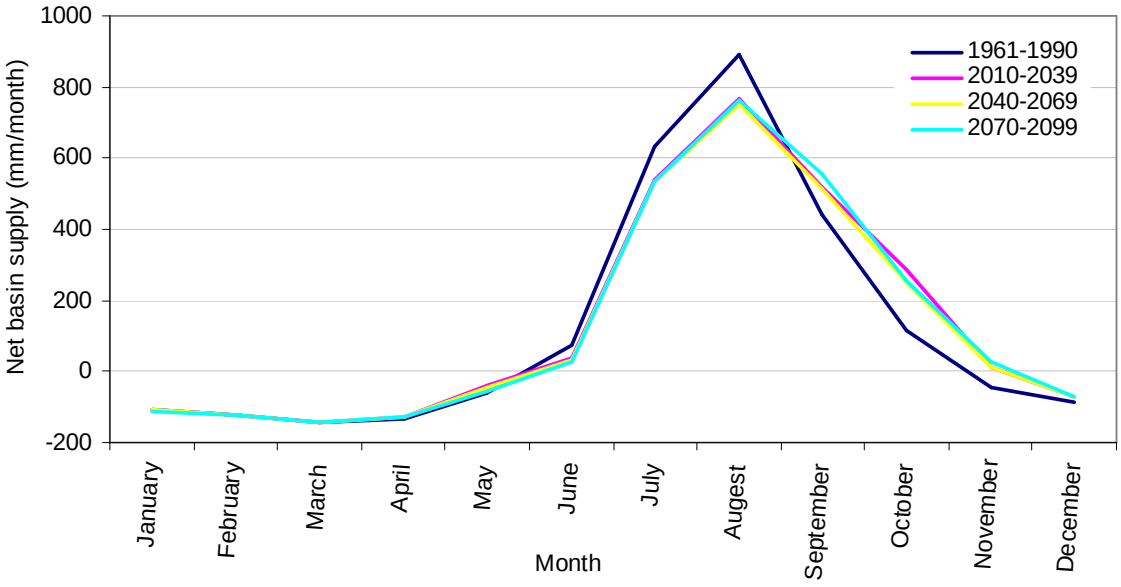

Figure 5-43: Mean monthly net basin supply with HadCM3B2a scenario output

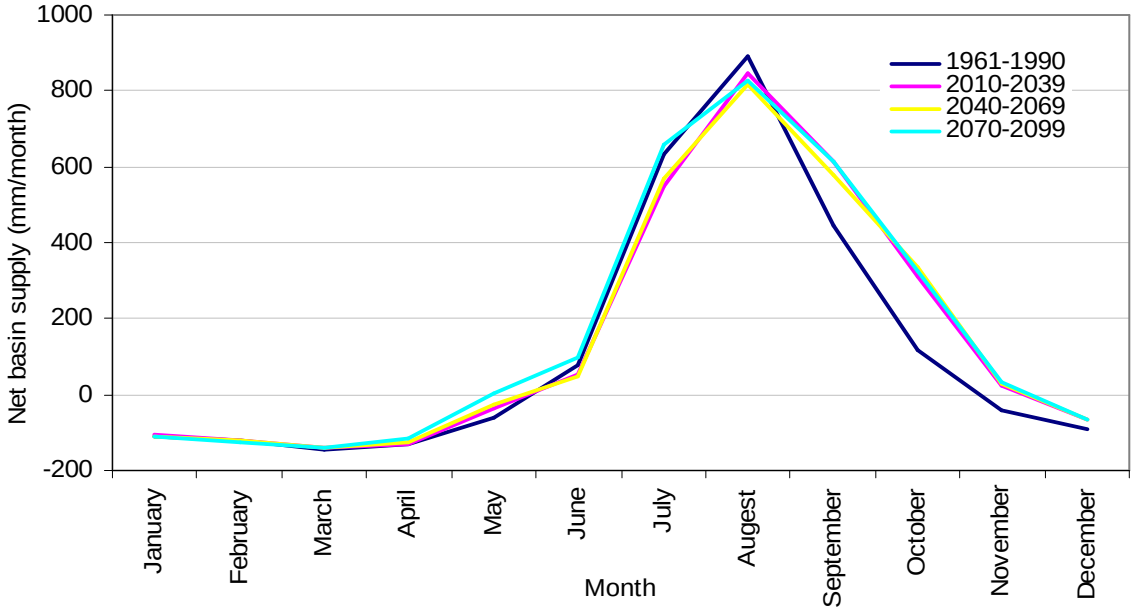

Figure 5-44: Mean monthly net basin supply with HadCM3A2a scenario output

5.7. Analysis on lake water balance

The water balance of the Lake Tana from 1997-2006 is estimated based the inflow and the outflow component of the Lake Tana. The inflow component is the sum of the lake areal precipitation and inflow from gauged and unguagde rivers. The outflow component is the sum of the lake areal evaporation and outflow from the lake. The lake level is simulated by the area-volume and elevation-volume relation of (Abeyou, 2008).

The lake evaporation is computed by Bahir Dar and Gonder meteorological data with Penman combination equation of Vallet-Coulomb et al. (2001) and the Lake areal precipitation is estimated by the surrounding five stations (see Figure: 5-45). The weight of each station for estimation of lake precipitation and lake evaporation is computed by inverse distance weighting method.

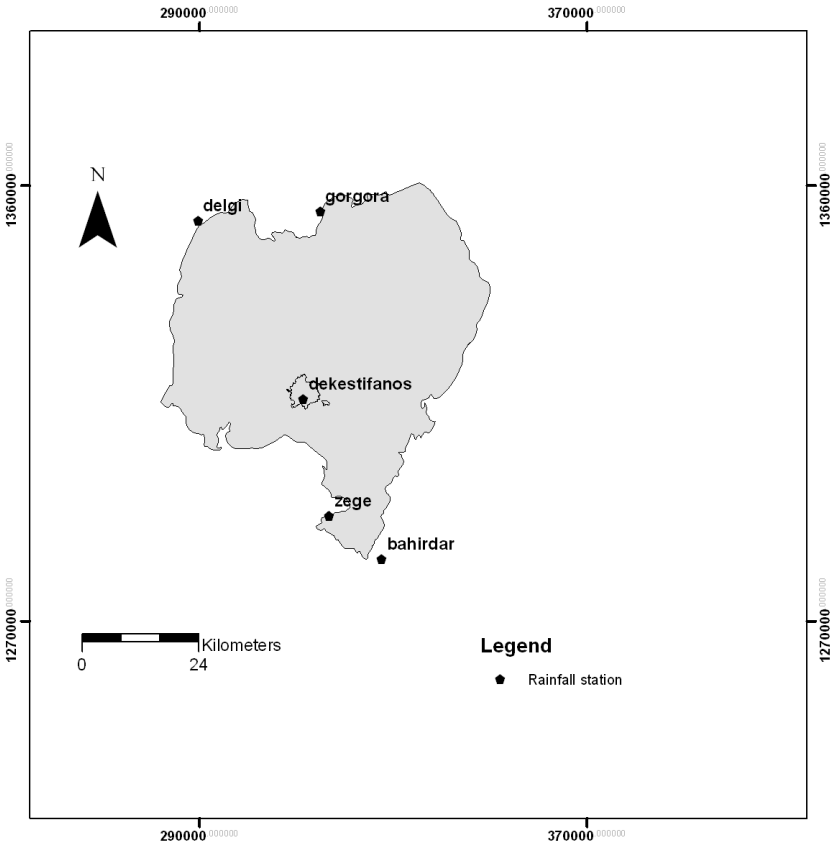

Figure 5-45: Rainfall stations for estimation of lake area precipitation

Table 5-7: Weight of rainfall station

Station	Weight
Bahir Dar	0.05
Delgi	0.1
Zege	0.08
Gorgora	0.2
Dek estifanos	0.57

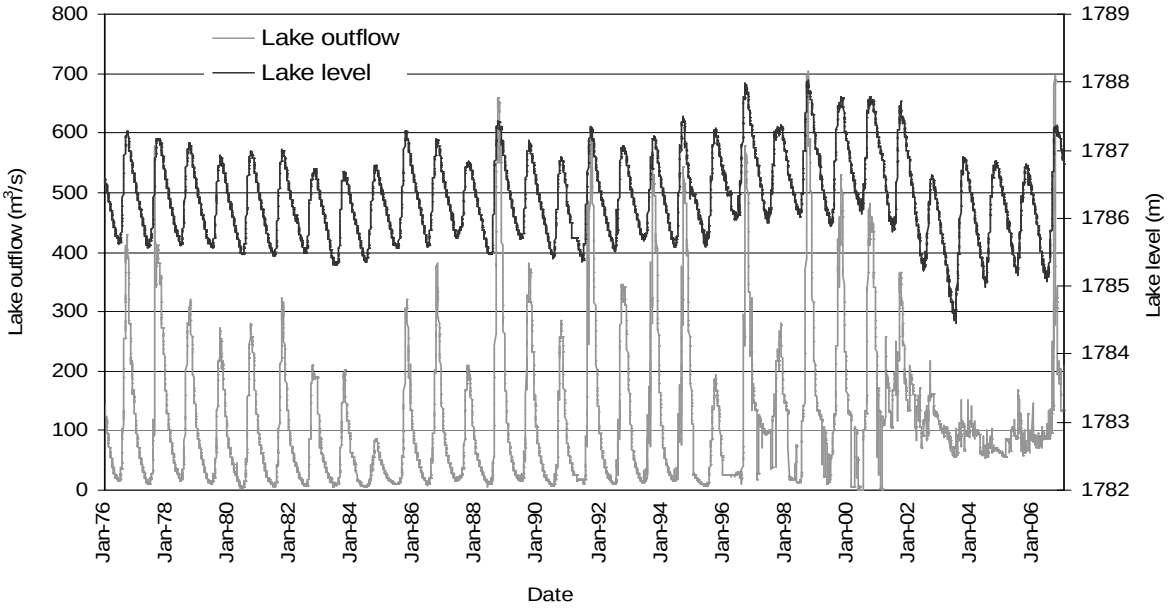

Figure 5-46: Lake level and lake outflow of Lake Tana (1976-2006)

In Lake Tana the low height weir is constructed in 1996 at Chara-chara across the Abbay River at the outlet of the lake. The weir operation begins in 2002 to supply the water to Tis-Abbay hydropower plant. After this period the lake level decreases dramatically and reaching the historic minimum level of 1784.46 mm in 6/30/2003 (Abeyou, 2008). The outflow from the lake is maximum during the wet season and minimum during the dry season of the year but after the operation of the weir the trend shows an erratic pattern since the water is diverted to the hydropower before reaching the outflow gauging station.

In order to see the impact of climate change on the lake level and the lake outflow it is necessary to observe the trend before the construction of the weir. The outflow and the lake level in dry season of the years have almost the same trend. But as it is indicate in the Figure 5-46 the outflow of the lake in wet season become the lowest value in 10/5/84. This year was the drought year in Lake Tana basin due to the decrease in precipitation. This decrease in precipitation and outflow is the result of climate change.

The general water balance equation for simulation of the lake level is as follow:

$$\frac{\Delta S}{\Delta T} = \left(P + SI_{guaged} + SI_{unguaged}\right) - \left(E_o + S_o\right) \quad [5\text{-}1]$$

Where:

$\frac{\Delta S}{\Delta T}$ = change in storage with time

P = precipitation

SI_{guaged} = sum of gauged inflow

$SI_{unguaged}$ = sum of unguagde inflow

E_o = lake evaporation

S_o = lake outflow

The FORTRAN code (obtained from personal communication of Janaka) is used in order to calculate the lake level using lake volume based on the polynomial interpolation of (Abeyou, 2008). Based on these water balance components the change in storage is calculated by using an initial value of storage for the programme. After that the change in storage is converted to the lake level and the lake area. The lake area is used for computation of the volume of lake precipitation and lake evaporation for the next time step using the daily observed data. In such away the lake level is computed with iteration for a series of time steps.

$$V_{Lake(i)} = V_{Lake(i-1)} + \Delta S_{(i)} \quad [5\text{-}2]$$

Where:

$V_{Lake(i)}$ = Lake total volume at day i, $V_{Lake(i-1)}$ = Lake total volume at day $i-1$ and $\Delta S(i)$ = change in storage at day i.

Table 5-8: Water balance component of Lake Tana (1997-2006)

Water balance components	mm/year	MCM/year
Lake preciptation	+1381	+4227
Guaged river inflow	+1313	+4018
Unguaged river inflow	+648	+1983
Lake evaporation	-1729	-6380
Lake outflow	-1447	-4430
Closure term	-166	-508

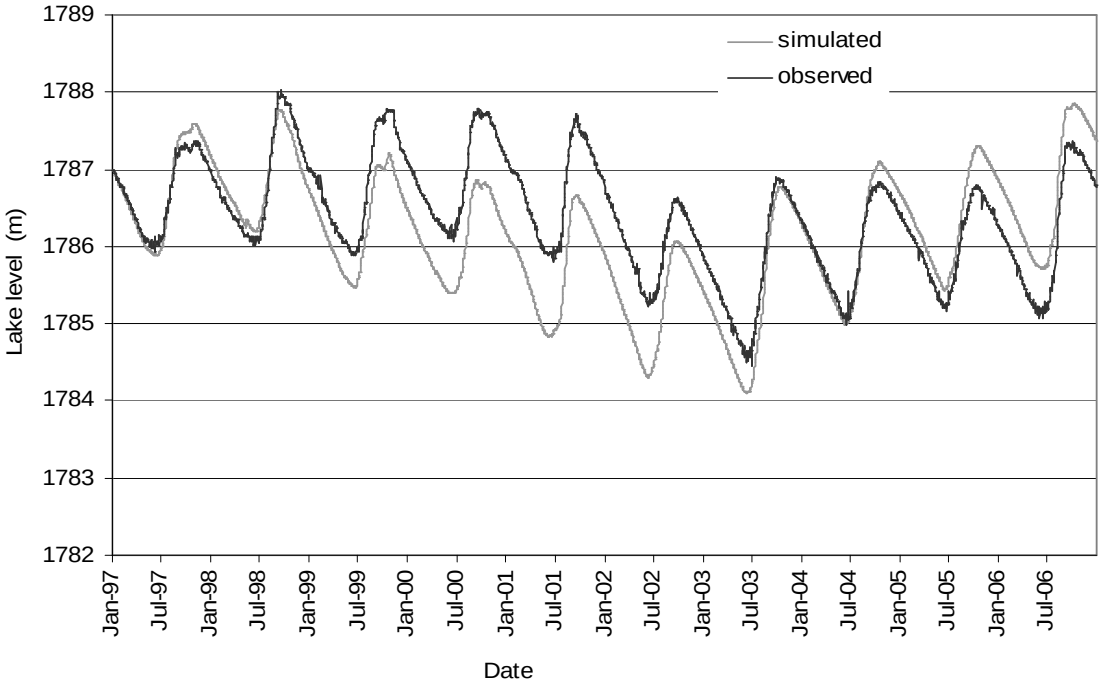

Figure 5-47: Simulation of Lake Tana water level (1997-2006)

The closure term indicates the water balance error is 5 % and the relative volume error of 1 %. The Nash-Sutcliffe coefficient is 0.70.

Table 5-9: Water balance components of (Abeyou, 2008), (Gieske et.al , 2008) and (SMEC, 2007)

	Wale (2008)		Gieske et.al (2008)		SMEC (2007)	
Water balance terms	mm	MCM	mm	MCM	mm	MCM
Lake areal rainfall	1220	3784	1255	3891	1260	3906
Guaged river inflow	1280	3970	1297	4021	1622	5028
Unguaged river inflow	880	2729	473	1466	nd	nd
Lake evaporation	-1690	-5242	-1671	-5180	-1650	-5115
Outflow	-1520	-4714	-1348	-4179	-1231	-3813
Closure term	-170	-527	6	19	1	3

5.8. Uncertainty and sensitivity analysis

The HadCM3A2a and HadCM3B2a scenarios are the most widely used GCM in climate change impact studies. The temporal resolution of both models is monthly but hydrological models for forecasting of the future inflow to the lake requires daily precipitation and temperature. Therefore computation of the difference between the current and the future climate data and addition of this change to the 30 years daily data is the most widely used method. This technique is one of the sources of uncertainty because it assumes that the same anomalies persist every year, which might smooth inter annual variability of climate variables.

The other source of uncertainty in climate change impact assessment is the emission scenarios. For this study two emission scenarios (A2 and B2) are used. The CO_2 concentration for both scenarios in 1990 is 354 parts per million (ppm) but in 2050s the concentration increases to 536 ppm and 478 ppm with A2 and B2 emission scenarios respectively. But temperature increase as a result of increase in CO_2 concentration for both scenarios is 1.4 ^oC compared to the 1990 temperature. There are also other emission scenarios with the same emission of carbon dioxide concentration produces different climate change scenarios.

In addition to the climate change scenarios synthetic scenarios is used for this study to determine the sensitivity of the climate variables for the net basin supply of Lake Tana water balance. This scenario is based on the increasing of the baseline temperature and the precipitation by an arbitrary but reasonable amount to check the sensitivity of the net basin supply for the climate variables.

Table 5-10: Change of Annual average net basin supply with incremental scenario

Scenario number	S-1	S-2	S-3	S-4	S-5	S-6	S-7	S-8	S-9	S-10	S-11
Change in Precipitation (%)	0	0	0	-10	10	-20	20	-10	10	-20	20
Change in Temperature (^oC)	1	2	3	1	1	1	1	2	2	2	2
Change in Evaporation (%)	2.7	5.4	8.2	2.7	2.7	2.7	2.7	5.4	5.4	5.4	5.4
Change of net basin supply (%)	-7.4	-15	-21	-39	44.6	-69	59	-45	17	-75	33

The sensitivity analysis result indicates that an increase in 1^oC in temperature reduces the annual average net basin supply by 7.4 % but the increase in 1^oC and a reduction of precipitation by 10 % reduces the average net basin supply by 38.7%. In the same way the percentage change in precipitation in the whole scenario shows significant changes to the average annual net basin supply as compared to the change in temperature. This indicates that net basin supply for Lake Tana is more sensitive to precipitation than temperature.

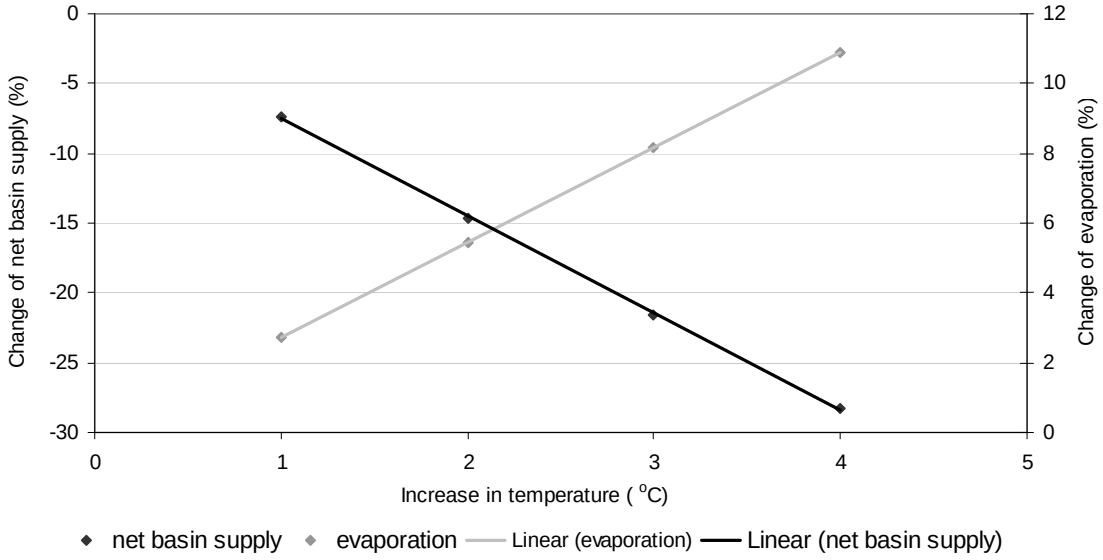

Figure 5-48: Annual average change of net basin supply and evaporation for change of temperature

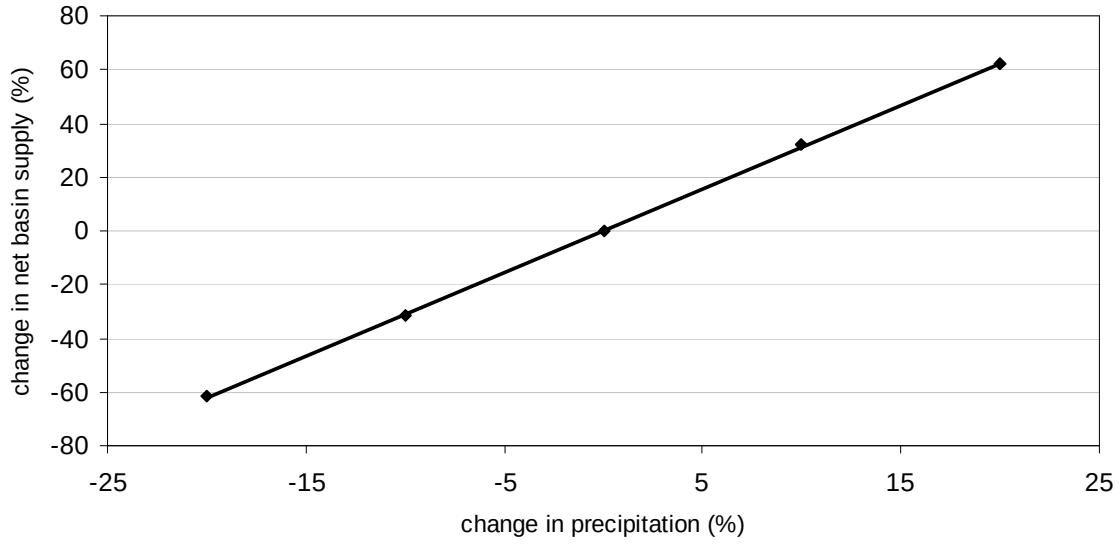

Figure 5-49: Annual average change of net basin supply for change of precipitation.

As it is indicated in Figure 5-48 and Figure 5-49 the decrease of precipitation by 10 % and 20 % reduces the annual mean net basin supply by 32 % and 62 % respectively and the same percentage increase in precipitation results increases of the net basin supply by 32 % and 62 %. The increase in temperature by 1, 2 and 3 °C decreases the mean annual net basin supply by 7, 15 and 21 % respectively. This shows the change in precipitation is more sensitive than change in temperature for annual average net basin supply. The change in temperature also causes the change in evaporation. Therefore the sensitivity analysis is made for the mean annual evaporation of Bahir Dar and Gonder station due to increase in temperature from the baseline period. The sensitivity result indicates an increase of 1°C, 2 °C, 3 °C and 4 °C for the both maximum and minimum temperature results the increases of the evaporation by 2.7%, 5.4%, 8.2% and 10.9 % respectively.

6. Conclusions and Recommendations

6.1. Conclusions

The objective of this study is the assessment of climate change impact on the net basin supply of Lake Tana water balance. Therefore downscaling of large scale climate variables from GCM outputs to local scale or regional scale is very essential in order to investigate the hydrological impact of future climate change scenarios. For this study regression based statistical downscaling methods which correlate the predictors (regional climate variables) and the predictand (local scale climate variable) with multiple linear regression equation is applied. The precipitation and temperature data of Bahir Dar, Gonder and Debre Markos is used for downscaling.

The study confirmed that the statistical downscaling model is able to simulate all climatic variables. The model simulates the maximum temperature and minimum temperature more accurately than precipitation. However all simulated climatic variables follow the same trend with the observed one. The lower performance of the precipitation simulation is based on its nature of being a conditional process.

The result of the downscaling models indicates that the mean monthly maximum temperature is increasing by 0.5, 1 and 1.5 ^{o}C in 2020s, 2040s and 2070s respectively for HadCM3B2a scenario out put. For HadCM3A2a scenario output the maximum temperature also increases by 0.52, 1.2 and 2.1^{o}C in 2020s, 2040s and 2070s respectively compared to the base line period (1961-1990). The increase in mean monthly minimum temperature 0.66, 1.13 and 1.75 ^{o}C for the HadCM3B2a scenario and for HadCM3A2a scenario the increase is 0.65, 1.4 and 2.35^{o}C in 2020s, 2040s and 2070s respectively. As a result of increase in maximum and minimum temperature the lake evaporation also increases as compared to the baseline period. The lake evaporation based on the HadCM3A2a scenario output indicates that the mean annual evaporation is 1685, 1706 and 1741 mm in the period of 2020s, 2040s and 2070s respectively. The lake evaporation based on the baseline climate variable is 1674 mm/year.

The downscaled result of precipitation indicates that the mean monthly precipitation is increases by 15.5, 17.8 and 17.4 % for HadCM3B2a scenario output in 2020s, 2040s and 2070s respectively. For HadCM3A2a scenario output the increase in precipitation is 13.6, 18.5 and 24.8 % in 2002s, 2040s and 2070s respectively. This increase in precipitation in the future causes for increasing in lake precipitation and inflow to Lake Tana. The analysis made on the mean annual lake precipitation indicates that the lake precipitation is 1425mm, 1444 mm and 1540 mm/year for the HadCM3B2a scenario output in 2020s, 2040s and 2070s and this increase in precipitation for HadCM3A2a scenario output is 1360 mm, 1361 mm and 1386 mm in the same periods. The lake precipitation in the base line period is 1312 mm/year.

The ultimate objective of the study is the assessment of climate change impact on the net basin supply of the Lake Tana water balance. Then a hydrological model is required in order to forecast the inflow

to the lake based on the downscaled climate variables. For this the HBV-96 is selected because the model is tested by many countries for climate change impact studies, it is applicable for different geographical and climatological regions and it is easily available.

The hydrological analysis indicates that the mean annual inflow to the lake is 1878mm, 1848mm and 1866 mm for the HadCM3B2a scenario and 2062 mm, 2045 mm and 2192 mm with HadCM3A2a scenario in 2020s, 2040s and 2070s respectively. The mean annual inflow for the baseline period is 1821mm/year. The inflow estimated by HadCM3B2a scenario output is less compared to the HadCM3A2a scenario outputs. This is because the downscaled precipitation by HadCM3B2a scenario for all the station is less than the precipitation downscaled by the HadCM3A2a scenario.

The net basin supply in the future time is computed based on the lake evaporation, the lake precipitation and the inflow to the lake. Even though all component of the net basin supply shows an increasing trend, the lake evaporation is obscured by the increase in inflow and lake precipitation. The mean annual net basin supply of Lake Tana based on the HadCM3A2a scenario output is 1801mm, 1783 mm and 1991 mm in 2020s ,2040s and 2070s respectively while the net basin supply within these successive periods for HadCM3B2a scenario output is 1554, 1481 and 1530. For the baseline period the mean annual net basin supply is 1459 mm.

The water balance estimation of the Lake (1997-2006) indicates that the mean annual lake precipitation is 1381 mm, gauged inflow is 1313 mm, unguaged inflow is 648 mm, lake evaporation is 1729mm and outflow is 1447 mm. The contribution of the unguaged inflow is 37 % of the total inflow discharge to the lake. In Lake Tana the operation of the weir to deliver water to the hydropower project is begin in 2002. Then it is difficult to observe the impact of climate change on the outflow and lake level after this period because the water balance components are influenced by supply to the hydropower plant. But the outflow of Lake Tana was the lowest record in 1984 before the weir construction. At that time the precipitation of the Lake Tana catchment is decline due the climate change impact.

The sensitivity analysis made with the incremental scenario method indicates that the net basin supply of Lake Tana is sensitive to climate change impact. The increase in temperature by $1^{o}C$ and $2^{o}C$ reduce the net basin supply by 7.4 % and 15 % from the baseline period net basin supply while the decrease in precipitation by 10 % and 20 % reduces the net basin supply by 32 % and 62 % from the baseline net basin supply. The sensitivity analysis made for evaporation indicates that the increase of temperature by 1 ^{o}C , 2 ^{o}C , 3 ^{o}C , and 4 ^{o}C increase the evaporation by 2.7%, 5.4%, 8.2% and 10.9 % respectively. Generally the sensitivity result indicates that the net basin supply is more sensitive to precipitation change than change in temperature.

6.2. Recommendations

The GCM outputs, the emission scenarios and the downscaling methods used for this study have certain level of uncertainty. Therefore further studies should reduce the uncertainty by the use of different GCM outputs, downscaling methods and emission scenarios. The use of several general circulation models for climate change studies able to get the better result. Further downscaling methods especially improves the simulation of the precipitation result is very essential. In this study only two emission scenarios are applied but in the actual case all SRES emission scenarios have equal probability of occurrence, then the future study should also consider the entire range of possible emission scenarios.

For downscaling of climate variables with statistical downscaling model only maximum temperature, minimum temperature and rainfall data of Bahir Dar, Gonder and Debre Markos stations are applied. But these stations are not sufficient for downscaling of the entire Lake Tana basin. Therefore further studies should consider other stations data. Besides, this study can be extended by considering change in land used, soil type and other climate variables in addition to the change in precipitation and temperature.

References:

Abdo Kedir, S., 2008. Assessment of climate change impacts on the hydrology of Gilgel Abbay catchment in Lake Tana basin, Ethiopia, ITC, Enschede, 72 pp.

Abeyou, W., 2008. Hydrological balance of Lake Tana upper Blue Nile basin, Ethiopia, ITC, Enschede, 94 pp.

Allen, R.G., Pereria, L.S., Rase, D. and Smith, M., 1998. Crop Evaporanspiration: FAO Irrigation and Drainage Paper No.56 326pp.

Bergström, S. and Graham, L.P., 1998. On the scale problem in hydrological modeling. Journal of Hydrology, 211(1-4): 253-265.

Booij, M.J., 2005. Impact of climate change on river flooding assessed with different spatial model resolutions. Journal of Hydrology, 303(1-4): 176-198.

Carter, T.R.,2007. General guide lines on the use of scenario data for climate impact and adaptation assessment. Finnish Environmental Institute, Helsinki, Finland.

Clair , E. Hanson, Tom Holt and Jean P Paluikof, February 2004. An Integrated Assessment of the potential for change in storm activity over Europe: Implications for insurance and forestry in the UK .Tyndall centre for climate change research technical report12, 10-11pp.

Conway, D., 2000. The Climate and Hydrology of the Upper Blue Nile River. The Geographical Journal, 166: 49-62.

Das, T., Bárdossy, A., Zehe, E. and He, Y., 2008. Comparison of conceptual model performance using different representations of spatial variability. Journal of Hydrology, 356(1-2): 106-118.

Dawson, C.W. & Wilbey, R.L., 2007. Statistical Downscaling Model, version 4.2. Department of Geography , Lancaster University, UK.

deBoer, B., 2007. Climate change and impacts on the extreme rainfall over the Blue Nile region. KNMI, Royal Netherlands Meteorological Institute, De Bilt, Netherlands.

Dibike, Y.B. and Coulibaly, P., 2005. Hydrologic impact of climate change in the Saguenay watershed: comparison of downscaling methods and hydrologic models. Journal of Hydrology, 307(1-4): 145-163.

Gieske, Abeyou, W., Getachew, HA., Alemseged TH., Rientjes, T.H.M, 2008. Non-linear parameterization of Lake Tana flow system.Hydrology and ecology of Nile River Basin under extreme conditions, Wossenu Abtew, Assefa M. Melesse (eds). Proceeding of the workshop, Addis ababa, 2008; 128-145.

Goodess, C.M., Osborn, C.T., Hulme, M. and Tyndall Centre for Climate Change, R., 2003. The Identification and Evaluation of Suitable Scenario Development Methods for the Estimation of Future Probabilities of Extreme Weather Events. Tyndall Centre for Climate Change Research.

Hay, L.E. and Clarck, M.P., 2003. Use of statistically and dynamically downscaled atmospheric model output for hydrologic simulations in three mountainous basins in the western United States. Journal of Hydrology , 282 (1-4) : 56-75.

Kaba Ayana, E., 2007. Validation of radar altimetry lake level data and it's application in water resource management, ITC, Enschede, 76 pp.

Kebede, S., Travi, Y., Alemayehu, T. and Marc, V., 2006. Water balance of Lake Tana and its sensitivity to fluctuations in rainfall, Blue Nile basin, Ethiopia. Journal of Hydrology, 316(1-4): 233-247.

Krysanova, V., Bronstert, A. and Müller-Wohlfeil, D.-I., 1999. Modelling river discharge for large drainage basins: from lumped to distributed approach. Hydrological Sciences Journal, 44: 313-331

Luis, A.J. and Pandey, P.C., 2005. Characteristics of atmospheric divergence and convergence in the Indian Ocean inferred from scatterometer winds. Remote Sensing of Environment, 97(2): 231-237.

Maidment, D.R., 1993. Handbook of Hydrology, McGraw-Hill.

Menzel, L. and Bürger, G., 2002. Climate change scenarios and runoff response in the Mulde catchment (Southern Elbe, Germany). Journal of Hydrology, 267(1-2): 53-64.

Mujumdar, P.P., 2008. Implications of climate change for sustainable water resources management in India. Physics and Chemistry of the Earth, Parts A/B/C, 33(5): 354-358.

Palmer, Richard N., Erin Clancy , Nathan T. Van Rheenen, and Mattew W.Wiley, 2004. The impacts of climate change on the Tualatine River basin water supply: An investigation into projected hydrologic and management impacts. Department of civil and environmental engineering, University of Washington, 67pp.

Rientjes, T.H.M., 2007. Modelling in hydrology. Department of water resources, ITC, Enschede.

Seibert, J., 2002. HBV light: version 2 User's Manual. Department of Earth Science, Hydrology, Uppsala University, Sweden.

SMHI, 2006. Integrated Hydrological Modelling System Manual, Version 5.1.

SMEC International Pty Ltd, 2007. Hydrological Study of the Tana-Beles Subbasins Interim Report, Snowy Mountain Engineering Corporation, Australia, 77pp.

Ungtea Kim and Jagath Kaluarachchi., 2008. Analysis of hydrology and water resources of the Upper Blue Nile river basin under climate change. Hydrology and Ecology of the Nile river basin under extreme conditions, Wossenu Abtew, Assefa M. Melesee (eds). Proceeding of the workshop, Addis ababa, 2008; 15-34.

Vallet-Coulomb, C., Legesse, D., Gasse, F., Travi, Y. and Chernet, T., 2001. Lake evaporation estimates in tropical Africa (Lake Ziway, Ethiopia). Journal of Hydrology, 245(1-4): 1-18.

Wilby, R. et al., 2004. Guidelines for use of climate scenarios developed from statistical downscaling methods. IPCC Data Distribution Centre Report, UEA, Norwich, UK, 27.

Annexes:

Appendix A : Catchment extraction procedures

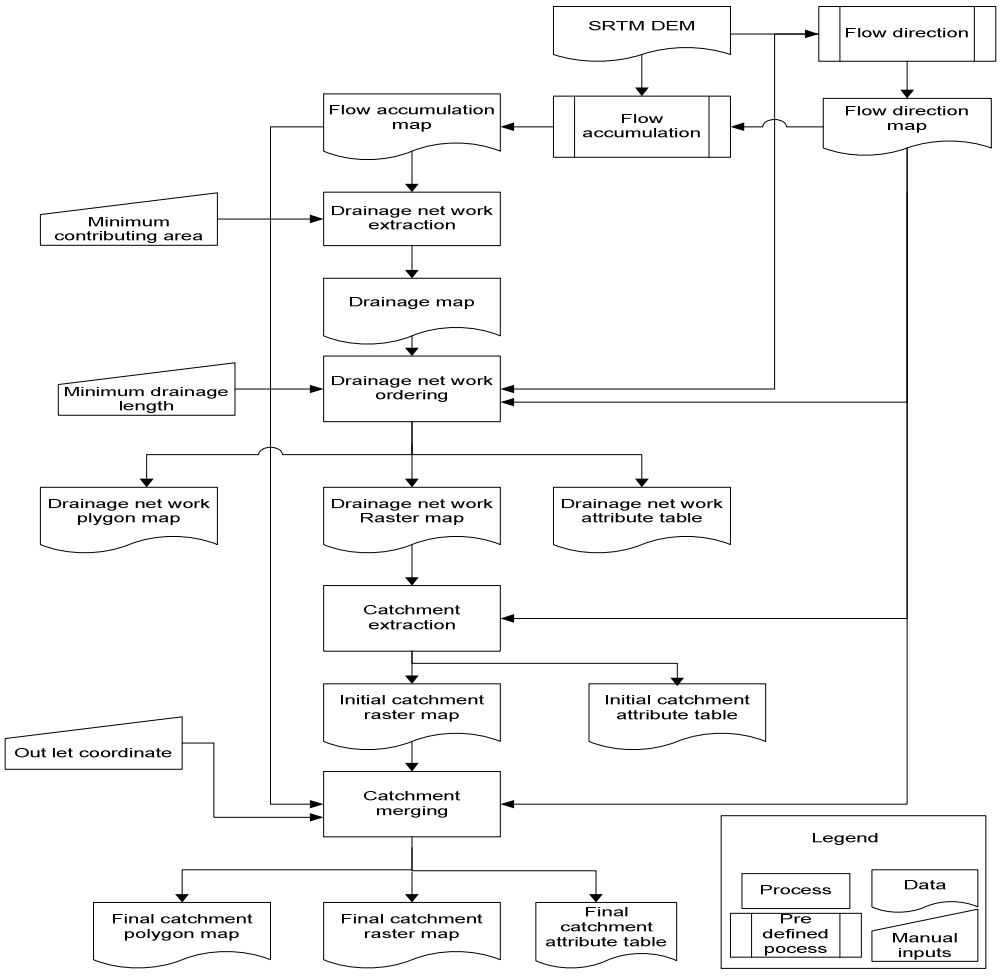

Appendix B: Hydrological and meteorological station and their location

Hydrological stations and their locations

River	Guaging station	Latitude (utm)	Longitude (utm)	outlet elevation (m amsl)
Gilgel Abbay	Near Merawi	285380.315	1257135.310	1889
Koga	At Merawi	287199.781	1257123.048	1898
Kelti	Nera Delgi	276374.243	1270104.996	1876
Ribb	Near Addis Zemen	360283.969	1326759.723	1796
Gumara	Near Bahir Dar	351119.160	1308370.538	1794
Megech	Near Azezo	331552.842	1380369.401	1865
Gemero	Near Maksegnit	342362.313	1369247.425	1879
Garno	Near Enfranze	349525.939	1352618.885	1856
Gelda	Near Ambesame	351605.015	1404223.536	2036

Meteorological stations and their location

Staions	Longitude (utm)	Latitude (utm)	Elevation (m amsl)
Addis zemen	1376576.884	376576.884	2117
Debre Tabour	1309918.026	401873.898	2714
Gondar	1387682.311	327881.649	2074
Bahir Dar	1282605.753	325456.442	1828
Dangila	1245380.969	265187.251	2126
Sekella	1216350.924	305057.004	2584
Enjibara	1212886.813	270418.731	2580
Gundil	1210918.62	288991.214	2546
Adet	1245695.593	332531.137	2230
Kidamaja	1216653.109	259512.914	2456
Abbay Sheleko	1259013.797	267107.339	2000
Enfranze	1346966.733	356659.457	1889

Appendix C: Catchment characteristics of unguaged catchment

Sub catchment	Area	Hypsometric Integral	Average Slope %	% Level	% Hilly	% Steepy	Average Elevation (m amsl)
Gelda	356.1	0.48	17.91	69.64	29.23	1.13	2116
Unguaged Gumara	517.3	0.39	17.29	79.04	20.28	0.69	2010
Unguaged Ribb	711.5	0.46	35.19	64.29	27.15	8.56	2421
UnguagedMegechh	462.3	0.43	18.03	76.72	22.30	0.98	2237
Unguaged Gilgelabbay	1991	0.45	19.93	89.83	9.21	1.93	2186
Garno	256.5	0.46	37.65	28.89	41.03	30.08	2337
Gumero	389.9	0.5	34.04	52.56	31.13	16.3	2313
Derma	376	0.48	16.6	72.78	26.46	0.76	2144
Gabikura	382.5	0.49	14.53	84.18	15.45	0.37	2002
Tana west	610.6	0.49	20.91	59.87	38.11	2.02	2038

Sub catchment	% of Leptosols	% of Nitisols	% of Luvisols	% of Vertisols	% of Fluvisols	Elongation Ratio	Length of longest flow path
Gelda	0.74	0.00	96.74	2.52	0.00	1.88	42.42
Unguaged Gumara	0.30	0.00	50.32	26.82	22.56	0.60	14.83
Unguaged Ribb	28.56	0.56	9.08	14.46	47.35	0.58	17.53
Unguaged G.Abbay	22.5	4.5	54.38	13.27	4.9	2.04	76.96
Ungauged Megech	17.48	0.00	12.40	50.09	20.0	1.42	34.93
Garno	59.51	6.64	2.95	21.53	9.37	1.73	37.03
Gumero	42.33	2.04	13.68	41.12	0.83	1.67	44.12
Derma	23.39	0.00	5.11	69.39	2.11	2.07	45.38
Gabi Kura	1.32	0.00	11.87	69.04	17.78	1.44	31.54
Tana west	0.10	0.00	39.21	2.79	57.89	0.72	20.34

Appendix D: Correlation coefficient between model parameters and catchment characteristics.

Alfa= 1.65-0.26 *Percentage of bare land -0.02*Percentage of hilly [1]

Beta =1.17+0.000808*Catchment area-0.014*Percentage of hilly [2]

FC=2142.81-0.803*Catchment area -17.33*Percentage of hilly [3]

K4=0.049-0.057*Hypsometric integral-o.001*Percentage of nitsols [4]
-0.001*Percentage of Fluvisols

Perc=-0.23 +0.36*log (Percentage of Luvisols) [5]
-0.114*log (Percentage of Bare Land)

KHQ=0.113-0.000036*Catchment area +0.000602*Percentage of luvisols [6]

LP=0.06+0.0006*Catchment area -0.12*Percentage of bare land [7]

Hq=4.64+0.0019*Catchment area -2.34 *Percentage of bare land [8]

NB.The unit of the catchment area is in Km^2

Appendix E: Double mass curve for some of gauged catchments and Rainfall Stations.

Double mass curve is the hydrological method used to analyse the consistence of precipitation and discharge. To check the consistency of the discharge data the cumulative daily rainfall with the cumulative daily discharge of Megech, Ribb, Gilgel Abbay, and Gumara are made in the excel. Beside this the cumulative daily rainfall of 10 stations are made with the cumulative rainfall of Bahir Dar station. Bahir Dar station is taken as the base station since it has long time series data and it is reliable.

In double mass analysis the cumulative rainfall is directly related the cumulative discharge. During the dry season the cumulative rainfall is almost constant since the daily rainfall is almost negligible. As a result the cumulative discharge could not show an increasing trend. If an increment of discharge with out rainfall distribution there may be a problem in the discharge record at that period. In same way there must be an increasing trend in the main wet season due to increasing rainfall. Generally by observing the trend of the cumulative rainfall and cumulative discharge it is possible to identify the problem in the discharge record.

The double mass curve between the base station (Bahir Dar) and other rainfall stations is used to identify the homoginty of the records between each other. Even tough the spatial distribution of the rainfall is different; the cumulative rainfall between the stations could not show an abrupt change. During the dry seasons both the base station and the other station records less amount of rainfall then the slope of the plot become almost zero. But in rainy seasons there is considerable amount of rainfall in both stations then the slope the plot become positive. With visual interpretation of the plot it is possible to identify where the error in rainfall record.

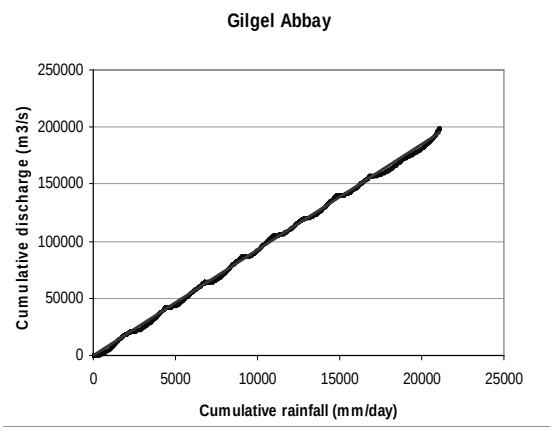

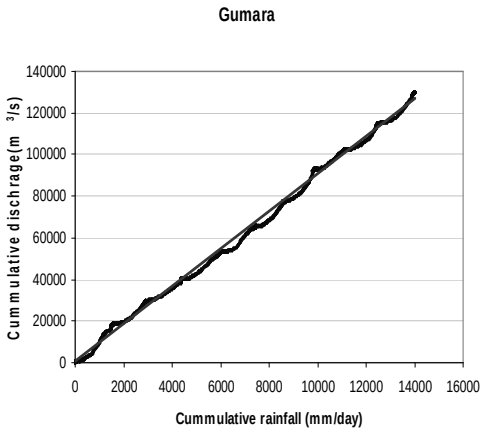

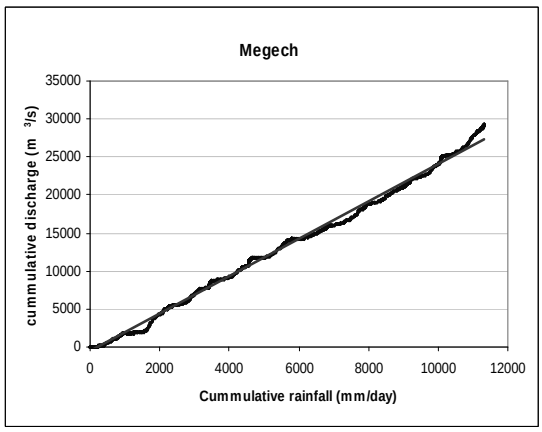
Megech
cummulative discharge (m 3/s)
35000
30000
25000
20000
15000
10000
5000
0
0
2000
4000
6000
8000
10000
12000
Cummulative rainfall (mm/day)

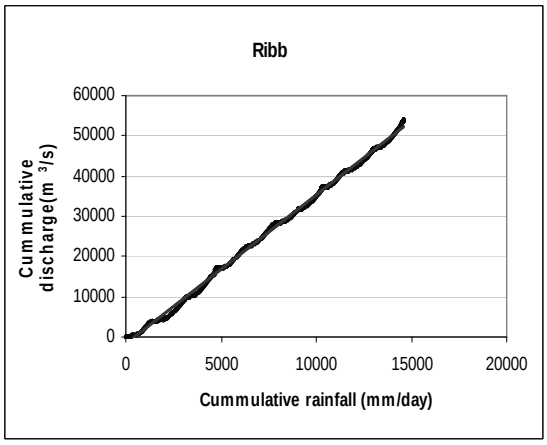
Ribb
Cummulative discharge(m 3/s)
60000
50000
40000
30000
20000
10000
0
0
5000
10000
15000
20000
Cummulative rainfall (mm/day)

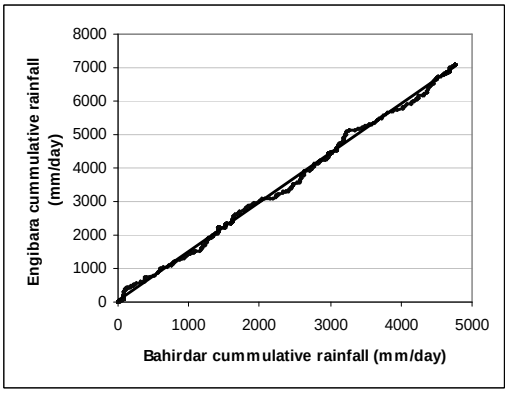
Engibara cummulative rainfall (mm/day)
8000
7000
6000
5000
4000
3000
2000
1000
0
0
1000
2000
3000
4000
5000
Bahirdar cummulative rainfall (mm/day)

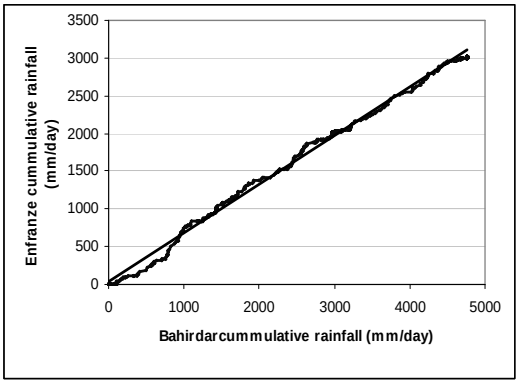
Enfranze cummulative rainfall (mm/day)
3500
3000
2500
2000
1500
1000
500
0
0
1000
2000
3000
4000
5000
Bahirdarcummulative rainfall (mm/day)

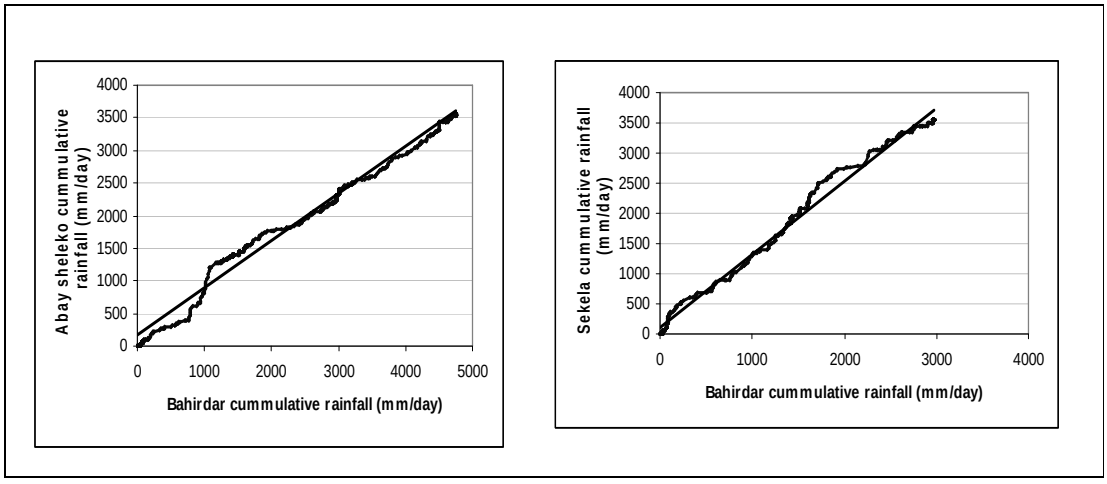
Abay sheleko cummulative rainfall (mm/day)
4000
3500
3000
2500
2000
1500
1000
500
0
0
1000
2000
3000
4000
5000
Bahirdar cummulative rainfall (mm/day)
Sekela cummulative rainfall (mm/day)
4000
3500
3000
2500
2000
1500
1000
500
0
0
1000
2000
3000
4000
Bahirdar cummulative rainfall (mm/day)

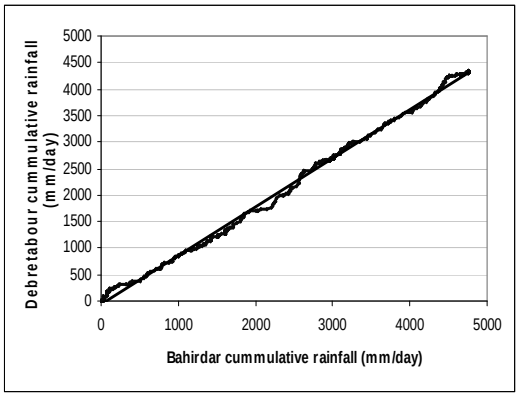
Debretabour cummulative rainfall (mm/day)
5000
4500
4000
3500
3000
2500
2000
1500
1000
500
0
0
1000
2000
3000
4000
5000
Bahirdar cummulative rainfall (mm/day)

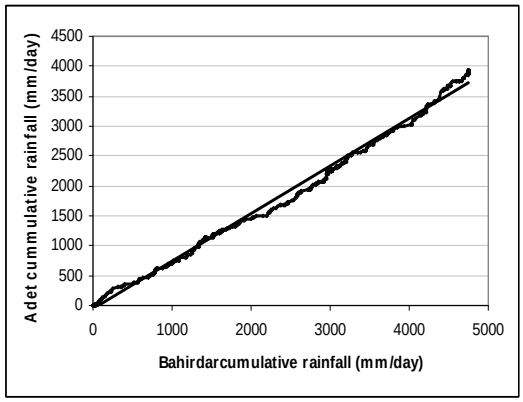
Adet cummulative rainfall (mm/day)
4500
4000
3500
3000
2500
2000
1500
1000
500
0
0
1000
2000
3000
4000
5000
Bahirdarcumulative rainfall (mm/day)

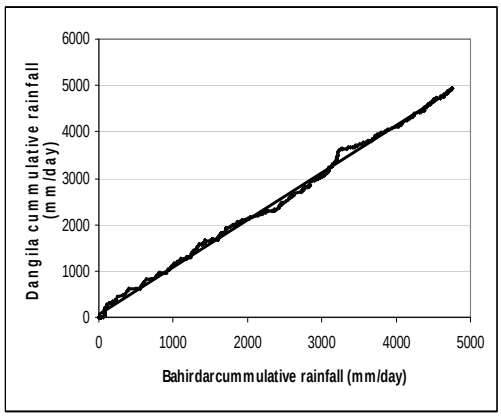
Dangila cummulative rainfall (mm/day)
6000
5000
4000
3000
2000
1000
0
0
1000
2000
3000
4000
5000
Bahirdarcummulative rainfall (mm/day)

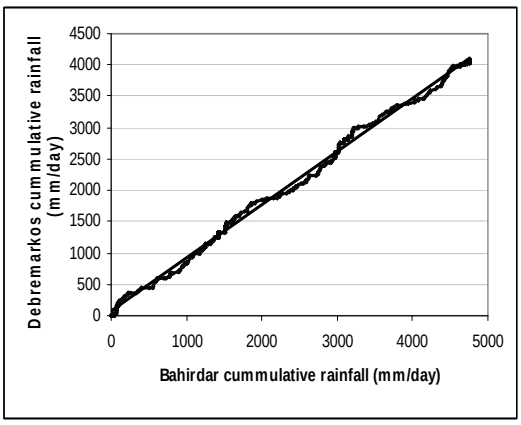
Debremarkos cummulative rainfall (mm/day)
4500
4000
3500
3000
2500
2000
1500
1000
500
0
0
1000
2000
3000
4000
5000
Bahirdar cummulative rainfall (mm/day)

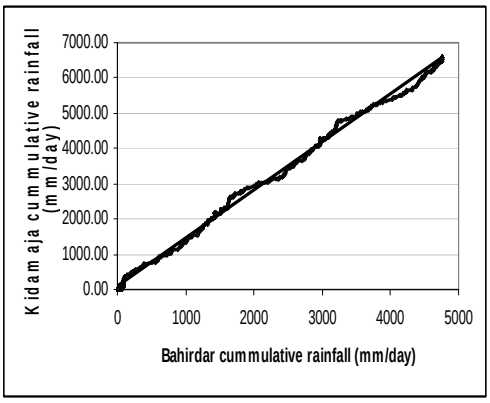
Kidamaja cummulative rainfall (mm/day)
7000.00
6000.00
5000.00
4000.00
3000.00
2000.00
1000.00
0.00
0
1000
2000
3000
4000
5000
Bahirdar cummulative rainfall (mm/day)

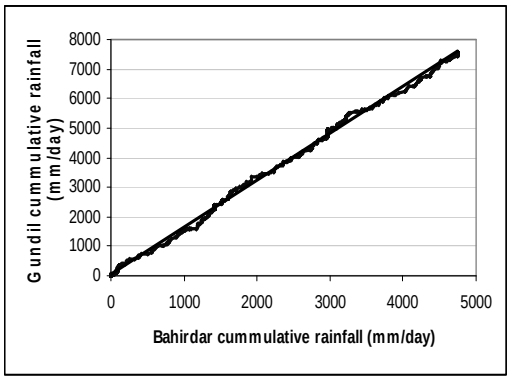
Gundil cummulative rainfall (mm/day)
8000
7000
6000
5000
4000
3000
2000
1000
0
0
1000
2000
3000
4000
5000
Bahirdar cummulative rainfall (mm/day)

Appendix F: Downscaled maximum temperature, minimum temperature and rainfall

Maximum temperature change with HadCM3A2a scenario output of Debre Markos station

Months	Monthly average maximum temperature (°C)					Temperature change compared to the 1961-1990 (°C)			
	1961-1990	1991-2006	2010-2039	2040-2069	2070-2099	1991-2006	2010-2039	2040-2069	2070-2099
January	24.41	24.04	24.88	25.40	26.15	-0.37	0.47	0.99	1.74
February	24.66	23.18	24.98	25.47	25.99	-1.48	0.32	0.81	1.33
March	25.05	25.74	25.54	26.01	27.07	0.69	0.49	0.96	2.02
April	25.06	24.42	25.38	25.69	26.22	-0.64	0.32	0.63	1.16
May	23.35	24.45	24.30	25.18	26.62	1.1	0.95	1.83	3.27
June	21.34	20.30	22.81	24.14	26.30	-1.04	1.47	2.80	4.96
July	19.14	18.88	19.56	19.99	20.64	-0.26	0.42	0.85	1.50
August	19.10	18.94	19.38	19.75	20.32	-0.16	0.28	0.65	1.22
September	19.73	19.87	20.01	20.27	20.58	0.14	0.28	0.54	0.85
October	21.33	21.82	21.91	22.50	23.23	0.49	0.58	1.17	1.90
November	22.04	22.11	22.50	23.04	23.79	0.08	0.46	1.00	1.75
December	22.60	23.45	23.02	23.62	24.27	0.85	0.42	1.02	1.67

Maximum temperature change with HadCM3B2a scenario output of Debre Markos

Months	Monthly average Maximum temperature (°C)					Temperature change compared to 1961-1990 (°C)			
	1961-1990	1991-2006	2010-2039	2040-2069	2070-2099	1991-2006	2010-2039	2040-2069	2070-2099
January	24.41	24.04	24.88	25.40	26.15	-0.37	0.48	0.99	1.74
February	24.66	23.18	24.98	25.47	25.99	-1.48	0.32	0.80	1.33
March	25.05	25.74	25.54	26.01	27.07	0.69	0.49	0.96	2.02
April	25.06	24.42	25.38	25.69	26.22	-0.64	0.32	0.63	1.16
May	23.35	24.45	24.30	25.18	26.62	1.10	0.94	1.83	3.27
June	21.34	20.30	22.81	24.14	26.30	-1.04	1.47	2.80	4.96
July	19.14	18.88	19.56	19.99	20.64	-0.26	0.42	0.85	1.50
August	19.10	18.94	19.38	19.75	20.32	-0.16	0.28	0.64	1.21
September	19.73	19.87	20.01	20.27	20.58	0.14	0.28	0.54	0.85
October	21.33	21.82	21.91	22.50	23.23	0.49	0.57	1.17	1.90
November	22.04	22.11	22.50	23.04	23.79	0.08	0.47	1.01	1.75
December	22.60	23.45	23.02	23.62	24.27	0.85	0.42	1.01	1.67

Minimum temperature change with HadCM3B2a scenario output of Debre Markos station

Months	Monthly average Minimum temperature (^{o}C)					Temperature change compared to 1961-1990 (^{o}C)			
	1961-1990	1991-2006	2010-2039	2040-2069	2070-2099	1991-2006	2010-2039	2040-2069	2070-2099
January	7.30	9.15	8.09	8.56	9.35	1.85	0.79	1.27	2.05
February	8.85	9.38	9.44	9.87	10.50	0.54	0.59	1.02	1.66
March	10.21	11.36	10.98	11.55	12.39	1.15	0.77	1.34	2.18
April	10.89	11.78	11.96	12.80	14.06	0.89	1.06	1.91	3.17
May	10.62	11.90	11.25	11.71	12.35	1.28	0.63	1.09	1.73
June	9.81	10.53	10.27	10.59	10.99	0.72	0.46	0.78	1.18
July	10.05	11.03	10.34	10.54	10.79	0.97	0.28	0.49	0.73
August	9.77	10.99	10.07	10.29	10.63	1.22	0.30	0.52	0.86
September	9.36	9.91	10.18	10.70	11.52	0.56	0.82	1.34	2.16
October	8.89	9.91	9.50	9.84	10.33	1.02	0.61	0.94	1.44
November	7.49	8.70	8.38	8.90	9.62	1.21	0.89	1.41	2.13
December	6.83	8.67	7.66	8.38	9.27	1.84	0.83	1.55	2.44

Minimum temperature change with HadCM3A2a scenario out put of Debre Markos station.

Months	Monthly average Minimum temperature (^{o}C)					Temperature change compared to 1961-1990 (^{o}C)			
	1961-1990	1991-2006	2010-2039	2040-2069	2070-2099	1991-2006	2010-2039	2040-2069	2070-2099
January	7.30	9.15	8.06	9.01	10.07	1.85	0.77	1.71	2.77
February	8.85	9.38	9.49	10.28	11.18	0.54	0.65	1.44	2.34
March	10.21	11.36	10.94	11.88	13.26	1.15	0.73	1.67	3.05
April	10.89	11.78	12.13	13.32	15.19	0.89	1.24	2.43	4.30
May	10.62	11.90	11.29	11.96	12.97	1.28	0.67	1.34	2.35
June	9.81	10.53	10.28	10.75	11.38	0.72	0.47	0.94	1.57
July	10.05	11.03	10.32	10.62	11.06	0.97	0.27	0.57	1.01
August	9.77	10.99	10.08	10.42	10.89	1.22	0.30	0.65	1.12
September	9.36	9.91	10.14	11.07	12.35	0.56	0.78	1.72	2.99
October	8.89	9.91	9.47	10.08	10.93	1.02	0.57	1.18	2.03
November	7.49	8.70	8.34	9.22	10.52	1.21	0.85	1.73	3.03
December	6.83	8.67	7.70	8.79	10.15	1.84	0.87	1.96	3.33

Precipitation change with HadCM3A2a scenario output of Debre Markos station

Months	Monthly average precipitation (mm/day)					Precipitation change Compared to 1961-1990 (%)			
	1961-1990	1991-2006	2010-2039	2040-2069	2070-2099	1991-2006	2010-2039	2040-2069	2070-2099
January	0.45	0.49	0.46	0.43	0.51	0.04	0.03	-0.03	0.13
February	0.76	0.34	0.63	0.75	0.74	-0.41	-0.17	-0.01	-0.03
March	1.49	1.49	1.42	1.61	1.47	0.00	-0.05	0.08	-0.02
April	1.90	2.61	1.75	1.93	1.90	0.71	-0.08	0.02	0.00
May	3.04	3.03	3.95	4.09	4.04	-0.01	0.30	0.35	0.33
June	5.20	5.54	5.33	5.21	4.93	0.34	0.03	0.00	-0.05
July	9.54	8.71	8.68	8.75	8.69	-0.83	-0.09	-0.08	-0.09
August	9.53	9.88	9.09	9.05	9.08	0.35	-0.05	-0.05	-0.05
September	6.92	7.05	6.56	6.43	6.35	0.13	-0.05	-0.07	-0.08
October	2.25	3.10	2.87	3.11	3.30	0.85	0.28	0.38	0.46
November	0.89	0.83	1.14	1.18	1.44	-0.06	0.28	0.34	0.63
December	0.49	0.73	0.61	0.57	0.63	0.24	0.25	0.16	0.27

Precipitation change with HadCM3B2a scenario output of Debre Markos station

Months	Monthly average precipitation (mm/day)					Precipitation change Compared to 1961-1990 (%)			
	1961-1990	1991-2006	2010-2039	2040-2069	2070-2099	1991-2006	2010-2039	2040-2069	2070-2099
January	0.45	0.49	0.38	0.43	0.39	0.04	-0.16	-0.05	-0.12
February	0.76	0.34	0.65	0.70	0.80	-0.41	-0.14	-0.08	0.06
March	1.49	1.49	1.32	1.45	1.42	0.00	-0.12	-0.03	-0.04
April	1.90	2.61	1.92	1.88	1.92	0.71	0.01	-0.01	0.01
May	3.04	3.03	4.01	4.05	4.11	-0.01	0.32	0.33	0.35
June	5.20	5.54	5.23	5.14	5.19	0.34	0.01	-0.01	0.00
July	9.54	8.71	8.88	8.78	8.78	-0.83	-0.07	-0.08	-0.08
August	9.53	9.88	9.08	9.15	9.15	0.35	-0.05	-0.04	-0.04
September	6.92	7.05	6.44	6.51	6.42	0.13	-0.07	-0.06	-0.07
October	2.25	3.10	2.98	3.04	2.80	0.85	0.32	0.35	0.24
November	0.89	0.83	1.21	1.20	1.21	-0.06	0.36	0.35	0.37
December	0.49	0.73	0.60	0.64	0.56	0.24	0.21	0.30	0.13

Maximum temperature change with HadCM3A2a scenario output of Bahir Dar station

	Monthly average					Temperature change			
	maximum temperature (^{o}C)					compared to 1961-1990 (^{o}C)			
Months	1961-1990	1991-2007	2010-2039	2040-2069	2070-2099	1991-2007	2010-2039	2040-2069	2070-2099
January	26.16	26.75	26.78	27.62	28.48	0.58	0.61	1.46	2.31
February	27.81	28.77	28.27	29.03	29.82	0.95	0.46	1.22	2.01
March	29.51	29.68	29.82	30.24	31.10	0.17	0.31	0.73	1.59
April	29.57	30.09	30.23	30.74	31.62	0.52	0.66	1.17	2.05
May	28.35	29.32	28.77	29.16	29.84	0.97	0.42	0.81	1.49
June	26.42	26.88	27.20	28.02	29.51	0.46	0.79	1.60	3.10
July	23.77	24.29	24.16	24.95	26.25	0.52	0.39	1.18	2.47
August	23.44	24.30	23.98	24.82	26.21	0.85	0.54	1.38	2.77
September	24.70	25.59	24.96	25.52	26.12	0.89	0.27	0.82	1.42
October	26.19	26.55	26.85	27.65	28.76	0.35	0.66	1.46	2.57
November	25.98	26.70	26.56	27.32	28.24	0.71	0.57	1.34	2.25
December	25.76	26.70	26.38	27.17	28.20	0.94	0.62	1.41	2.45

Maximum temperature change with HadCM3B2a scenario output of Bahir Dar station

	Monthly average					Temperature change			
	maximum temperature (^{o}C)					Compared to 1961-1990 (^{o}C)			
Months	1961-1990	1991-2007	2010-2039	2040-2069	2070-2099	1991-2007	2010-2039	2040-2069	2070-2099
January	26.16	26.75	26.84	27.24	27.88	0.58	0.67	1.04	1.71
February	27.81	28.77	28.20	28.69	29.14	0.95	0.39	0.94	1.33
March	29.51	29.68	29.80	30.14	30.57	0.17	0.29	0.77	1.06
April	29.57	30.09	30.02	30.51	31.05	0.52	0.45	1.04	1.49
May	28.35	29.32	28.65	29.11	29.46	0.97	0.30	0.81	1.12
June	26.42	26.88	27.29	27.85	28.84	0.46	0.87	1.56	2.43
July	23.77	24.29	24.24	24.77	25.71	0.52	0.47	1.47	1.94
August	23.44	24.30	23.93	24.62	25.35	0.85	0.49	1.42	1.90
September	24.70	25.59	25.06	25.23	25.72	0.89	0.36	0.66	1.02
October	26.19	26.55	26.96	27.44	28.12	0.35	0.77	1.16	1.93
November	25.98	26.70	26.64	27.03	27.61	0.71	0.66	0.97	1.63
December	25.76	26.70	26.34	26.84	27.54	0.94	0.58	1.20	1.78

Minimum temperature change with HadCM3A2a scenario output of Bahir Dar station

Months	Monthly average					Temperature change			
	Minimum temperature (^{o}C)					compared to 1961-1990 (^{o}C)			
	1961-1990	1991-2007	2010-2039	2040-2069	2070-2099	1991-2007	2010-2039	2040-2069	2070-2099
January	6.52	8.87	7.12	8.12	8.92	2.35	0.60	1.60	2.40
February	8.27	10.88	9.07	10.07	11.67	2.60	0.80	1.80	3.40
March	11.30	13.09	12.70	13.90	15.70	1.79	1.40	2.60	4.40
April	12.51	15.18	14.31	15.91	18.31	2.67	1.80	3.40	5.80
May	13.47	15.50	14.67	15.87	17.27	2.03	1.20	2.40	3.80
June	13.36	14.70	14.76	15.96	17.56	1.34	1.40	2.60	4.20
July	13.24	14.35	13.64	14.44	15.04	1.12	0.40	1.20	1.80
August	13.14	14.16	13.74	14.54	15.24	1.01	0.60	1.40	2.10
September	12.37	13.53	13.57	15.17	16.97	1.16	1.20	2.80	4.60
October	11.91	13.87	12.71	13.71	15.11	1.96	0.80	1.80	3.20
November	9.81	11.79	10.81	12.21	13.41	1.98	1.00	2.40	3.60
December	6.94	9.56	8.34	10.14	12.34	2.62	1.40	3.20	5.40

Minimum temperature change with HadCM3B2a scenario output of Bahir Dar station

Months	Monthly average					Temperature change			
	Minimum temperature (^{o}C)					compared to 1961-1990 (^{o}C)			
	1961-1990	1991-2007	2010-2039	2040-2069	2070-2099	1991-2007	2010-2039	2040-2069	2070-2099
January	6.52	8.87	7.09	7.89	8.29	2.35	0.57	1.37	1.77
February	8.27	10.88	9.05	9.85	10.65	2.60	0.78	1.58	2.38
March	11.30	13.09	12.64	13.64	14.64	1.79	1.34	2.34	3.34
April	12.51	15.18	14.00	15.20	16.80	2.67	1.49	2.69	4.29
May	13.47	15.50	14.67	15.27	16.27	2.03	1.20	1.80	2.80
June	13.36	14.70	14.76	15.56	16.56	1.34	1.39	2.19	3.19
July	13.24	14.35	13.86	14.06	14.66	1.12	0.62	0.82	1.42
August	13.14	14.16	13.96	14.36	14.96	1.01	0.82	1.22	1.82
September	12.37	13.53	13.70	14.10	15.70	1.16	1.33	1.73	3.33
October	11.91	13.87	12.67	13.47	14.07	1.96	0.76	1.56	2.16
November	9.81	11.79	10.95	11.55	12.55	1.98	1.14	1.74	2.74
December	6.94	9.56	8.28	9.68	11.08	2.62	1.34	2.74	4.14

Precipitation change with HadCM3A2a scenario output of Bahir Dar station

Months	Monthly average Precipitation (mm/day)					Precipitation change compared to 1961-1990 (%)			
	1961-1990	1991-2007	2010-2039	2040-2069	2070-2099	1991-2007	2010-2039	2040-2069	2070-2099
January	0.10	0.05	0.11	0.13	0.15	-0.05	0.08	0.32	0.51
February	0.08	0.08	0.09	0.09	0.10	0.00	0.19	0.16	0.28
March	0.22	0.44	0.22	0.24	0.23	0.22	-0.04	0.08	0.03
April	0.73	0.95	0.75	0.84	0.97	0.23	0.03	0.16	0.33
May	2.67	2.42	3.57	3.75	3.85	-0.25	0.34	0.41	0.44
June	5.97	7.28	5.43	5.32	5.26	1.31	-0.09	-0.11	-0.12
July	14.38	13.60	13.90	14.23	13.93	-0.78	-0.03	-0.01	-0.03
August	12.65	11.93	12.31	11.91	11.83	-0.72	-0.03	-0.06	-0.06
September	6.75	6.89	9.10	8.75	9.07	0.14	0.35	0.30	0.34
October	2.89	3.22	5.22	5.78	6.29	0.33	0.80	1.00	1.17
November	0.75	0.43	1.42	1.51	1.63	-0.31	0.90	1.03	1.19
December	0.12	0.09	0.27	0.24	0.29	-0.02	1.31	1.07	1.49

Precipitation change with HadCM3B2a scenario output of Bahir Dar station

Months	Monthly average Precipitation (mm/day)					Precipitation change Compared to 1961-1990 (%)			
	1961-1990	1991-2007	2010-2039	2040-2069	2070-2099	1991-2007	2010-2039	2040-2069	2070-2099
January	0.10	0.05	0.09	0.11	0.09	-0.05	-0.08	0.11	-0.11
February	0.08	0.08	0.08	0.09	0.10	0.00	0.05	0.13	0.22
March	0.22	0.44	0.20	0.23	0.23	0.22	-0.10	0.04	0.01
April	0.73	0.95	0.83	0.85	0.80	0.23	0.14	0.17	0.10
May	2.67	2.42	3.38	3.26	3.43	-0.25	0.27	0.22	0.29
June	5.97	7.28	4.79	4.93	4.53	1.31	-0.20	-0.17	-0.24
July	14.38	13.60	13.36	13.72	13.42	-0.78	-0.07	-0.05	-0.07
August	12.65	11.93	11.25	11.17	10.83	-0.72	-0.11	-0.12	-0.14
September	6.75	6.89	8.20	8.10	8.15	0.14	0.21	0.20	0.21
October	2.89	3.22	5.22	4.81	4.47	0.33	0.80	0.66	0.55
November	0.75	0.43	1.37	1.43	1.38	-0.31	0.84	0.91	0.85
December	0.12	0.09	0.25	0.24	0.24	-0.02	1.12	1.05	1.00